7848

DIFFUSION AND TRANSFORMATION IN TERNARY AUSTENITES

DIFFUSION AND DIFFUSION-CONTROLLED TRANSFORMATION IN DILUTE TERNARY AUSTENITES

By

GARY RUSH PURDY, M.Sc.

A Thesis

Submitted to the Faculty of Graduate Studies

in Partial Fulfilment of the Requirements

for the Degree

Doctor of Philosophy

McMaster University

August 1962

DOCTOR OF PHILOSOPHY (1962) McMASTER UNIVERSITY
(Metallurgy) Hamilton, Ontario.

TITLE: Diffusion and Diffusion-controlled Transformation in Dilute Ternary Austenites

AUTHOR: Gary Rush Purdy, B.Sc. (University of Alberta)
M.Sc. (University of Alberta)

SUPERVISOR: Professor J. S. Kirkaldy

NUMBER OF PAGES: vii, 74

SCOPE AND CONTENTS:

The interstitial concentration and temperature dependence of the diffusion coefficient ratio D_{12}/D_{11} in ternary austenites containing silicon or manganese has been experimentally determined using diffusion couples based on the concept of "transient equilibrium". The results are compared with values predicted theoretically from statistical and thermodynamic considerations.

The kinetics of the growth of proeutectoid ferrite in binary and ternary austenites have been determined, using two-phase diffusion couples. The results are consistent with the premise that carbon diffusion controls the rate of interface migration. It is demonstrated, theoretically and experimentally, that the ternary results fall into two classes - one in which local equilibrium may be assumed, and one in which "constrained local equilibrium" may be postulated.

ACKNOWLEDGMENTS

The author is indebted to his supervisor, Dr. J. S. Kirkaldy, for suggesting the problems treated here, and for his continuing guidance throughout the course of the work. The financial assistance of the National Research Council of Canada (in the form of two graduate studentships) and of the American Iron and Steel Institute (in the form of a research grant to Dr. Kirkaldy) is gratefully acknowledged.

The author wishes to express his thanks to the staff and graduate students of the McMaster Metallurgy Department for many stimulating discussions; to the technical staff of the McMaster Engineering Building for technical assistance; to Dr. H. I. Aaronson of the Ford Motor Company for providing some of the alloys; and to Mr. J. H. Kelly of the Steel Company of Canada for assistance with the chemical analyses.

TABLE OF CONTENTS

INTRODUCTION		1
I	PREVIOUS EXPERIMENTAL WORK	2
	(a) Diffusion in Multicomponent Systems	2
	(b) Phase Transformation Studies - (Austenite decomposition)	5
II	THEORY	11
	(a) Phenomenological Theory of Diffusion	11
	(b) Phenomenological Theory for Ternary Austenites	17
	(c) Thermodynamics of Dilute Ternary Austenites	20
	(d) Statistical Theory of Diffusion in Ternary Austenites	25
	(e) Analysis of a Diffusing System in the Transient Equilibrium State	27
	(f) Application of the Diffusion Formalism to Phase Transformations	30
	(g) Ferrite Growth in Binary Iron-Carbon Austenite	34
	(h) Ferrite Growth in Ternary Austenite	36
III	DETERMINATION OF DIFFUSION COEFFICIENTS	43
	(a) Experimental	43
	(b) Results and Discussion	47
IV	INVESTIGATION OF THE GROWTH OF PROEUTECTOID FERRITE IN BINARY AND TERNARY AUSTENITES	52
	(a) Experimental	52
	(b) Results and Discussion	58
V	CONCLUSIONS	69
REFERENCES		71

LIST OF TABLES*

1. Interaction Parameters in Binary and Ternary Austenites.

2. Analyses of Alloys.

3. Analytical Results for Diffusion Layer Couples.

4. Measured Ferrite Growth Parameters.

*Tables have been placed at the end of thesis.

LIST OF ILLUSTRATIONS*

1. Penetration curve for an iron-carbon-silicon diffusion couple, after Darken[3].

2. Portion of the Fe-Fe_3C constitution diagram.

3. Micrograph showing grain boundary and Widmanstatten ferrite.

4. Austenite to austenite + ferrite surface of the iron, carbon, manganese constitution diagram.

5. Analytic representation of experimental activity data for the ternary systems Fe-C-Si, Fe-C-Mn, Fe-C-Ni.

6. Schematic representation of jump configuration in a ternary system containing an interstitial component.

7. Schematic representation of the energy relationships involved in the jump of an interstitial atom from site to site in a ternary alloy.

8. Initial and final solute distributions (schematic) in a layer diffusion couple.

9. Schematic isothermal section of the Fe-C-Mn constitution diagram.

10. Schematic penetration curves for ferrite growth in a ternary Fe-C-Mn austenite.

11. Schematic isothermal free energy surfaces for ferrite and austenite in the ternary Fe-C-Mn system.

12. Melting and casting apparatus.

13. Annealing furnace and clamp.

14. Microanalytic apparatus for carbon determination.

15. Penetration curve for Fe-C-Si layer diffusion couple in the "transient equilibrium" state.

16. Macrograph of a cross section of a typical "transient equilibrium" diffusion layer couple.

17. The interstitial concentration dependence of D_{12}/D_{11} in Fe-C-Si and Fe-C-Mn.

*Illustrations have been placed at the end of thesis.

18. The temperature dependence of D_{12}/D_{11} in Fe-C-Si and Fe-C-Mn.

19. Quenching furnace.

20. Macrograph of a binary ferrite-austenite diffusion couple.

21. Lead baths.

22. Micrographs of ternary Fe-C-Mn diffusion couples.

23. Austenite growth data for the binary ferrite - 0·567% C austenite diffusion couple.

24. Penetration curve for the binary ferrite-austenite diffusion couple.

25. Penetration curve for the binary ferrite-austenite diffusion couple.

26. Ferrite growth data for ternary 1·52% Mn, 0·210% C diffusion couples.

27. Ferrite growth data for ternary 1·52% Mn, 0·335% C diffusion couples.

28. Ferrite growth data for ternary 1·52% Mn, 0·405% C diffusion couples.

29. Ferrite growth data for ternary 3·16% Mn, 0·282% C diffusion couples.

30. Microhardness traverses of ternary Fe-C-Mn diffusion couples.

31. Iron, carbon, manganese constitution diagram, showing equilibrium tie-line.

32. Summary of ferrite growth data for all ternary compositions studied.

33. Calculated "constrained" tie-lines for ferrite growth in 0·282% C, 3·16% Mn austenite.

DIFFUSION AND DIFFUSION-CONTROLLED TRANSFORMATIONS IN DILUTE TERNARY AUSTENITES

Introduction:

The behaviour of austenite in diffusion and phase transformation is of interest from two standpoints. Firstly, a simple or alloyed form of austenite is invariably the starting point for the production of carbon or alloy steel. It is expected that, with a fuller understanding of these processes in austenite, many of the empirical rules of heat treatment currently in use may be supplemented or modified to improve the alloys and their treatments. Secondly, the austenite decomposition reactions, particularly the eutectoid, (pearlite) reaction, have invited much theoretical speculation, since it is assumed that an investigation of the more fundamental aspects of these reactions will cast light upon the broad field of solid state transformations.

The aim of this investigation has been to experimentally determine the diffusion coefficients required to designate diffusive behaviour in selected ternary austenites, and armed with this information, to attack the problem of phase transformations in these alloys. Towards these ends, new techniques have been evolved for the determination of diffusion coefficients, and of the growth kinetics of proeutectoid ferrite in supersaturated austenite. It is expected that the latter investigation will have a direct bearing on the kinetics of the more complex eutectoid (pearlite) reaction.

I PREVIOUS EXPERIMENTAL WORK

(a) Diffusion in Multicomponent Systems

Although diffusion in binary systems has been extensively investigated, the problem of diffusion in ternary and higher order systems has received comparatively little attention. Only recently have phenomenological schemes capable of describing the general case of diffusion been developed. (see section IIa).

The experiments of Bramley et al[1] represent the first significant studies of diffusion in ternary systems. Penetration curves for carbon in steels containing previously established gradients of sulphur and phosphorous were obtained. In both systems it was observed that the carbon distribution was drastically affected by the gradient of the alloying element.

Seith and Bartschat[2] and Darken[3] studied the effect of an abrupt change in concentration of a sluggish substitutional solute (e.g. Ni, Si, Mn) on the behaviour of carbon in austenite. The diffusion couples employed were variations of the semi-infinite couple common in binary diffusion experiments. In many cases, a distinct discontinuity in carbon concentration corresponded to the discontinuity in alloy concentration.

Darken's couple design, in particular, emphasized the fact that the diffusive flow of one element must be considered a function of all independent concentration gradients. It consisted of an iron-carbon alloy welded to an iron-carbon-silicon alloy such that the carbon

distribution was initially approximately uniform. After 13 days at 1050°C, the carbon concentration had changed as shown in figure 1.

Seith and Wever[4] suggested that, although the carbon penetration curves in the above experiments exhibited discontinuities, the carbon activity should be a smooth function of distance. Hirth et al[5] have recently analysed ternary couples (similar to Darken's) to determine the activity of carbon in iron-carbon-cobalt, implicitly making this assumption. As Darken[6] has pointed out, such an assumption is in need of experimental verification.

Gosting et al[7] studied diffusion in ternary liquid electrolytes with the object of testing the Onsager relations (see section IIa). The distribution of a diffusing species was found to be a function of all independent activity gradients, and the Onsager relations were verified within the probable experimental error.

Kirkaldy and co-workers have addressed themselves to the problem of determining diffusion coefficients in ternary substitutional alloys, again by means of semi-infinite couples[8,9].

The diffusion coefficients of carbon and manganese in austenite have been determined to good precision (approximately ± 15%) by Wells and Mehl[10,11]. Their work[12] has also shown that moderate amounts of alloy additions (in particular ~ 1% of Mn, Ni, or Si) do not significantly affect the rate of diffusion of carbon in austenite, although, in manganese steels, carbon has a pronounced effect on the rate of diffusion of manganese. Kurdjumov[13] on determining diffusivities of substitutional solutes in ternary austenites, found that they were greatly enhanced by the $\alpha + Fe_3C \rightarrow \gamma$ reaction, presumably because of the large number of

subgrains attending the first stages of austenite formation. No such increase was found when the above reaction did not immediately precede the diffusion anneal, (i.e. when a tracer was plated onto retained austenite rather than a ferrite-carbide mixture or martensite). The diffusion couples were slowly heated in vacuum.

As will be demonstrated in the following sections, thermodynamic data are of great value in interpreting multicomponent diffusion data. The results of Smith[14,15,16] on the activity of carbon in binary and ternary austenites are particularly relevant to this investigation, and will subsequently be discussed from a theoretical point-of-view. The binary activities were determined by equilibrating pure iron samples with calibrated $CO-CO_2$ and CH_4-H_2 mixtures. Activities determined by the two methods showed small consistent discrepancies, but, in general, were in good accord. Fe-C-Mn and Fe-C-Si activities were obtained by equilibrating pure iron and appropriate iron-base alloys with CH_4-H_2 mixtures, then comparing the carbon contents of the binary and ternary alloys. Recently, Kaufman et al[17] have stated that "there is evidence that the CH_4-H_2 ratios are open to question because of the formation of other hydrocarbons".

(b) Phase Transformation Studies

Many workers have studied the morphology, crystallography, and kinetics of phase transformations[18]. The following section will be devoted largely to pertinent observations of the various austenite decomposition processes, although the results will often be of general application in the field of condensed state transformations.

Before proceeding with a discussion of the austenite decomposition reactions, some of their elementary characteristics should be noted. The portion of the Fe-Fe_3C phase diagram shown in figure 2 is based on that presented by Hansen[19], modified slightly to comply with the recent work of Smith[20]. Austenite (γ) is an interstitial solid solution of carbon in face-centered-cubic iron, and ferrite (α) is an interstitial solid solution of carbon in body-centered-cubic iron. In both phases, the dissolved carbon atoms occupy octahedral interstices in the respective host lattices[21,22]. Cementite, (Fe_3C) is a complex orthohombic intermetallic compound. Pearlite, a product of eutectoid decomposition, consists of alternating lamellae of α and Fe_3C. Martensite, (α') is a body-centered-tetragonal product of non-equilibrium γ decomposition, produced by a shear process involving cooperative atom movements at the γ-α' phase interface. Here we will primarily be concerned with reactions between the α and γ solid solutions.

(i) Morphology

It is not the writer's intent to present an extensive account of previous detailed morphological investigations[23,27]. Morphology is of interest here, only in that it is often possible to infer interface struc-

tures from observations of precipitate shape and habit. Therefore, a simplified account of the sometimes complex morphology of the pro-eutectoid reactions will be given.

When austenite is supersaturated (i.e. cooled into the $\alpha + \gamma$ or $Fe_3C + \gamma$ regions of the iron-carbon diagram, the first stages of transformation usually occur in such a manner that the precipitated phase exhibits two distinct types of morphology*:

1. Grain Boundary Allotriomorphs: (figure 3)

The precipitate nucleates at the grain boundaries, and quickly grows preferentially along them (linear rate[24]). The precipitate films then tend to grow into the austenite (i.e. normal to the grain boundaries) with an approximately planar interface. Since there will, in general, be no rational orientation between two adjacent austenite grains, the daughter phase can only be rationally oriented with respect to one of the parent grains at most.

Aaronson[23] holds the view that grain boundary ferrite nucleates in an austenite grain, and grows into that grain. Smith[25] hypothesized that ferrite nucleates coherently with one grain, and grows into the adjacent grain, an opinion that is supported by the observation that ferrite usually grows predominantly into one austenite grain[23]. In any case, an incoherent α-γ interface is to be expected on at least one side of the ferrite film.

---

*These morphologies are common in a wide variety of ferrous and non-ferrous alloys when a single-phase precipitate forms in a single phase matrix by nucleation and growth involving long range diffusion.

2. Widmanstatten Plates and Sideplates: (figure 3)

These plates are formed in the interiors of γ grains, or develop from grain boundary allotriomorphs, and are therefore not kinetically constrained to grow along γ grain boundaries. In the case of proeutectoid ferrite, the parent and daughter phases are related approximately by the Kurdjumov and Sachs relations,[26]

$$(111)_\gamma \text{ ll } (110)_\alpha$$
$$[\bar{1}10]_\gamma \text{ ll } [\bar{1}11]_\alpha,$$

so that there is a chance of partial lattice matching, and an attendant semi-coherent interface structure. It appears that the habit plane of proeutectoid cementite is not unique[27].

(ii) Kinetics

Previous workers have failed to unequivocally demonstrate whether diffusion controls the grain boundary proeutectoid ferrite reaction. Some possible reasons for this failure are listed below:

(1) The usual practice has been to austenitize a steel, react isothermally in the $\alpha + \gamma$ range for various times, and metallographically evaluate the thickness of the grain boundary ferrite. Since the time of nucleation of each plate is not known, and the ferrite platelets intersect the plane of polish at random angles, evaluation of the rate of thickening presents a formidable problem in quantitative statistical metallography.

(2) High purity iron-carbon alloys transform with such rapidity that many investigators have found complex alloy steels attractive[28,29]. Even in the case of alloy steels, the carbon diffusion

fields from opposite sides of a grain impinge after a time $t = 0{\cdot}035\ a^2/D$ [30], (a is the grain radius, D the diffusion coefficient of carbon) so that, unless the γ grains are very large or penetration times very short, the boundary conditions will be altered during the experiment.

(3) The ease with which steels decarburize has occasionally led to error. Heidenreich[31], using hot-stage thermionic emission microscopy, found that grain boundary ferrite thickened more rapidly than could be accounted for by volume diffusion control, and concluded that proeutectoid ferrite forms by a shear mechanism. However, since decarburization apparently took place during the experiment[23], this conclusion is probably not warranted.

Aaronson[23] has calculated diffusion coefficients from the best available information on ferrite allotriomorph thickening, and finds that the values obtained are within about $\pm$ 50% of those measured by Wells and Mehl[10].

Rouze and Grube[23] measured the rate of thickening of a Widmanstatten α plate using thermionic emission microscopy, and found the rate too slow for diffusion control. Heckel and Paxton[27] metallographically determined growth rates of grain boundary cementite in a high purity hypereutectoid steel, and, observing that the rates were too slow for diffusion control, concluded that interfacial reaction must be partially controlling.

According to Heckel and Paxton[27], various attempts to metallographically demonstrate the existence of carbon gradients near precipitated ferrite have not been conclusive, although Barrett et al[32] have

presented a photomicrograph showing solute depletion near silver-rich allotriomorphs in aluminum-silver alloys.

The austenite-pearlite reaction in high-purity steels apparently proceeds too quickly for volume diffusion control[33], an observation which led Cahn and Hagel[34] to suggest that a large proportion of the carbon is transported laterally along phase boundaries as the pearlite grows. However, there is evidence[35] that interstitial components diffuse less rapidly along austenite grain boundaries than in bulk austenite, so that the assumption of enhanced interstitial phase boundary diffusion is in need of experimental justification.

Published isothermal transformation diagrams[36] for various steels indicate that alloying elements usually have inhibiting effects on both nucleation and growth in the austenite decomposition reactions. Manganese, in particular, is a very effective hardenability agent[37]. Wells and Mehl[12] showed that the observed inhibitions are not due to a change in the carbon diffusion coefficient.

Of considerable pertinence to the alloy transformation problem is the work of Aaronson[38] and of Bowman[39] who have demonstrated that no alloy partition occurs during the proeutectoid ferrite reaction in the systems Fe-C-Cr and Fe-C-Mo, respectively. The analyses were carried out on ferrite formed isothermally at various temperatures.

In the pearlite reaction, partition of alloying elements to the ferrite or carbide has frequently been observed[40,41,42]. Cahn and Hagel[34] have shown that, for pearlite to form in slightly supersaturated austenite some alloy partition is necessary, but that pearlite formation in highly supersaturated austenite is thermodynamically possible without alloy

partition. Recently, Pickelsimer et al[41] observed that negligible manganese partition occurred during the early stages of transformation in a manganese steel, which suggests that measured alloy partition is often the result of subsequent lateral alloy diffusion behind the growth front. Zener[43] concluded that alloying elements only affect the rate of pearlite growth by changing the interlamellar spacing, a conclusion that is not borne out by experiment[34].

The portion of the ternary Fe-C-Mn phase diagram in figure 4 is based on that suggested by Wells[44], but modified to comply with the $Fe-Fe_3C$ diagram of figure 2, and with the Fe-Mn diagram determined by Troiano and McGuire[45].

II THEORY

(a) Phenomenological Theory of Diffusion

The formal basis for diffusion theory was established in 1855 by Fick[46], who proposed a linear relationship between the diffusive flow, J, and the concentration gradient ∇C, of the form

(1) $$J = - D\nabla C.$$

The proportionality constant, D, is called the diffusion coefficient. Relation (1) has survived the discovery that D is a function of concentration by becoming, in part, a definition of the diffusion coefficient.

Combination of (1) with the mass balance,

(2) $$\text{div } J = - \frac{\partial C}{\partial t} ,$$

yields the time-dependent diffusion equation

(3) $$\frac{\partial C}{\partial t} = \nabla \cdot \left(D_{(C)} \nabla C \right) .$$

Equations (1) and (3), known as Fick's first and second laws respectively, are sufficient to describe binary volume diffusion in crystals, whatever the mechanism by which the atoms involved migrate. If the diffusing species is dissolved substitutionally in the solvent, the origin is chosen as the Matano interface[47]. If the solute occupies interstices in the solvent lattice, the origin is chosen fixed relative to the host lattice. Other choices of coordinate axes usually require that two "intrinsic" diffusion coefficients be specified.

Onsager[48] proposed, as a generalization of Fick's first law for application to multicomponent systems, that the flux of each component be assumed a linear function of all the concentration gradients:

$$J_i = -\sum_{k=1}^{n} D'_{ik} \nabla C_k \qquad (i = 1, 2, \cdots n). \tag{4}$$

On combining equations (4) with the mass balances,

$$\text{div } J_i + \frac{\partial C_i}{\partial t} = 0 \qquad (i = 1, 2, \cdots n), \tag{5}$$

the generalized diffusion equations are obtained,

$$\frac{\partial C_i}{\partial t} = \sum_{k=1}^{n} \nabla \cdot (D'_{ik} \nabla C_k) \quad (i = 1, 2, \cdots n). \tag{6}$$

In general, n^2 coefficients (all functions of concentration) are required to completely describe diffusion in an n-component system. However, since it is usually possible to write concentrations in such units that

$$\sum_{i=1}^{n} C_i = \text{constant}, \tag{7}$$

equations (4) can be written

$$J_i = -\sum_{i=1}^{n-1} D_{ik} \nabla C_k \qquad (i = 1, 2, \cdots n-1) \tag{4a}$$

$$\text{where} \quad D_{ik} = D'_{ik} - D'_{in} \tag{8}$$

By an appropriate choice of coordinate axes, one of the fluxes has been eliminated.* The number of coefficients required is thus reduced to $(n-1)^2$.

---

*Such a choice of origin makes it impossible to treat the motion of markers in the diffusion zone (the Kirkendall effect). While of great interest because of the light it casts on the mechanism of substitutional diffusion, the Kirkendall effect can usually be ignored in a phenomenological scheme designed only to designate flow relative to a fixed lattice[49].

The analogue of equation (6) in the reduced system is

$$\frac{\partial C_i}{\partial t} = \sum_{k=1}^{n-1} \nabla\cdot(D_{ik}\nabla C_k) \quad (i = 1, 2, \cdots n-1). \tag{6a}$$

Equations (4a) and (6a) lend themselves to mathematical manipulation (especially in cases where the D_{ik} can be considered constant) and have been the subject of considerable investigation. Kirkaldy,[50] in particular, has developed a theorem for determining solutions of (6a) from solutions of the binary diffusion equation (2) for analogous boundary conditions.

An alternative, and complementary, approach to the description of diffusive flows is based on the thermodynamics of irreversible processes[51]. In this scheme, the local rate of entropy production is written as a sum of fluxes and corresponding forces,

$$\sigma = \sum_i J_i X_i \tag{9}$$

The phenomenological equations describing the irreversible phenomena are introduced as linear equations between these two sets of quantities,

$$J_i = \sum_{k=1}^{n} L'_{ik} X_k \tag{10}$$

Onsager[52] has advanced statistical arguments to the effect that the matrix of coefficients is symmetric, i.e.

$$L'_{ik} = L'_{ki} \,. \tag{11}$$

Onsager's original result is valid only for the description of scalar phenomena. De Groot and Mazur[53] have extended Onsager's proof to include processes of a vectorial nature. The "proper choice" for a diffusive force in an isothermal system (so that equations 11 hold) has

been ascertained from considerations of equation 9:[51]

(12) $$X_k = - \text{grad } \mu_k$$

where the μ_k are chemical potentials.

In the statistical arguments leading to the Onsager relations, it is assumed that the fluxes are measured with respect to the local centre of mass, and that the fluxes, as well as the forces, are independent of one another. The formalism should therefore be applied with care when fluxes are specified with respect to some more common frame of reference, or when linear dependencies exist between the fluxes or the forces.

Hooyman and de Groot[54] have treated the case where the fluxes and forces are not independent, and show that the L'_{ik} scheme need not be symmetric, although the L'_{ik} can always be chosen so as to satisfy the Onsager relations.

Hooyman[55] and Kirkwood et al[56] have investigated the case where the flows are referred to a frame in which the net flow of solvent is zero. The forces are related through the Gibbs-Duhem relation, which can be written

(13) $$\sum_{k=1}^{n} C_k \frac{\partial \mu_k}{\partial x} = 0 \, .$$

In this particular frame of reference, the unidirectional flux equations take the simpler form,

(14) $$J_i = - \sum_{k=1}^{n-1} L_{ik} \frac{\partial \mu_k}{\partial x} \, , \quad (i = 1, 2, \text{---} n-1),$$

and the Onsager relations are

(15) $$L_{ik} = L_{ki} \, .$$

The L_{ik} in (15) are uniquely defined.

Equations (14) and (15) are valid when the concentrations are

measured in grams per unit volume, and the chemical potentials in μ per gram, or when the concentrations, C, are measured in moles per unit volume, and the chemical potentials in μ per mole. Hereafter, the latter system of units will be used unless otherwise stated.

Since $\mu_k = \mu_k (C_1, C_2, \text{---} C_{n-1})$,

$$\frac{\partial \mu_k}{\partial x} = \sum_{j=1}^{n-1} \mu_{kj} \frac{\partial C_j}{\partial x} \tag{16}$$

where $$\mu_{kj} = \frac{\partial \mu_k}{\partial C_j} \quad . \tag{17}$$

Combining equations (14) and (16),

$$J_i = - \sum_{k=1}^{n-1} L_{ik} \sum_{j=1}^{n-1} \mu_{kj} \frac{\partial C_j}{\partial x} \quad , \quad (i = 1, 2, \text{---} n-1) \tag{18}$$

which defines the D's in terms of the L's:

$$D_{ij} = \sum_{k=1}^{n-1} L_{ik} \mu_{kj} \quad . \tag{19}$$

As a consequence of (15), it is possible to write

$$\sum_{j,\ell=1}^{n-1} \mu_{ji} L_{j\ell} \mu_{\ell k} = \sum_{j,\ell=1}^{n-1} \mu_{jk} L_{\ell j} \mu_{\ell i} \quad , \tag{20}$$

so that the Onsager relations in terms of diffusion coefficients read

$$\sum_{j=1}^{n-1} \mu_{ji} D_{jk} = \sum_{j=1}^{n-1} \mu_{jk} D_{ji} \quad . \tag{21}$$

The transformation properties of the Onsager relations have been investigated by Hooyman et al[57]. If the fluxes in a new frame of reference (A) are related to the fluxes in the original frame (B) by

$$J_k^{A} = \sum_{i=1}^{n-1} P_{ki} J_i^{B}, \quad (k = 1, 2, \text{---} n-1) \tag{22}$$

then, if the Onsager relations are to be preserved, the forces must be

$$X_k^{A} = \sum_{i=1}^{n-1} P_{ik}^{-1} X_i^{B}, \tag{23}$$

which also leaves the expression for the entropy production (9) unchanged.

Hooyman[55] has presented a general equation for the Onsager relations in terms of diffusion coefficients for fluxes and forces transformed by (22) and (23). This is

$$\sum_{j,\ell=1}^{n-1} D_{jk} P^{-1}_{\ell j} \mu_{\ell i} = \sum_{j,\ell=1}^{n-1} \mu_{\ell k} P^{-1}_{\ell j} D_{ji} \,. \tag{24}$$

(b) Phenomenological Theory for Ternary Austenites*

In the special case where one dilute interstitial component (designated 1) diffuses in a face-centered-cubic binary substitutional austenite (substitutional solute; 2, iron; 3), equations of type 4 may be applied to fluxes measured with respect to a fixed face-centered-cubic lattice (i.e. lattice parameter changes and the shift of the Matano interface are neglected). Subject to these specifications,

$$J_2 + J_3 = 0 \tag{25}$$

so that equations (4) can be written, (for unidirectional diffusion)

$$J_1 = - D_{11} \frac{\partial C_1}{\partial x} - D_{12} \frac{\partial C_2}{\partial x} , \tag{26}$$

and

$$J_2 = - D_{21} \frac{\partial C_1}{\partial x} - D_{22} \frac{\partial C_2}{\partial x} , \tag{27}$$

where $D_{11} = D'_{11}$, $D_{12} = (D'_{12} - D'_{13})$, $D_{21} = D'_{21}$,

and $D_{22} = (D'_{22} - D'_{23})$.

The alternate flux equations may be found by transforming equations (14) via

$$J_i^L = J_i^N + C_i \, v_{NL} \tag{28}$$

where J_i^L is the flux of i measured in the lattice fixed frame, (L), J_i^N is the flux of i measured in the solvent-fixed frame, (N), and v_{NL} is the velocity of frame N with respect to frame L.

Since

$$J_3^N = 0, \tag{29}$$

---

*The essential content of the following sections (b) through (e) has been published by the author and Professor Kirkaldy[58,59].

and

$$J_3^L = - J_2^L , \tag{30}$$

then, according to (28)

$$v_{NL} = - \frac{J_2^L}{C_3} . \tag{31}$$

The transformed fluxes are:

$$J_1^L = J_1^N - \frac{C_1}{C_2 + C_3} J_2^N \tag{32}$$

and

$$J_2^L = \frac{C_3}{C_2 + C_3} J_2^N , \tag{33}$$

and the forces, according to (23), are

$$X_1^L = X_1^N \tag{34}$$

and

$$X_2^L = \frac{C_1}{C_3} X_1^N + \frac{C_2 + C_3}{C_3} X_2^N . \tag{35}$$

The flux equations are now

$$J_1^L = - L_{11} \frac{\partial \mu_1}{\partial x} - L_{12} \left[\frac{C_1}{C_3} \frac{\partial \mu_1}{\partial x} + \frac{C_2 + C_3}{C_3} \frac{\partial \mu_2}{\partial x} \right] \tag{36}$$

and

$$J_2^L = - L_{21} \frac{\partial \mu_1}{\partial x} - L_{22} \left[\frac{C_1}{C_3} \frac{\partial \mu_1}{\partial x} + \frac{C_2 + C_3}{C_3} \frac{\partial \mu_2}{\partial x} \right] \tag{37}$$

subject to

$$L_{12} = L_{21} . \tag{38}$$

In terms of diffusion coefficients, the Onsager relation (from (24), is

$$D_{11}\mu_{12} + D_{21} \frac{C_1}{C_3} \mu_{12} + D_{21} \frac{C_2 + C_3}{C_3} \mu_{22} = D_{12}\mu_{11} + D_{22} \frac{C_1}{C_3} \mu_{11} + D_{22} \frac{C_2 + C_3}{C_3} \mu_{21} , \tag{39}$$

which reduces to the ternary form of (21) for dilute solutions (C_1, $C_2 \ll C_3$).

Combining equation (36) with equations (16) gives

$$J_1 = -\left[L_{11}\mu_{11} + L_{12}\frac{C_1}{C_3}\mu_{11} + L_{12}\frac{C_2+C_3}{C_3}\mu_{21}\right]\frac{\partial C_1}{\partial x} - \left[L_{11}\mu_{12} + L_{12}\frac{C_1}{C_3}\mu_{12} + L_{12}\frac{C_2+C_3}{C_3}\mu_{22}\right]\cdot\frac{\partial C_2}{\partial x} \tag{40}$$

The ratio of diffusion coefficients D_{12}/D_{11} may be obtained by comparing (40) with (26). This yields

$$\frac{D_{12}}{D_{11}} = \frac{L_{11}\mu_{12} + L_{12}\frac{C_1}{C_3}\mu_{12} + L_{12}\frac{C_2+C_3}{C_3}\mu_{22}}{L_{11}\mu_{11} + L_{12}\frac{C_1}{C_3}\mu_{11} + L_{12}\frac{C_2+C_3}{C_3}\mu_{21}}, \tag{41}$$

which, to the extent that the off-diagonal interactions as measured by L_{12} are small, becomes purely thermodynamic, i.e.,

$$\frac{D_{12}}{D_{11}} = \frac{\mu_{12}}{\mu_{11}} = \frac{\partial\mu_1/\partial N_2}{\partial\mu_1/\partial N_1}. \tag{42}$$

To the same approximation, D_{21}/D_{22} is given by

$$\frac{D_{21}}{D_{22}} = \frac{\partial\mu_2/\partial N_1}{\partial\mu_2/\partial N_2}. \tag{43}$$

(c) The Thermodynamics of Dilute Ternary Austenites

It is apparent that any test of equation (42) requires that analytic expressions for the thermodynamic properties of the solutions involved be available. The data accumulated by Smith[14,15,16] on the activity of carbon in binary and ternary austenites provides a strong incentive for theoretical interpretation. The binary iron-carbon results have often been discussed on the basis of geometric models,[17] which assume that some or all of the interstitial sites adjacent to an occupied site are inaccessible for other carbon atoms. Darken[60] has treated the binary system, using an energetic model, by calculating the partition function for the system. Iwase and Kachi[61] have extended this calculation to ternary austenites. In the following section, an approximate expression for the Gibbs free energy,

(44) $$F = E - TS^{*}$$

is obtained by calculating the energy E as a sum of pair energies, and S as the configurational entropy. The differentiation of F with respect to the number of atoms of institial component leads directly to an expression for the activity.

In ternary austenites of the type considered here, the interstitial component (1) occupies octahedral sites in the face-centered-cubic alloy host lattice. The substitutional solute (2) replaces iron (3) in the solvent lattice. The octahedral interstices form another f.c.c. lattice with the same number of sites as the solvent lattice.

---

*The correct expression for F is E + PV - TS. In the solid state, the PV term is usually negligible in comparison with the others, and F is satisfactorily approximated by (44).

The entropy is assumed to be purely configurational (i.e. regular behaviour) so that, in formation of the dilute solution, there is no tendency towards ordering, nor is there any significant change in the vibrational and electronic modes. The energy is regarded as made up of the interaction energy of nearest-neighbour pairs in the lattice. This enumeration includes interstitial pairs on adjacent octahedral sites, although these are not strictly nearest neighbours.

The total energy E, is given by the sum of pair energies,

(45) $$E = \eta_{11}\epsilon_{11} + \eta_{22}\epsilon_{22} + \eta_{33}\epsilon_{33} + \eta_{12}\epsilon_{12} + \eta_{23}\epsilon_{23} + \eta_{31}\epsilon_{31}$$

where the η's represent numbers of pairs, and the ϵ's are the corresponding interaction energies based on any convenient standard state. In particular ϵ_{11} is the energy of an interstitial pair from atoms at isolated interstitial sites, and ϵ_{12} and ϵ_{31} are the energies of formation of an interstitial-substitutional pair from a completely isolated interstitial atom. The η's are related to the number of atoms of the three species, n_1, n_2, and n_3 by the relations,

(46) $$6\, n_1 = \eta_{12} + \eta_{13} ,$$

(47) $$12\, n_2 = 2\eta_{22} + \eta_{23} ,$$

(48) $$12\, n_3 = 2\eta_{33} + \eta_{23} ,$$

(49) $$6\, n_1^2/(n_2 + n_3) = \eta_{11} ,$$

(50) $$6\, n_1 n_2/(n_2 + n_3) = \eta_{12} ,$$

(51) $$6\, n_2^2/(n_2 + n_3) = \eta_{22} ,$$

subject to the condition that $n_3 >> n_1, n_2$.

On substitution, equation (45) becomes ,

$$E = 6n_1\epsilon_{31} + 6n_3\epsilon_{33} + \frac{12n_2n_3}{n_2+n_3}\left(\epsilon_{23} - \frac{\epsilon_{33}}{2}\right) + \frac{1}{n_2+n_3}\left\{6n_1^2\epsilon_{11} + 6n_2^2\epsilon_{22} + 6n_1n_2\left(\epsilon_{12} - \epsilon_{31}\right)\right\} . \tag{52}$$

The total number of configurations of the ternary solution is equal to the number of distinct ways that n_1 atoms can be distributed among the $n_2+ n_3$ interstitial sites multiplied by the number of ways the n_2 and n_3 atoms can be arranged among the same number of substitutional sites. This is

$$W = \frac{(n_2+ n_3)!}{n_1!(n_2+ n_3 - n_1)!} \quad \frac{(n_2+ n_3)!}{n_2!\, n_3!} . \tag{53}$$

The configurational entropy is

$$S = k\, \ell n\, W \tag{54}$$

which, with the help of the Stirling approximation becomes

$$S = k\left\{- n_1 \ell n\, n_1 - (n_2+ n_3- n_1)\ell n(n_2+ n_3- n_1)\right\} + S_o \tag{55}$$

where S_o is a sum of terms independent of n_1.

By definition, the partial molal free energy is

$$\mu_1 = A\, \frac{\partial F}{\partial n_1} \tag{56}$$

where A is Avogadro's number. Thus, in terms of mole fractions,

$$\mu_1 = 6A\epsilon_{31} + 12AN_1\epsilon_{11} + 6AN_2(\epsilon_{12}-\epsilon_{31}) + AkT\ell n \frac{n_1}{n_2+ n_3- n_1} \cong 6A\epsilon_{31} + RT\ell nN_1\left\{1 + \left(\frac{12\epsilon_{11}}{kT} + 2\right)N_1\right\}\left\{1 + 6\frac{(\epsilon_{12}- \epsilon_{31})}{kT} N_2\right\} \tag{57}$$

subject to the approximation that N_1 and N_2 are sufficiently small compared with N_3, and that $\ell n\ (1 + x) \cong x$. Hence the activity of the interstitial component referred to the standard state at infinite dilution is:

$$(58) \qquad a_1 = N_1 \left\{1 + \left(\frac{12\epsilon_{11}}{kT} + 2\right)N_1\right\}\left\{1 + 6\,\frac{(\epsilon_{12} - \epsilon_{31})}{kT}\,N_2\right\}$$

By identical procedures,

$$(59) \qquad a_2 = N_2 \left\{1 - \frac{24}{kT}\left(\epsilon_{23} - \frac{\epsilon_{22} + \epsilon_{33}}{2}\right)N_2\right\}\left\{1 + 6\,\frac{\epsilon_{12} - \epsilon_{31}}{kT}\,N_1\right\}$$

and

$$(60) \quad a_3 = N_3 \left\{1 - (1 + \frac{6\epsilon_{11}}{kT})N_1^2 - 6\,\frac{\epsilon_{12} - \epsilon_{31}}{kT}\,N_1N_2 + \frac{12}{kT}\left(\epsilon_{23} - \frac{\epsilon_{22} + \epsilon_{33}}{2}\right)N_2^2\right\}$$

so that an internal check can be made through the Gibbs-Duhem relation. The standard partial molal free energies are $\mu_1^\circ = 6A\epsilon_{31}$, $\mu_2^\circ = 6A(2\epsilon_{23} - \epsilon_{33})$ and $\mu_3^\circ = 6A\epsilon_{33}$.

The equality of the second coefficients in (58) and (59) suggests that there may exist a general thermodynamic relation of this sort for a set of arbitrary dilute solutions with activities of the form,

$$(61) \qquad a_1 = k_1N_1(1 + bN_1 + cN_2) \cong k_1N_1(1 + bN_1)(1 + cN_2)$$

and

$$(62) \qquad a_2 = k_2N_2(1 + eN_2 + fN_1) \cong k_2N_2(1 + eN_2)(1 + fN_1)$$

Substituting these in the Gibbs-Duhem equation gives

$$(63) \qquad \begin{aligned} d(\ell n\, a_3) &= -\left[1 + (1 + b)N_1 + (1 + f)N_2\right]dN_1 \\ &\quad - \left[1 + (1 + c)N_1 + (1 + e)N_2\right]dN_2 \\ &= -\,P_1dN_1 - P_2dN_2\,. \end{aligned}$$

Since this must be an exact differential,

$$(64) \qquad \frac{\partial P_1}{\partial N_2} = \frac{\partial P_2}{\partial N_1}$$

or

$$(65) \qquad c = f.$$

Hence the symmetry of (58) and (59) is a thermodynamic imperative,

rather than a consequence of the model. This result, originally due to Wagner[62] represents a significant aid to experimental economy in tabulating the thermodynamic properties of dilute solutions, and in tabulating multicomponent diffusion data.

Relation (58) has been fitted to the experiments of Smith (at 1000°C) for the systems Fe-C, Fe-C-Si, Fe-C-Mn, and Fe-C-Ni and the results plotted in figure 5. Calculated values for ϵ_{11}/kT and $(\epsilon_{12} - \epsilon_{31})/kT$ are indicated in Table I.

Although the near-neighbour, regular solution approximation is generally an inaccurate one,[63] and the interaction energies are atomistically rather ill-defined, this theory does give a qualitative physical description of the thermodynamic functions of interstitial solutions, and provides a convenient framework for the representation of thermodynamic data.

(d) Statistical Theory of Diffusion in a Ternary Solution

Seitz[64] has presented a method for calculating a diffusion flux in terms of atomic parameters. In the case of interstitial diffusion in ternary austenites, the carbon atoms (1) in octahedral sites, have 6 near substitutional neighbours. The statistics of diffusion across a (111) substitutional plane will now be considered. In figure 6, lines a and b separated by the lattice spacing, λ, ($\lambda = d_{(111)}$) represent planes of octahedral sites, while c, d, and e represent adjacent planes of substitutional sites. Let n_1^a, n_2^a, n_3^a and n_1^b, n_2^b, n_3^b be the average number of moles per unit area at planes a and b respectively, subject to

$$n_2^a + n_3^a = n_2^b + n_3^b \tag{66}$$

Let $\nu^{ab} = \nu(n_1^a, n_1^b, n_2^a, n_2^b)$ be the probability per unit time that a 1 atom will jump from a to b and $\nu^{ba} = \nu(n_1^b, n_1^a, n_2^b, n_2^a)$ the probability of a jump from b to a. The flux of component 1 is

$$J_1 = n_1^a \nu^{ab} - n_1^b \nu^{ba} \tag{67}$$

Expanding this as a Taylor series in the spacing λ,

$$J_1 = n_1^a \nu^{ab} - \left(n_1^a + \lambda \frac{dn_1}{dx}\right)\left\{\nu^{ab} + \lambda \frac{dn_1}{dx}\left[\frac{\partial \nu^{ab}}{\partial n_1^a} - \frac{\partial \nu^{ab}}{\partial n_1^b}\right] + \lambda \frac{dn_2}{dx}\left[\frac{\partial \nu^{ab}}{\partial n_2^a} - \frac{\partial \nu^{ab}}{\partial n_2^b}\right]\right\}, \tag{68}$$

$$= -\lambda^2\left\{\nu^{ab} - n_1\left[\frac{\partial \nu^{ab}}{\partial n_1^a} - \frac{\partial \nu^{ab}}{\partial n_1^b}\right]\right\}\frac{\partial C_1}{\partial x} - \lambda^2\left[\frac{\partial \nu^{ab}}{\partial n_2^a} - \frac{\partial \nu^{ab}}{\partial n_2^b}\right] n_1 \frac{\partial C_2}{\partial x}$$

dropping insignificant superscripts and noting that $n_1 = \lambda C_1$. Neglecting the high order coefficient of $\frac{\partial C_1}{\partial x}$,

$$\frac{D_{12}}{D_{11}} = \frac{n_1}{\nu^{ab}}\left[\frac{\partial \nu^{ab}}{\partial n_2^a} - \frac{\partial \nu^{ab}}{\partial n_2^b}\right] . \tag{69}$$

Let us now consider a statistical representation of the jump frequency according to figure 7, where a 1 atom in plane a which is adjacent to a 2 atom in any one of its six possible sites has its potential well deepened by an amount $\epsilon_{31} - \epsilon_{12}$. Then the jump frequency can be written in terms of Boltzmann factors.

$$(70)\quad \nu^{ab} = 6\,\frac{n_2^{\,a}}{r_2^{\,a} + n_3^{\,a}}\,\frac{\nu_o}{m}\,e^{-\left\{\frac{\epsilon + [\epsilon_{31} - \epsilon_{12}]}{kT}\right\}} + \left(1 - 6\,\frac{n_2^{\,a}}{n_2^{\,a} + n_3^{\,a}}\right)\frac{\nu_o}{m}\,e^{-\epsilon/kT},$$

where ν_o is the mean vibration frequency, m is a geometric factor, and ϵ is the activation energy for diffusion of 1 in 3. Thus, via (69),

$$(71)\qquad \frac{D_{12}}{D_{11}} \cong 6\,\frac{\epsilon_{12} - \epsilon_{31}}{kT}\cdot N_1 .$$

Equation (71) may now be compared with the result obtained by substituting (61) into (42). For $N_1, N_2 \ll 1$, this gives

$$(72)\qquad \frac{D_{12}}{D_{11}} \cong cN_1 .$$

From relation (58),

$$(73)\qquad c = 6\,\frac{\epsilon_{12} - \epsilon_{31}}{kT},$$

so that (72) is identical with (71).

This indicates that a thermodynamic theory of interstitial diffusion which neglects the off-diagonal terms in the L-matrix is equivalent to a statistical theory which considers only near-neighbour interactions, and first order terms in a Taylor series expansion of the flux as a function of lattice spacing.

(e) Analysis of a Diffusing System in the Transient Equilibrium State

Kirkaldy[65] has proposed a boundary condition which has a particularly simple integral of the ternary diffusion equation (26). This is any finite system which has one very slowly diffusing component and one very rapidly diffusing one - precisely the situation described in previous sections where the interstitial element tends to diffuse much faster than the substitutional ones. The fast component diffusing on the gradient of the slow one will rapidly come to a state of "transient equilibrium", and the distribution of the fast component will thereafter change slowly in unison with the slow one. If the initial solute concentrations in a layer couple (for example Fe-C-2% Si) are as shown schematically in figure 8(a), at diffusion temperature, the substitutional element (2) diffuses slowly outward while the interstitial carbon (1) rapidly comes to "transient equilibrium" (figure 8(b)). When the latter state has been reached, the condition can be described to a first approximation by

$$J_1 = - D_{11} \frac{\partial C_1}{\partial x} - D_{12} \frac{\partial C_2}{\partial x} = 0 \ . \tag{74}$$

A solution for constant coefficients may be obtained by integrating (74) from the outside to the centerline. This gives

$$\frac{D_{12}}{D_{11}} = \frac{C_1^{\,o} - C_1}{C_2} \ , \tag{75}$$

where $C_1^{\,o}$ is the outside concentration of component 1, C_1 is any inside concentration of component 1, and C_2 is the corresponding inside concentration of component 2. Thus a measurement of the outside and the centerline concentrations of the couple ($C_1^{\,i}$ and $C_2^{\,i}$) gives a first estimate of

D_{12}/D_{11} at the mean concentrations $(C_1^{\circ} + C_1^{i})/2$ and $C_2^{i}/2$.

Approximation (74) may be improved by taking into account the first order time dependence of the configuration but again assuming constant coefficients. The time dependent diffusion equations are, from (6a),

$$\frac{\partial C_1}{\partial t} = \frac{\partial}{\partial x}\left(D_{11}\frac{\partial C_1}{\partial x}\right) + \frac{\partial}{\partial x}\left(D_{12}\frac{\partial C_2}{\partial x}\right) = D_{11}\frac{\partial^2 C_1}{\partial x^2} + D_{12}\frac{\partial^2 C_2}{\partial x^2}, \tag{76}$$

and

$$\frac{\partial C_2}{\partial t} = \frac{\partial}{\partial x}\left(D_{22}\frac{\partial C_2}{\partial x}\right) + \frac{\partial}{\partial x}\left(D_{21}\frac{\partial C_1}{\partial x}\right) = D_{22}\frac{\partial^2 C_2}{\partial x^2} + D_{21}\frac{\partial^2 C_1}{\partial x^2}, \tag{77}$$

where the latter equalities hold for constant coefficients.

An approximation to the time derivative of (76) is obtained by substituting (75) into the time derivative of (77) and neglecting the last term in (77):

$$\frac{\partial C_1}{\partial t} \cong \frac{D_{12}\cdot D_{22}}{D_{11}}\frac{\partial^2 C_2}{\partial x^2}. \tag{78}$$

On integrating (76) twice, a solution which takes account of the first order time dependence of the configuration is obtained:

$$\frac{D_{12}}{D_{11}} \cong \frac{C_1^{\circ} - C_1}{C_2\left(1 + \frac{D_{22}}{D_{11}}\right)}. \tag{79}$$

For all ternary austenites of the type considered here, the ratio $\frac{D_{22}}{D_{11}} \ll 1$, so (74) can be regarded as a highly accurate representation of the transient equilibrium state.

The concentration dependence of the diffusion coefficients* may be taken into account by noting that the thermodynamic relation (42), operating on the general expansion for the activity (61) gives

$$\frac{D_{12}}{D_{11}}(N_1,N_2) = \frac{cN_1(1 - bN_1)}{1 + cN_2} \tag{80}$$

In the same way, equations (43) and (62) yield

$$\frac{D_{21}}{D_{22}}(N_1,N_2) = \frac{cN_2(1 - eN_2)}{1 + cN_1} \quad . \tag{81}$$

For purposes of integration, the empirical relation

$$\frac{D_{12}}{D_{11}} = \frac{c'N_1}{1 + cN_2} \tag{82}$$

will be assumed. c is given the thermodynamic value of equation (61) and c' is a purely empirical coefficient which is eliminated in the integration. The result obtained by integrating (74) from the outer surface of the couple to the centerline, and assuming the concentration dependence of (82) is

$$\frac{D_{12}}{D_{11}}(N_1^{\,i},N_2^{\,i}) = \frac{cN_1^{\,i}\,\ell n\,(N_1^{\,o}/N_1^{\,i})}{(1 + cN_2^{\,i})\ell n(1 + cN_2^{\,i})} \quad . \tag{83}$$

The time required for a finite layer couple to come to transient equilibrium may be estimated from the following expression (simplified from

---

*It is usually found that on-diagonal D's approach constant values for dilute solutions. Off-diagonal D's, however, show a sensitive concentration dependence[66], since they must vanish with the appropriate concentrations. For example, in the equation for the flux of component 1,

$$J_1 = - D_{11}\frac{\partial C_1}{\partial x} - D_{12}\frac{\partial C_2}{\partial x} \quad ,$$

J_1 must vanish as $C_1 \rightarrow 0$. Therefore $D_{12} \rightarrow 0$ as $C_1 \rightarrow 0$.

a solution for heat flow in plates of similar thickness)[67]:

$$(84) \qquad \frac{C}{C_o} = \frac{d_1}{d_1 + d_2} + \frac{2}{\pi} \sum_{n=1}^{\infty} \frac{e}{n} - \left\{\left(\frac{n\pi}{d_1 + d_2}\right)^2 Dt\right\} \sin\left\{\frac{n\pi d_1}{d_1 + d_2}\right\}$$

where C is the surface concentration at time t, C_o is the initial (uniform) concentration in the outside plate (width d_1), and d_2 is the width of the inside (originally void of solute) layer.

Considering one half of a symmetrical layer couple of the type shown in figure 8, $\left(d_2 = 1/2 d_1\right)$, numerical evaluation of (84) indicates that the surface concentration will be within one percent of its ultimate value when $t = \frac{d_1^2}{D}$, and that it will be substantially constant (within 0·01%) after a time $t = 2 \frac{d_1^2}{D}$

(f) Application of the Diffusion Formalism to Phase Transformations

In this section, extensive use will be made of the "principle of local equilibrium" which may be stated as follows[68]: "For most irreversible processes involving moderate gradients, it will generally be true that the change in an intensive variable (T, P, μ) within one mean free path will be negligible compared with the magnitude of the variable at that point." The region in which this statement is valid is the realm of application of the thermodynamics of irreversible processes.

When the above postulate is applied in transformation theory (in particular, to a volume element containing the interface in an isothermal multi-phase system) it allows the specification of equilibrium interfacial concentrations, as given by the constitution diagram*.

The assumption of equilibrium interface conditions is at best a good approximation, since there must always be some free energy difference across the interface if the boundary is to migrate. Kirkaldy[49] has pointed out that this deviation from local equilibrium is most likely to affect experimental findings near the time origin, although, in many cases, the variations should be negligible from the point of view of measured macroscopic variables.

Boltzmann[69] first showed that unique solutions of equation (3)

---

*If the interface is non-planar,[68] a knowledge of the variation of equilibria with surface tension is required, since, if the system is to be in local mechanical equilibrium, the resolved stress due to surface tension must be balanced by pressure in the enclosed material.

of the form

(85) $$C = C(\lambda),\ \lambda = x/\sqrt{t},$$

exist, provided that the boundary conditions can be expressed in terms of λ (i.e. the semi-infinite boundary conditions). Kirkaldy[70], and Gosting and Fujita[71] have extended this statement to the general case (equations 6a). For a ternary system, equations 76 and 77 have solutions of the parametric $(x/\sqrt{t})$ class, which satisfy the ordinary equations

(86) $$-\frac{\lambda}{2}\frac{dC_1}{d\lambda} = \frac{d}{d\lambda}\left(D_{11}\frac{dC_1}{d\lambda}\right) + \frac{d}{d\lambda}\left(D_{12}\frac{dC_2}{d\lambda}\right)$$

and

(87) $$-\frac{\lambda}{2}\frac{dC_2}{d\lambda} = \frac{d}{d\lambda}\left(D_{21}\frac{dC_1}{d\lambda}\right) + \frac{d}{d\lambda}\left(D_{22}\frac{dC_2}{d\lambda}\right).$$

Any point of constant composition in the diffusion zone of a semi-infinite configuration must, according to the above statements, move with a $\sqrt{t}$ dependence. If the compositions on either side of a phase boundary are constant, the boundary will move according to a parabolic law. Accordingly, the observation of a parabolic growth rate suggests strongly that volume diffusion controls the growth process. If, further, the observed growth rates can be reconciled with independently determined diffusion data, diffusion control may be considered proven.

Exceptions to diffusion control of phase transformations are to be expected when the daughter and parent phases have the same composition throughout, or when a low mobility (coherent or semi-coherent) interface separates the two phases (in which case, chemical reaction may control the transformation[68]). If, however, the interface is of the random, or incoherent, type, a high mobility is to be expected, since

atoms are presumably transferred, more or less independently, across an amorphous boundary layer separating the two structures. (A striking example of the potential mobility of an incoherent interface may be found in the "massive" transformations[72], where interface velocities approaching those involved in martensitic transformations are observed).

(g) Ferrite Growth in Binary Iron-Carbon Austenite

Wagner[73] originally produced the appropriate solution of (3) for the velocity of a planar phase interface in a binary two-phase diffusion couple. The parametric solution, obtained by solving for the interface velocity using two simultaneous mass balances for the diffusing substance on either side of the interface is:

$$(88)\quad \alpha = 2\left[\frac{(C_1^I - C_e^I)}{(C_e^I - C_e^{II})}\sqrt{\frac{D_I}{\pi}}\,\frac{e^{-\frac{\alpha^2}{4D_I}}}{1+\operatorname{erf}\frac{\alpha}{2\sqrt{D_I}}} - \frac{(C_e^{II} - C_2^{II})}{(C_e^I - C_e^{II})}\sqrt{\frac{D_{II}}{\pi}}\,\frac{e^{-\frac{\alpha^2}{4D_{II}}}}{1-\operatorname{erf}\frac{\alpha}{2\sqrt{D_{II}}}}\right]$$

where α is the position of the interface in λ-space, C_e^I and C_e^{II} are the equilibrium interfacial concentrations in phases I and II, C_1^I and C_2^{II} are the initial bulk concentrations in phases I and II, and D_I and D_{II} are diffusion coefficients (assumed constant). This expression will be valid as long as the semi-infinite boundary conditions are applicable.

An approximate form of (88), which should apply to the initial stages of thickening of ferrite allotriomorphs is obtained by setting $C_1^I - C_e^{II} = 0$ (see figure 2):

$$(89)\qquad \alpha = 2\,\frac{C_e^{II} - C_2^{II}}{C_e^{II} - C_e^I}\sqrt{\frac{D_{II}}{\pi}}\,\frac{e^{-\frac{\alpha^2}{4D_{II}}}}{1-\operatorname{erf}\frac{\alpha}{2\sqrt{D_{II}}}}$$

where ferrite is phase I, and austenite is phase II.

If a diffusion couple, consisting of homogeneous layers of ferrite and austenite in equilibrium, is quenched up to a higher temperature (below 911°C), the austenite layer will grow at the expense of the ferrite layer. In this case, the appropriate form of (88) is

$$\alpha = 2 \frac{c_2^{II} - c_e^{II}}{c_e^{II} - c_e^{I}} \sqrt{\frac{D_{II}}{\pi}} \frac{e^{-\frac{\alpha^2}{4D_{II}}}}{1 + \operatorname{erf} \frac{\alpha}{2\sqrt{D_{II}}}} \cdot \tag{90}$$

(h) Ferrite Growth in Ternary Austenites

This section is based on Kirkaldy's analysis of the multi-component growth problem[74]. Popov[75] used a similar approach to growth in ternary austenites, but neglected possible coupling of the diffusive fluxes (as specified by the off-diagonal elements of the D-matrix). Here, interest will be centered upon the motion of planar phase interfaces in ternary austenites. The required parametric solutions of (6a) for constant coefficients, subject to the boundary conditions at infinity and at the interface, $\lambda = \alpha$,

(91) $$C_i(\lambda = \infty) = C_{i0},\ C_i(\lambda = \alpha+) = C_{i1},\ C_i(\lambda = \alpha-) = C_{i2},\ (i = 1,2)$$

are

(92) $$C_1 = a_{10} + \frac{d_{11}}{I_1} \int_{\lambda}^{\infty} e^{-(\lambda^2/4u_1)}\, d\lambda + \frac{d_{12}}{I_2} \int_{\lambda}^{\infty} e^{-(\lambda^2/4u_2)}\, d\lambda ,$$

and

(93) $$C_2 = a_{20} + \frac{d_{21}}{I_1} \int_{\lambda}^{\infty} e^{-(\lambda^2/4u_1)}\, d\lambda + \frac{d_{22}}{I_2} \int_{\lambda}^{\infty} e^{-(\lambda^2/4u_2)}\, d\lambda ,$$

where $$I_k = \int_{\alpha}^{\infty} e^{-(\lambda^2/4u_k)}\, d\lambda .$$

The coefficients take the values

$$a_{10} = C_{10},\quad a_{20} = C_{20},$$

$$d_{11} = \left\{ D_{12}(C_{21} - C_{20}) + \left[(D_{11} - D_{22}) + D\right](C_{11} - C_{10})/2 \right\} / D$$

$$d_{21} = \left\{ D_{21}(C_{11} - C_{10}) - \left[(D_{11} - D_{22}) - D\right](C_{21} - C_{20})/2 \right\} / D$$

$$d_{12} = C_{11} - C_{10} - d_{11},\quad d_{22} = C_{21} - C_{20} - d_{21},$$

$$D = \sqrt{(D_{11} - D_{22})^2 + 4D_{12}D_{21}}$$

$$u_1 = (D_{11} + D_{22} + D)/2,\quad u_2 = (D_{11} + D_{22} - D)/2.$$

The flux continuity equations are

$$(C_{i2} - C_{i1})v = - J_i(\alpha) \tag{94}$$

where the J_i are given by equations (26) and (27), and the interface velocity is

$$v = \frac{\alpha}{2\sqrt{t}} \quad . \tag{95}$$

The basis of the problem is that, in general, the two independent diffusing species will move at different rates. If, as in the binary case, the interfacial concentrations were fixed, no solutions would exist, since the two flux balances would yield two different interface velocities. There is, however, a degree of freedom afforded by the indeterminate tie-line (in the two-phase region) between the interfacial concentrations. (i.e. Local equilibrium can obtain at the termini of any tie-line).

When, as is usual in ternary austenites, the diffusion coefficient of the substitutional alloying element (D_{22}) is much smaller than that of carbon (D_{11}) the mass balance may demand that a diffusion solution exist such that the daughter phase has approximately the same substitutional component concentration as the bulk parent phase. Equivalently, component 2 must not partition. The introduction of this as an approximation from the start allows the "a priori" specification of a tie-line upon which to base growth rate calculations, thus significantly simplifying the calculations. The preceding considerations may be illustrated by referring to the approximate isothermal section of the Fe-C-Mn phase diagram in figure 9. If a homogeneous austenite of composition A is quenched to the temperature of interest, then, once ferrite nucleates, the interfacial concentrations will be given by the equilibrium tie-line (BD) between ferrite of composition B and the austenite

phase field. Schematic penetration curves are shown in figure 10 (to be compared with that for a binary iron-carbon austenite of similar carbon content). It is apparent that manganese additions have two possible effects on ferrite growth kinetics. One is a constitutional effect: the carbon potential (ΔC in figures 9 and 10) is drastically reduced; the other effect is due to off-diagonal interactions as measured by D_{12}, D_{21}.

In the case of Fe-C-Mn, where $D_{11} \cong 10^7 D_{22}$, and D_{21} can probably be assumed negligible in comparison with D_{12}, D_{11}, the flux balance equations (94), on combination with (92) and (93), yield an approximate expression for the growth parameter $\beta = \frac{\alpha}{2\sqrt{D_{11}}}$,

$$\beta = \frac{\Delta C}{2C_{11}} \left(1 + \frac{D_{12}}{D_{11}} \frac{\Delta Mn}{\Delta C}\right) \frac{e^{-\beta^2}}{\int_{\beta}^{\infty} e^{-u^2} du} \tag{96}$$

where $\Delta C = C_{11} - C_{10}$ and $\Delta Mn = C_{21} - C_{20}$.

For $\beta \ll 1$,

$$\beta = \frac{2}{\sqrt{\pi}} \frac{\Delta C}{2C_{11}} \left(1 + \frac{D_{12}}{D_{11}} \frac{\Delta Mn}{\Delta C}\right) \frac{(1 - \beta^2)}{(1 - \frac{2}{\sqrt{\pi}} \beta)} \tag{97}$$

$$\cong \frac{2}{\sqrt{\pi}} \frac{\Delta C}{2C_{11}} \left(1 + \frac{D_{12}}{D_{11}} \frac{\Delta Mn}{\Delta C}\right). \tag{98}$$

(Standard approximations have been used for the exponential and integral in (96)).

The condition for zero growth rate is found by setting $\beta = 0$ in (96) to obtain

$$\frac{D_{12}}{D_{11}} = - \frac{\Delta C}{\Delta Mn} \tag{99}$$

The above considerations indicate that transformations in some supersaturated Fe-C-Mn austenites can be analysed by extensions of the methods employed in binary transformation theory. There is, however, a class of transforming systems which cannot be so analysed, because, for these alloy constitutions, there is no equilibrium tie-line which allows a finite rate of growth with negligible manganese partition.

Referring to figure 9, it is apparent that there is no tie-line which would allow negligible manganese partition for alloys containing more than 2·5% manganese (the approximate solubility of manganese in α-iron at the temperatures of interest). Therefore, if manganese were to come to local equilibrium in such an alloy, the transformation would proceed extremely slowly, being forced to wait for the redistribution of manganese. A further restriction on the system is that, for solutions of type (92) and (93) to be applicable, the carbon potential, ΔC, must be greater than $-\Delta Mn \frac{D_{12}}{D_{11}}$. (cf. equation 99). Smaller values of ΔC would result in negative growth rates in a supersaturated alloy. Clearly, there is no composition in the region shown hatched in figure 9 which is not subject to one of these restrictions. (For purposes of illustration, D_{12} has been assumed much less than D_{11}).

To accommodate the possibility that ferrite forms rapidly by a diffusion-controlled mechanism in such alloys, it will be postulated that the high mobility interstitial component, carbon, is in local equilibrium, but that the low mobility substitutional components, iron and manganese, are not. A similar postulate has been made by Hillert[76] in his treatment of grain growth in binary austenite. This condition will be called "constrained local equilibrium".[77]

The consequences of such a postulate may be investigated with the aid of the generating (isothermal) free energy surfaces implied by the ternary phase diagram[78] (figure 11). Here, the variation of the free energy of mixing, F^*, with concentration is shown schematically. The F^* surfaces are analogous to the binary free energy curves commonly used to demonstrate the thermodynamic origin of binary phase diagrams[6]. The lowest free energy of a phase mixture is assumed to be a weighted average of the bulk free energies of the respective phases (i.e. the effects of surface tension are neglected). The chemical potentials of the three components in a phase are given, respectively, by the intercepts of a plane, tangent to the free energy surface (at the appropriate composition) with the three F^* axes[6]. The surfaces must meet the binary F^* curves with infinite tangents, so that zero third component concentration shall correspond to zero third component activity.

The two-phase field of an equilibrium diagram may be generated by rolling a doubly tangent plane about the surfaces corresponding to the two phases, and projecting the points of tangency onto the composition plane. Equilibrium tie-lines are projections of the lines (in the doubly tangent plane) that connect the points of tangency.

A tie-line describing the constrained equilibrium between ferrite and austenite may be constructed in the following way: A plane is constructed tangent to the α surface at the ferrite composition, A, and the intercept on the F^* carbon axis (μ_c) is noted. A line is then constructed from point A, tangent to the γ surface at a point, B, such that a plane, tangent to the γ surface at B intersects the F^* carbon axis at μ_c. The "constrained" tie-line (A'B') is a

projection of this line onto the composition plane. Thus, the equality of μ_c in the α and γ phases is assured, and the phase mixture has a minimum free energy consistent with the constraints.

The "constrained" phase boundary will differ from the equilibrium phase boundary (as shown in figure 11). It must be closer to the ferrite phase field, since the starting point of the tangent line (point A) will correspond to a higher free energy than will the α tangent point of the equilibrium tangent plane. It is expected that, in analogy with the small difference between the γ phase boundaries in the binary Fe-Fe_3C and Fe-C systems[6], the constrained phase boundary will differ but little from the equilibrium phase boundary.

The chemical potential of carbon must change rapidly with carbon concentration as point A is varied along a line of constant manganese concentration in the α surface. A small change in the position of point A may cause a considerable change in the direction of the constrained tie-line, depending on the particular geometry of the F^* surfaces. Thus, the assumed requirement that the non-equilibrium ferrite have a low carbon content is not sufficient to uniquely define the tie-line direction. The system therefore will contain a degree of freedom - it must choose from an infinite number of constrained tie-lines, there being no obvious thermodynamic or kinetic requirement to influence the choice.

Kirkaldy[79] has developed a variational principle applicable to non-steady-state processes, which may be stated:

$$\delta \int_{\text{volume}} \left[2 \sum_i J_i X_i - \sum_{i,k} L_{ik} X_i X_k \right] dV = 0 \qquad (100)$$

where the rate of entropy production

$$\sigma = \sum_{i,k} L_{ik} X_i X_k = \sum_i J_i X_i \ .$$

The variation is to be carried out subject to the artificial constraint on the flux, J_i = constant, and the integral is expected to attain a maximum at the optimum.

The application of this principle is expected to remove the degree of freedom mentioned above, and to allow the specification of a constrained tie-line for any given boundary condition.

III DETERMINATION OF DIFFUSION COEFFICIENTS

(a) Experimental

i) Alloys

The high-purity iron-carbon alloys used in this investigation were supplied by the Ford Motor Research Laboratories, Dearborn, Michigan, through the good offices of Dr. H. I. Aaronson. The major impurities were stated to be <0.007 wt% Si and <0.002 wt% Mn.

The iron-silicon and iron-manganese alloys were prepared in the crucible-mold arrangement shown in figure 12, which was designed to adapt a Stokes vacuum melting unit to bottom pouring. Gassy refractories were avoided in the construction of the apparatus, thereby enabling the attainment of a pressure of $\sim 10^{-3}$ torr. during the entire melting and casting cycle. 1000 gram charges (a) of electrolytic iron (see table II) and alloying elements (99.9% Mn or Si) were induction heated (b). The crucible (c) of recrystallized alumina, was supported and insulated with "pyrophyllite" (d) and zirconia powder (e). The temperature was measured with a platinum vs. platinum-10% rhodium thermocouple (f) located in a hollow alumina stopper (g). The stopper was manipulated by means of a steel rod (h), which entered the vacuum chamber through a Wilson seal. After melting, the charge was chill cast into a 1¾ inch diameter steel mold (i). The iron-silicon alloy was cast in vacuum. Before melting the iron-manganese alloy, the chamber was backfilled with argon (to approximately 200 torr.) to reduce manganese evaporation. These techniques produced sound ingots, which were judged clean, superficially as

well as metallographically.

The ingots were heated in a charcoal bed, and hot forged to 1 1/4 inch diameter, then homogenized for one week in argon at 1050°C, and turned to 1" diameter. The resulting bars were cut into thin discs with an abrasive wheel, and the manganese or silicon content of each disc determined by X-ray fluorescence spectroscopy. This comparison revealed no longitudinal macroscopic segregation. The chemical analyses for both ingots are reported in table II.

ii) The Diffusion Anneals

The alloy discs, together with similar iron-carbon discs, were surface-ground to produce accurately parallel plates, approximately 0·025, 0·035, or 0·045 inches thick (depending on the intended annealing temperature). The plates were cleaned, then clamped together to form three-layer finite diffusion couples of the type described in section IIe. The couples, separated by thin pyrophyllite discs, were welded and annealed in the vacuum furnace shown in figure 13.

The inconel furnace tube was heated by a Kanthal resistance element which, in turn, was controlled by a proportioning temperature controller. The ends of the furnace tube, as well as a manifold, were water cooled. The couples were manipulated in the furnace using an inconel push-rod, which contained a platinum vs. platinum-10% rhodium thermocouple. The thermocouple was subsequently compared with a standard furnished by the National Research Council, Ottawa. The furnace tube was evacuable by means of a diffusion pump. A system of vacuum valves provided for the admission of any desired furnace atmosphere. The uniform hot zone (± 1°C) was found to be 3 inches in

length at 850°C and 1000°C.

Welding was effected by heating the clamped couples to 1050°C for 6 hours in an atmosphere of catalytically purified hydrogen, after outgassing in $\sim 10^{-5}$ torr. at 400°C. The clamp (figure 13), made of molybdenum and type 316 stainless steel, was designed to apply pressure during the welding treatment by means of differential thermal expansion.

The diffusion anneals were carried out in a positive gauge pressure of argon at various temperatures (controlled to $\pm$ 2°C) in the austenite range. The temperature was continuously recorded with a chart recorder connected to the measuring thermocouple. One Fe-C-Si couple was annealed for a time $1 \cdot 7\ d_1^2/D_{11}$, and another for $28\ d_1^2/D_{11}$. The others were annealed for $7\ d_1^2/D_{11}$ (see section IIe). The couples were quenched (100°C/min) from temperature to avoid any solute segregation at the transformation temperatures[80]. The quench was effected by pushing the couples into the cooling manifold, and rapidly passing argon through the furnace.

iii) Analyses

The couples were sectioned by clamping in a lathe collet, and collecting turnings from the center 0.015 inches of each layer. The sampling was confined to within a 0.75 inch radius to minimize any edge effects.

The samples were analyzed using a modification of the micro-analytic technique of Frazer and Holzmann[81]. The apparatus, shown in figure 14, consists of a constant pressure oxygen supply, an oxygen purification train, a furnace (1200°C) for oxidizing the sample (5-30 mg of steel), a liquid air trap, and a capillary manometer

(1·60 mm. bore) for determining the volume of CO_2 produced. The trap volume (between stopcocks and etched line) and the manometer bore were determined using mercury as the calibrating fluid.

Frequent blanks, and standards (supplied by the National Bureau of Standards, Washington, D.C.), analysed during the course of the diffusion couple analyses, served as a check on the absolute accuracy of the method.

A complete penetration curve was determined for one half of one diffusion couple (Fe-C-Si at 1058°C). To ensure that the sections were taken parallel to the plane of the weld, the couple was aligned in the collet before each cut, using a dial gauge sensitive to variations of 0,0001 inches. The silicon concentrations were determined by vacuum x-ray fluorescence spectroscopy*, after calibrating the spectroscope with iron-base alloys of known silicon content.

---

*These analyses were carried out by counting (10^4 counts) on Si $K\alpha_1$ radiation (λ = 7·12Å), which is so readily absorbed by an iron matrix that its intensity is decreased to ~1% of its initial value after passing through ~ 2 microns of iron. Therefore, any silicon concentrations determined in this way are effectively surface concentrations.

(b) Results and Discussion

The experimental penetration curve shown in figure 15 and the macrograph of figure 16 clearly demonstrate the principle of the state of "transient equilibrium". While the slowly diffusing silicon effectively looks at an infinite medium, the fast diffusing carbon rapidly adjusts its distribution to that of the almost static silicon, and thereafter remains substantially invariant. An experimental determination of D_{12}/D_{11} accordingly requires only two carbon concentration measurements, one near the center of the couple, and one in an outer layer.

The results of measurements designed to determine the concentration and temperature dependence of $D_{12}/D_{11}(N_1^i, N_2^i)$ are summarized in table III. Each reported value of N_1^i or N_1^o represents the average of at least six independent determinations (R.M.S. errors* are shown). Values of D_{12}/D_{11}, calculated using equation (83), are included in table III. The errors in D_{12}/D_{11} were calculated from the errors in N_1^i, N_1^o, with the aid of approximation (75). The rather large experimental errors in the calculated D_{12}/D_{11} ratios are the result of relatively small errors in N_1^i and N_1^o ($\sim$1%), since the ratio of coefficients is sensitive to the difference $(N_1^o - N_1^i)$, which is small compared with the values of N_1^o and N_1^i.

The interstitial concentration dependence of the ratio D_{12}/D_{11}

*In this and following sections, the statistical methods suggested by Davies[82] are employed. Errors shown are $\pm$ twice the standard deviation of the mean.

is shown graphically in figure 17 (where the numbers on the points refer to the couple designations in table III). The point corresponding to couple No.4 has been adjusted slightly for silicon concentration, assuming the substitutional concentration dependence of equation (80). The close agreement of the results from couples 4 and 6 with those from the other Fe-C-Si couples indicates that the diffusion times chosen were more than sufficient to attain the "transient equilibrium" state.

In both sets of couples, the experimental results are in fair accord with the thermodynamic prediction of equation 82, which in turn rests on approximation 42. It therefore appears that the neglect of L_{12} in comparison with L_{11} is a valid approximation in the systems Fe-C-Si and Fe-C-Mn, so that D_{12} is related to D_{11} in a purely thermodynamic manner. In such a case, the value of D_{12} may be obtained from ternary activity data and a knowledge of the on-diagonal diffusion coefficients.

While the agreement between experimental and predicted values for D_{12} is satisfactory, there is a significant deviation in the case of Fe-C-Mn, (accepting Smith's results for the present), indicating that the off-diagonal L's are non-zero. This conclusion may be assessed by solving for $\frac{L_{12}}{L_{11}}$ from equation 41, assuming that N_1, $N_2 \ll N_3$ and that $\frac{D_{12}}{D_{11}} = k' N_1$ (where k' takes the [empirical] experimental value of ~ -3 for $N_2 = 0.0316$),

$$\frac{L_{12}}{L_{11}} = N_2 \left[k'(1 + b\ N_1) - \frac{c}{1 + cN_2} \right] \tag{101}$$

The μ_{ik} have been evaluated from the empirical expansions for the

activities, (61) and (62). If L_{12} is set equal to zero, (101) reduces to (81). Solving numerically for L_{12}/L_{11} indicates that the ratio $\longrightarrow 0.05$ as $N_1 \longrightarrow 0$ (N_2 constant), and that the ratio is relatively insensitive to N_1.

It is possible that, although L_{12} (and therefore L_{21}) is small compared with L_{11}, it is large compared with L_{22}. The consequences of this possibility will now be investigated.

In the dilute solution approximation, D_{21}/D_{22} may be written in the same manner as (41) i.e.,

$$\frac{D_{21}}{D_{22}} = \frac{L_{21}\mu_{11} + L_{22}\mu_{21}}{L_{21}\mu_{12} + L_{22}\mu_{22}} \cong \frac{L_{21}/N_1 + cL_{22}}{cL_{21} + L_{22}/N_2} \quad , \tag{102}$$

where the μ_{ik} have again been evaluated from (61) and (62). If $L_{21} \ll L_{22}$, equation (43) is obtained. In the event that $L_{21} \gg L_{22}$, the ratio of coefficients becomes

$$\frac{D_{21}}{D_{22}} = \frac{1}{cN_1} \quad , \tag{103}$$

which gives the theoretical maximum value of the ratio. Because L_{21} must go to zero with N_1, (103) is not expected to apply as N_1 goes to zero. Comparing (103) with (43) it is apparent that the most sensitive test for L_{21} (and L_{12}) would be a determination of the interstitial and substitutional concentration dependence of D_{21}.

The most promising type of experiment to determine D_{21} would be the use of a steady-state configuration in which a carbon gradient is maintained in, say, an iron-manganese plate. However, since $D_{21} \ll D_{11}$, the time required to perform a significant experiment would appear to be prohibitive. While the fact that $D_{21} \ll D_{11}$ makes measurement

difficult, it should be emphasized that this fact also decreases the desirability of such a measurement, since D_{21} and D_{22} can usually be set equal to zero without significantly altering concentration distributions. (cf. equation 96).

It should perhaps be pointed out that Smith's experiments[15,16] to determine the ternary activities were subject to the same sort of errors as are the "transient equilibrium" measurements reported here. In both experiments, the carbon content of a ternary austenite was compared with that of a binary austenite, and the difference in carbon contents, rather than their absolute values, is significant. Because Smith compared ternary alloys with binary standards, it is unlikely that the use of CH_4-H_2 mixtures rather than the favoured CO-CO_2 mixtures would significantly affect the results (i.e. the value of the coefficient "c", which enters so prominently into the expression for D_{12}/D_{11} (81)).

The results of the temperature-dependence investigation are plotted in figure 18. The data from couples 1,2,8,10, and 11,12,13,17 have been normalized to the same carbon content for purposes of comparison. The temperature dependence is very weak in both cases, indicating that D_{12} and D_{11} have similar Arrhenius factors, and are determined by the same activated rate process.

The thermodynamic approximation predicts no temperature dependence since according to Smith, the activities are independent of temperature. There is no general indication of the $\frac{1}{T}$ dependence suggested by the statistical theory, but, then, there is no reason why the ϵ's should be independent of temperature.

The only previous determination of D_{12} in ternary austenites, Kirkaldy's analysis[59] of Darken's experiment[3], yielded

$$\frac{D_{12}}{D_{11}} (N_1 = 0{\cdot}0206,\ N_2 = 0{\cdot}0369) = 0{\cdot}166$$

which may be compared with the "transient equilibrium" value,

$$\frac{D_{12}}{D_{11}} (N_1 = 0{\cdot}0206,\ N_2 = 0{\cdot}0363) = 0{\cdot}162$$

In view of the large experimental and analytical errors of the two methods, this excellent agreement is perhaps fortuitous.

IV AN INVESTIGATION OF THE GROWTH OF PROEUTECTOID FERRITE IN BINARY AND TERNARY AUSTENITES

(a) Experimental

The determination of kinetics of the proeutectoid ferrite reaction (as previously pointed out) has often been hampered by difficulties inherent in studying growth rates "in situ". The small diffusion lengths, varying nucleation time, necessarily random metallographic sections, and the onset of complex morphological development all contribute to the experimental and analytical difficulties.

A study of the problem by means of macroscopic ferrite-austenite diffusion couples appeared feasible, and the following techniques were developed to measure rates of growth under controlled conditions.

(i) Alloys

The alloys used in this investigation were the same as those described in section II(a) with the exception of an iron-1·5% manganese alloy (see table II for analysis). This was prepared in non-consumable-electrode arc furnace under a helium atmosphere. The 200 gram button was turned and melted four times. The resulting ingot was cold rolled to 3/8 inch thickness, annealed for two weeks at 1050°C (in argon), then ground to 1/4 inch and rolled to 0·040 inch sheet.

The iron-manganese alloys were carburized to desired carbon contents in CO-CO_2 mixtures with constant CO-CO_2 ratios, using an apparatus constructed by Brigham[83]. The samples, in the form of rolled

sheet, were carburized at 1000°C for a time such that $\left(\frac{D_{11}t}{\ell^2}\right) > 2.5$, ($\ell$ is the half-thickness of the sample). This equilibration time was sufficient to ensure the uniformity of carbon in the alloys[6]. The samples were then rapidly cooled to room temperature, and analysed for carbon.

(ii) The Binary Iron-Carbon System

A direct study of ferrite growth in supersaturated high-purity austenite was not attempted, since nucleation ahead of an advancing interface would immediately produce competing diffusion fields, and terminate the interface motion. Instead, the reverse reaction, the growth of austenite at the expense of ferrite, was investigated.

A diffusion couple with reasonably planar phase interfaces was produced in the following way:

A 0.035 inch thick disc, (1" diameter) of high purity Fe - 0·567 wt% C martensite was suspended from a fine tungsten wire in the quenching furnace shown in figure 19. The power supply and temperature controller were the same as those used for the vacuum furnace, (figure 13). The furnace was evacuated and wet hydrogen admitted. The furnace temperature was raised to 920°C, and the sample lowered into the hot zone. After 10 minutes in the decarburizing atmosphere, the hydrogen was replaced by argon, and the furnace was slowly cooled (~2°C/min) to 755°C, the temperature at which ferrite is in equilibrium with austenite containing 0·567 wt% C. Nucleation of ferrite presumably occurred at the surface as soon as the temperature passed the pure iron transition point at 911°C, and the ferrite grew inward, rejecting carbon

to the austenite, as the temperature was lowered further. The sample was equilibrated in argon at 755°C for 36 hours $\left(\frac{Dt}{\ell^2} = 2{\cdot}5\right)$, a time calculated to ensure that the austenite and ferrite were of uniform composition. The sample was quenched to martensite by dropping into the pool of mercury in the bottom of the furnace tube. The resulting diffusion couple was similar to that shown in the macrograph of figure 20.

The thickness of the ferrite layer was measured metallographically (2 sections at right angles) using a filar eyepiece calibrated with a stage micrometer. The magnification was 160X. 23 measurements were made on each side at regular intervals of 0·03 inches. Although the thickness did not vary appreciably from one measurement to the next, the phase boundary on one side (side II) was curved (0·001 inches variation from center to edge), while that on the other side (sideI) was relatively planar (within $\sim$ 0·0002 inches).

The diffusion anneals were carried out in lead pots (figure 21). The temperatures were controlled ($\pm$ 1°C) by proportioning controllers, and frequently measured during the course of the anneals using chromel-alumel thermocouples, (which were compared with an NRC standard). A thermocouple in the center of a dummy diffusion couple was up-quenched to 800°C, and required approximately 15 seconds to come to within 2°C of its final temperature.

The diffusion couple was up-quenched to 792°C $\pm$ 1°C, held for 5 minutes at temperature, then quenched in brine. 0·020 inches was ground from the edge, and the thickness of the ferrite layer again determined metallographically. This procedure was repeated for total

diffusion times of 15, 30 and 45 minutes. Before the calculated time required for impingement of the opposite diffusion fields had elapsed, the diffusion anneal was terminated, and the couple was sectioned in the same way as the Fe-C-Si couple of figure 15.

(iii) The Iron-Carbon Manganese System

A direct study of the growth of ferrite in the ternary Fe-C-Mn system was made possible by the delay of ferrite nucleation caused by the presence of manganese as an alloying element. Martensitic samples containing 3·16 or 1·52 wt% manganese and various amounts of carbon were hand ground (wet) from 0·040 inches thickness to 0·025 inches, polished, then plated with a thin layer of iron in a standard electroplating bath*.

The diffusion anneals were carried out in the lead baths at various temperatures within the $\alpha + \gamma$ region of the ternary phase diagram. It was found that the plated iron acted as a nucleating agent for ferrite, and that, once the diffusion temperature was reached, the ferrite grew toward the center of the sample with an approximately planar interface. The original interface was delineated by a series of pores (as shown in figure 22(a)) which apparently resulted from imperfect cleaning of the sample surface prior to plating.

In the case of the alloys containing 1·52% manganese, it was necessary to precede the actual diffusion anneals by austenitization treatments of one minute at 815°C (0·405 and 0·328 wt%C) or one-half minute at 825°C (0·210 wt%C). This treatment produced no detectable

---

*The bath contained 300 grams $FeC\ell_2.H_2O$ and 250 grams $CaC\ell_2$ per litre of water.

change in the position of the interface, and was evidently sufficient to transform the martensite to homogeneous austenite. One diffusion couple was annealed for each time at temperature, then quenched in brine. The average time required for a dummy sample containing a thermocouple to come to within 2°C of the reaction bath temperature (after transfer from the high temperature bath) was nine seconds. This time was subtracted from the total time in the low temperature bath to obtain the isothermal reaction time (t). The distance from the original interface position to the interface, (x') was evaluated metallographically. Ten to twenty measurements were taken for each couple, using a calibrated filar eyepiece and an oil immersion objective lens, (approximate magnification:1400X).

The alloy containing ·282 wt% carbon and 3·16 wt% manganese required no preliminary treatment in the austenite range, so that the couples could be quenched directly up to diffusion temperature, held for the required times, then quenched. One couple was used for each temperature, the diffusion anneal being interrupted whenever a measurement was desired, and then resumed by re-heating to the temperature of interest. One duplicate sample was reacted at 733°C, to test the reproducibility of the results.

As a measure of the carbon concentration profiles in advance of the interface, microhardness traverses were obtained for two couples (0·282 wt% C, 3·16 wt% Mn at 742 and 733°C) using a Reichert microhardness tester (32 gram load). Figure 22(b) shows a number of indentations made in the region of the interface.

In each series designed to determine a growth rate, the approximate time required for ferrite nucleation in the center of the couple

was noted.

The zero growth rate temperature was determined for the 0.282% C 3.16% Mn and the 0.405%C, 1.52%Mn alloys by finding the lowest temperature at which the ferrite-austenite boundary was immobile for times up to 20 minutes.

(b) Results and Discussion

(i) The Binary Fe-C System

The results of the metallographic measurements on the binary diffusion couple are shown in figure 23, where x', the mean distance of the interface from its original position is plotted against $(\text{time})^{1/2}$. Rms. errors ($\pm 2\sigma_M$) are shown for points corresponding to the more planar side (side I) while those points from side II serve as check points. The discrepancies are thought to be due to the fact that the variation of the initial position of the side II boundary with depth was not precisely known.

No deviation from parabolic behaviour is evident (within the experimental error), indicating that the rate of interface migration is volume diffusion controlled. This conclusion is further supported by the close agreement between the calculated rate ($\alpha = 73{\cdot}2 \times 10^{-6}$ cm/$\sqrt{\text{sec.}}$, calculated using equation (90), equilibrium data from figure 2, and a value of D_{11} from reference 10) and the experimental value ($\alpha = 71 \times 10^{-6} \pm 5 \times 10^{-6}$ cm/$\sqrt{\text{sec.}}$, calculated from the growth rate data from side I).

The experimental penetration curve (concentration vs. average distance from the final interface position) is shown in figure 24. An error function has been fitted to the pentration data in figure 25, and extrapolated to the interface concentration. The value so obtained is 0·36 wt% C, in satisfactory agreement with the equilibrium austenite composition of 0·350 wt% C obtained from the Fe-Fe_3C constitutional diagram.

The observed parabolic growth law, and the agreement with established diffusion and equilibrium data are considered to provide

the strongest evidence yet presented for the volume diffusion control of the proeutectoid ferrite reaction. Consequently, the postulate that local equilibrium prevails throughout the diffusing system is also validated.

As previously noted, the growth of austenite at the expense of ferrite, rather than the more usual ferrite growth reaction, was chosen for study. The results, however, apply equally well to the growth of an incoherent ferrite interface into austenite, since, by the principle of detailed balance[51], any reaction proceeding in the environs of equilibrium must proceed by the same mechanism in both the forward and backward directions.

(ii) The Ternary Fe-C-Mn System

The growth results are summarized in table IV, and shown graphically in figures 26 through 29. The microhardness traverses are shown in figure 30.

Since these experiments were performed using diffusion couples in which the austenite was supersaturated, nucleation of ferrite ahead of the interface inevitably terminated the time wherein the semi-infinite boundary conditions were valid. Usually, however, the ferrite precipitated near the centerline of the sample, but not near the interface, (figure 22(b)) presumably because of carbon enrichment of the interface region. In some cases, parabolic behaviour was observed to persist for a significant time after the initial ferrite precipitate was detected.

During the determination of the zero growth rate temperature for the 1·52 wt% Mn, 0·405 wt% C alloy (760°C), it was observed that precipi-

tated ferrite formed at temperatures below 760°C was rapidly redissolved if the couple was heated above 760°C (in this case, to 761°C).

The check points determined for the 3·16 wt% Mn 0·282 wt% C alloy at 733°C are in good accord with the original points (figure 29) signifying that the results are satisfactorily reproducible.

This investigation was initiated with the object of testing the local equilibrium hypothesis (and its consequences, as outlined in sections IIf and IIh) in ternary Fe-C-Mn austenites. The diffusion data (section IIIb) and the appropriate diffusion solutions (section IIh) being available, no difficulty in analysing the results was anticipated. During the course of the investigation, the author became aware of the fact that, for some ternary constitutions and boundary conditions, local equilibrium diffusion solutions predict extremely slow growth rates - much slower than those experimentally observed. In such cases, the local equilibrium analysis must necessarily be abandoned. A similar development was anticipated by Kirkaldy[74], who suggested that, in cases where no diffusion solution exists, transformation occurs according to the laws of diffusion in an associated metastable system.

In retrospect, the results may best be discussed as the results of two investigations; one dealing with growth rates obtained for high degrees of supersaturation, where local equilibrium may be assumed, and one dealing with situations where such an assumption cannot be made.

1. The Case Where Local Equilibrium is Possible

The direct study of the proeutectoid growth reaction was facilitated by the delay in ferrite nucleation due to the presence of manganese. As the supersaturation was increased, ferrite nucleation occurred earlier,

so that it became increasingly difficult to obtain measurements. It was possible, however, to measure growth kinetics for a highly supersaturated 1·52 wt% Mn, 0·210 wt% C alloy at 735 and 725°C.

These results (figure 26) show the effects of ferrite nucleation ahead of the interface. Assuming that the deviations from parabolic behaviour are due to impingement, the growth rate (given by α), may be obtained by determining the slope of the X' vs. $\sqrt{t}$ plot at the origin. The value of α_{735} obtained in this way depends on two measurements, one obtained before the onset of ferrite precipitation. Since the two points are consistent with parabolic behaviour, this value was not influenced by subsequent ferrite precipitation. For α_{725}, the initial slope yields, at worst, a minimum value. However, because the first point on the 725°C curve was determined for a value of x' at which the 735°C curve is still parabolic, it is probable that the value obtained for α_{725} is accurate.

These rates are of particular interest in this discussion, since it is possible to use the temperature dependence of α to check the local equilibrium hypothesis.

It will be assumed that the ternary constitution diagram is known. (This point will be discussed further in the next section). Slight deviations from the constitution diagram of figure 4 will not significantly affect the following calculations. Consideration of the free energy surfaces of figure 11 leads to the conclusion that the equilibrium tie-lines should not change direction appreciably with temperature, since the surfaces should change relative position, rather than shape, for small temperature changes. Tie-lines must connect the

α and γ phase fields, and the solubility of manganese in α-iron is nearly independent of temperature between 650°C and 750°C[45]. The tie-lines are therefore not required to change direction in order that the binary and ternary constitution diagrams be consistent.

The measured growth rate at 735°C may be used as a basis for the calculation of an equilibrium tie-line. Substituting a value of D_{12}/D_{11} from section IIIB, and α_{735} (measured) into equation (96), and solving for the interface concentrations yields C_{21} = 5·1 wt% manganese and C_{11} = 0·29 wt% carbon. The resulting tie-line is shown in figure 31. The corresponding tie-line for 725°C may be found by projecting the 735°C tie-line to the 725°C phase boundary. The value of α_{725} calculated using this new tie-line is 16.5 x 10^{-6} cm/$\sqrt{\text{sec}}$., in good agreement with the measured value of 18 x 10^{-6} cm/$\sqrt{\text{sec}}$.

Since the 735°C calculation has been used to determine the equilibrium tie-line, (the first such determination reported in this system) it cannot be used as a strong test of the diffusion model. However, the agreement between prediction and the independent experiment at 725°C indicates that diffusing systems in this region of high supersaturation can be treated by the methods of section IIf, and therefore, that local equilibrium may be assumed throughout the diffusion zone.

The two inhibiting effects of manganese on ferrite formation, as introduced in section IIh, are illustrated by the following calculation. The measured growth rate parameter, α, for 735°C is 10·4 x 10^{-6} cm/$\sqrt{\text{sec}}$. If the effect of D_{12} is neglected (i.e. D_{12} is set equal to zero), the calculated value of α_{735} is 33 x 10^{-6} cm/$\sqrt{\text{sec}}$. Finally, if it is assumed that the alloy contains no manganese, α_{735} (from equation 89)

becomes 146 x 10^{-6} cm/$\sqrt{\text{sec}}$. For the particular constitution involved, the two effects abet one another, so that the total effect of manganese as an alloying element is to drastically reduce the rate of growth of ferrite.

The results of this section have a direct bearing on the understanding of the kinetics of the pearlite reaction. Pearlite usually forms in highly supersaturated austenite, where local equilibrium is most likely to obtain during growth. Kirkaldy[74] has shown, with the aid of Hultgren extrapolations[84] of the ternary phase boundaries, and calculations similar to the above, that the linear growth of carbide as well as ferrite in Fe-C-Mn is inhibited for purely constitutional reasons (i.e. D_{12} was set equal to zero). In both cases, the sign of D_{12} is such that the calculated growth rates will be further reduced if D_{12} is taken into consideration. The experimental and numerical results of this section, confirming the validity of the calculation for the simple proeutectoid ferrite reaction, lend a measure of confidence in attacking the pearlite problem by these methods.

2. The Case Where Interfacial Local Equilibrium Is Not Possible

According to the determination of the equilibrium tie-line reported in the preceding section, and the discussion in Section IIh, the majority of the Fe-C-Mn growth curves (including those shown in figures 27, 28, 29 and the 760°C curve of figure 26) were obtained at degrees of supersaturation where no local equilibrium diffusion solution admits of a transformation rate which is not infinitesimal, i.e. which is not controlled by manganese diffusion. The results for all ternary

compositions studied are summarized in figure 32, where the growth parameter, α, is plotted against temperature for each composition. In contrast to those for other compositions, the results for 0·210 wt% C, 1·5 wt% Mn show a discontinuity at approximately 735°C, further verifying that there are two types of transformation to be considered.

The growth curves of figures 27, 28 and 29 all clearly indicate parabolic behaviour. The results are reproducible, as demonstrated by the duplicate points in figure 29.

The microhardness traverses of figure 30 demonstrate that appreciable carbon gradients exist in the region of the interface. The calibration points available for this manganese concentration are not sufficient to justify an absolute correlation of hardness with carbon content. However, it is sufficient for the present purpose to show the extent of the gradients. Assuming that the hardness of martensite is linearly related to carbon concentration (over a small composition range) it is possible[9] to obtain an estimate of the diffusion coefficient by constructing a line tangent to the penetration curve at the interface, and finding its intercept (Z) with the horizontal axis. The diffusion coefficient is then given by

$$D = \frac{Z^2}{\pi t} \cdot \tag{104}$$

The value of D estimated from the 742°C penetration curve is $\sim 10^{-8}$ $cm^2/sec.$, in agreement with the established diffusion coefficient of carbon at this temperature.

Consideration of the carbon mass balances for the two penetration curves, assuming simple binary carbon diffusion, indicates that C_{11} is

approximately 0·295 wt% C at 742°C and 0·305 wt% C at 733°C. (Actual values for C_{11} should be slightly higher, due to the proposed steep manganese gradients in advance of the interface, and the negative sign of D_{12}). Using equation (96) to calculate those "constrained" tie-lines (as discussed in section IIh) which would generate the observed growth rates yields C_{11} = 0.301 wt% C at 742°C and 0.314 wt%C at 733°C. The calculated "constrained" tie-lines are shown in figure 33.

It is conceivable that the value of D_{22} was drastically increased on austenite formation at the beginning of the diffusion anneals (as noted by Kurdjumov[13]). If D_{22} were increased by a factor of 10^4 (from 10^{-15} to 10^{-11}), the growth rate at 742°C could be reconciled with a local equilibrium diffusion solution. However, on calculating the value of D_{22} required to generate the observed growth rate at 733°C (assuming local equilibrium), it is found that, to account for the temperature dependence of the growth rate, D_{22} would be required to increase by a factor of 2 for a decrease in temperature of 9°C. The growth data for 1·52 wt% Mn, 0·405 wt% C and 1·52 wt% Mn, 0·335 wt% C yield qualitatively similar results; in all cases D_{22} would be required to increase with decreasing temperature.

Furthermore, the observed zero growth rate temperatures (for 1·52 wt% Mn, 0·405 wt% C and 3·16 wt% Mn, 0·282 w'%C) are not consistent with the ternary phase diagram if local equilibrium is assumed. They are, however, consistent with the premise that the zero growth rate temperature is one at which the carbon and manganese potentials (ΔC and ΔMn) balance one another, according to a "constrained" tie-line. A calculated "constrained" tie-line for zero growth rate (at 752°C) is shown in figure 33.

While the above considerations indicate that local equilibrium is highly unlikely in these cases, the possibility of greatly enhanced manganese diffusion cannot be entirely discounted on the basis of the experimental data. The author is of the opinion, however, that the rapid up-quench at the beginning of each diffusion anneal was sufficient to prevent the introduction into the austenite of the large numbers of defects observed in Kurdjumov's experiments.

Since the observed parabolic growth rates strongly suggest that a diffusion solution applies in these cases, (even in the absence of local equilibrium) the results will be discussed using the hypothesis of "constrained local equilibrium".

Such an assumption - that carbon comes to local equilibrium, but that manganese and iron do not - implies that the major effect of manganese additions (whatever the supersaturation) is to alter the boundary conditions for carbon diffusion, and that carbon diffusion controls the rate of growth. This appears reasonable, since a basic requirement for the formation of ferrite is the redistribution of carbon.

With complete generality, a linear approximation for the velocity of interface motion (V) may be written

$$V = M_1 A_1 + M_2 A_2 + M_3 A_3 \qquad (105)$$

where the M's are phenomenological coefficients, and the A's are given by

$$A_i = \mu_i^{\gamma} - \mu_i^{\alpha} \quad . \qquad (106)$$

Nothing is known of the values the coefficients take, but, according to the results discussed above, the velocity must be equal to that given by the diffusion solution, and A_1 must not be so large that the assumption of constant interface concentrations is invalidated.

Weichert[85] has applied himself to the difficult mathematical problem of calculating the growth rate (and its temperature dependence) for these alloys using the variational principle (equation 100) introduced in section IIh. While the preliminary results appear promising, the calculation has not yet progressed to the point where an unequivocal statement can be made concerning its validity.

The kinetic results of this section have considerable bearing on the equilibrium constitution diagram in the iron-carbon-manganese system. Previous investigators, notably Wells[44], determined the $\alpha + \gamma - \gamma$ phase boundary by standard metallographic and dilatometric techniques. As noted above, it is found that non-equilibrium ferrite, once precipitated, is quickly redissolved upon heating to a temperature just above that for zero growth rate - a temperature at which the austenite is supersaturated. This phenomenon is analogous to "retrogression" as observed in age-hardening systems containing non-equilibrium transformation products. The resulting behaviour closely resembles that for true equilibrium systems, so that it is probable that "constrained" equilibria, rather than true equilibria, have been determined by these investigators (particularly those employing dilatometric techniques). However, judging from the temperatures at which zero growth rate was observed, the "constrained" phase boundary differs but little from the equilibrium phase boundary. In fact, the precision of much of the equilibrium data is probably insufficient to distinguish between the two.

Several possible criticisms of the experimental configuration employed in this investigation have occurred to the author. These will now be discussed.

1. The use of a pure iron nucleus, rather than one of the α-Fe-Mn should not significantly affect the results, since the original interface, where the manganese gradient existed, was rapidly left behind by the growth front. The diffusion coefficient for manganese in α-iron has not been determined, but it may be estimated by assuming that the ratio of manganese diffusion coefficients in α and γ iron is similar to the ratio of self-diffusion coefficients in α and γ iron[86]. An approxiate calculation then indicates that, at the temperatures of interest, manganese diffusion would affect the ferrite composition for ~ 0·1 micron on either side of the original interface in ~ 1 minute. The measured penetrations were such that this concentration change occurred far behind the interface.

2. There is a possibility that the interface was coherent, due to epitaxy between the plated iron and the ternary alloy (which consisted of martensite and retained austenite at room temperature). Such coherency should not have affected the experimental results, since the plated ferrite was observed to recrystallize almost immediately after the beginning of the diffusion anneal. Any new ferrite grains with orientations markedly different from the original ferrite would be expected to possess high mobility boundaries, and would therefore soon become dominant, destroying any structural relationship at the interface.

V CONCLUSIONS

1. The concentration and temperature dependence of the diffusion coefficient ratio D_{12}/D_{11} in ternary manganese and silicon austenites has been found to be in good accord with values predicted theoretically from statistical and thermodynamic considerations. The results are expected to be of general application in ternary systems where one component has a mobility much greater than the others. In such systems, the diffusive behaviour can be specified to a good approximation from a knowledge of on-diagonal diffusion coefficients, and ternary activity data. This result constitutes a major simplification in the description of multicomponent diffusion.

2. Two phase diffusion couples have been successfully employed to isolate and study the growth of ferrite in austenite. In the binary Fe-C system, diffusion control of a ferrite-austenite interface has been demonstrated, and the concept of local equilibrium has been given strong experimental support.

3. The kinetics of ferrite growth in the ternary Fe-C-Mn system have been determined, again employing two-phase diffusion couples. It has been shown, both theoretically and experimentally, that the growth phenomena may be divided into two classes, one in which local equilibrium may be assumed, and one in which such an assumption cannot be made. The concept of "constrained local equilibrium" has been developed, and applied in order to rationalize the observed transformation behaviour in the second case. Variational methods are required to predict the reaction

path in situations like the latter, where an internal degree of freedom may be said to exist.

4. The results, and the conclusions drawn from them, represent a useful contribution to our understanding of the complex processes involved in diffusion and transformation in the solid state; in particular, in the processes of austenite decomposition.

REFERENCES

1. A. Bramley, F. W. Haywood, A. T. Cooper and J. Watts: Trans. Faraday Soc. 31, 707, (1935).

2. W. Seith and F. Bartschat: Z. Metallkunde 34, 125, (1942).

3. L. S. Darken: Trans.AIME, 180, 430, (1949).

4. W. Seith and H. Wever: Z. Elektrochem. 55, 380, (1951).

5. V. K. Chandhok, J. P. Hirth, and E. J. Dulis: Trans. AIME, 224, 858, (1962).

6. L. S. Darken and R. W. Gurry: "Physical Chemistry of Metals", McGraw-Hill, (1953).

7. P. J. Dunlop and L. J. Gosting: J. Phys. Chem. 63, 86, (1959).

8. J. S. Kirkaldy, G. R. Mason and W. J. Slater: Trans. CIM, 64, 53, (1961).

9. A. H. M. Zia-Ul-Haq: Master's Thesis, McMaster University (1962).

10. C. Wells and R. F. Mehl: Trans. AIME, 188, 553 (1950).

11. C. Wells and R. F. Mehl: Trans. AIME, 144, 315, (1941).

12. C. Wells and R. F. Mehl: Metals Technol. 7, Tech. publication, 1180, (1940).

13. G. Kurdjumov: "Proc. International Conference on Peaceful Uses of Atomic Energy", 15, 81, (1955).

14. R. P. Smith: J. Am. Chem. Soc. 68, 1163, (1946).

15. R. P. Smith: J. Am. Chem. Soc. 70, 2724, (1948).

16. R. P. Smith: Trans. AIME, 218, 62, (1960).

17. L. Kaufman, S. V. Radcliff and M. Cohen: "AIME Symposium on the Decomposition of Austenite by Diffusional Processes" Interscience (1962).

18. A. H. Geisler: "Phase Transformations in Solids", Chapter XIV, Wiley,(1951).

19. M. Hansen: "Constitution of Binary Alloys", McGraw-Hill, (1958).

20. R. P. Smith and L. S. Darken: Trans. AIME, 215, 727, (1959).

21. N. J. Petch: J. Iron Steel Inst. 145, 111, (1942).

22. C. Zener: "Imperfections in Nearly Perfect Crystals", Chapter XI, Wiley, (1952).

23. H. I. Aaronson: "AIME Symposium on the Decomposition of Austenite by Diffusional Processes", Interscience, (1962).

24. C. A. Dube, H. I. Aaronson, and R. F. Mehl, Rev. de Met. 55, 201, (1958).

25. C. S. Smith: Trans. ASM 45, 533, (1953).

26. G. V. Kurdjumov and G. Sachs: Z. Physik, 64, 325, (1939).

27. R. W. Heckel and H. W. Paxton: "The Growth of Proeutectoid Cementite in Steels", Carnegie Institute of Technology, (1959).

28. K. Manzanec and J. Cadek: Rev. de Met., 212, 501, (1958).

29. C. Hickley and J. Woodhead: J. Iron Steel Inst. 176, 129, (1954).

30. J. Crank: "Mathematics of Diffusion", Oxford, Clarendon Press, (1956).

31. R. D. Heidenreich: J.A.P. 26, 879, (1955).

32. C. S. Barrett, A. H. Geisler and R. F. Mehl: Trans. AIME, 134, (1941).

33. R. F. Mehl: "ASM Symposium on the Hardenability of Alloy Steels" (1938).

34. J. W. Cahn and W. C. Hagel: "AIME Symposium on the Decomposition of Austenite by Diffusional Processes" Interscience (1962).

35. I. E. Kontorovich and I. M. Mermel'shtein: Fiz. Met. Metalloved, 6 no5. 40, (1958).

36. "Atlas of Isothermal Transformation Diagrams". U. S. Steel, (1951).

37. M. A. Grossman: "Elements of Hardenability", ASM (1952).

38. H. I. Aaronson: Trans. AIME, 224, 870, (1962).

39. F. E. Bowman: Trans. ASM, 36, 61, (1946).

40. F. E. Bowman: Trans. ASM, 35, 112, (1945).

41. M. L. Picklesimer, D. L. McElroy, T. M. Kelly, E. E. Stansbury, and J. H. Frye: Trans. AIME 218, 473 (1960).

42. A. Hultgren: Rev. de Met. 50, 737, (1953).

43. C. Zener: Trans. AIME, 167, 550, (1946).

44. C. Wells: Metals Handbook, ASM (1948).

45. A. R. Troiano and F. T. McGuire: Trans. ASM. 31, 340, (1943).

46. A. Fick: Pogg. Ann. 94, 59, (1855).

47. C. Matano: Japan J. Phys. 8, 109, (1933).

48. L. Onsager: Ann. N. Y. Acad. Sci. 46, 241, (1945).

49. J. S. Kirkaldy: Can. J. Phys. 36, 917, (1958).

50. J. S. Kirkaldy: Can. J. Phys. 37, 30, (1959).

51. S. R. de Groot: "Thermodynamics of Irreversible Processes", Interscience, (1951).

52. L. Onsager: Phys. Rev. 37, 405, (1931); 38, 2265, (1932).

53. S. R. de Groot and P. Mazur: Phys. Rev. 94, 218, (1954).

54. G. J. Hooyman and S. R. de Groot: Physica, 21, 73, (1955).

55. G. J. Hooyman: Physica, 22, 751, (1956).

56. J. G. Kirkwood, R. L. Baldwin, P. J. Dunlop, L. J. Gosting, and G. Keyeles: J. Chem. Phys. 33, 1505, (1960).

57. G. J. Hooyman, S. R. de Groot, and P. Mazur: Physica, 21, 360, (1955).

58. J. S. Kirkaldy and G. R. Purdy: Can. J. Phys. 40, 202, (1962).

59. J. S. Kirkaldy and G. R. Purdy: Can. J. Phys. 40, 208, (1962).

60. L. S. Darken: Appendix to paper by R. P. Smith: J. Am. Chem. Soc., 68, 1163, (1946).

61. K. Iwase and S. Kachi: Nippon Kinzoku Gakkaishi, 15, 189, (1951).

62. C. Wagner: "Thermodynamics of Alloys", Addison-Wesley (1952).

63. R. A. Oriani: "Symposium on the physical Chemistry of Metallic Solutions and Intermetallic Compounds 1", Chemical Publishing, (1960).

64. F. Seitz: Acta Cryst. 3, 355, (1950).

65. J.S. Kirkaldy: Can. J. Phys. 36, 899, (1958).

66. I. J. O'Donnell and L. J. Gosting: "Symposium on Electrolytes", Wiley, (1957).

67. H. S. Carslaw and J. C. Jaeger: "Conduction of Heat in Solids", Oxford; Clarendon Press, (1959).

68. J. S. Kirkaldy: "AIME Symposium on the Decomposition of Austenite by Diffusional Processes" Interscience (1962).

69. L. Boltzmann: Ann. Phys. (Leipsig), 53, 959, (1894).

70. J. S. Kirkaldy: Can. J. Phys. 35, 435, (1957).

71. L. J. Gosting and H. Fujita: J. Am. Chem. Soc. 78, 1099, (1956).

72. T. B. Massalski: Acta Met. 6, 243, (1958).

73. H. Buckle: Metallforshung, 1, 175, (1946).

74. J. S. Kirkaldy: Can. J. Phys. 36, 907, (1958).

75. A. A. Popov: Fiz. Met. Metalloved, 6, no.4, 643, (1958).

76. M. Hillert: Jernkont. Ann. 141, 757, (1957).

77. J. Cahn: Private communication.

78. J. W. Gibbs: "Scientific Papers 1", Longmans, Green, (1906).

79. J. S. Kirkaldy: Can. J. Phys. 38, 1356, (1960).

80. J. S. Kirkaldy, J. von Destinon-Forstmann, and R. J. Brigham: Trans. CIM, (to be published.)

81. J. W. Frazer and R. T. Holzmann: University of California Research Report UCRL-6020, (1960).

82. O. L. Davies: "Statistical Methods in Research and Production" Oliver and Boyd (1949).

83. R. J. Brigham and J. S. Kirkaldy: In preparation.

84. A. Hultgren: "Hardenability of Alloy Steels". ASM (1938).

85. D. Weichert: Private communication.

86. C. E. Birchenall and R. F. Mehl: Trans. AIME, 188, 144,(1950).

NOMENCLATURE

a	Thermodynamic activity
A	Avogadro's number
A_i	Chemical affinity (equation 105)
α	Phase boundary position in λ-space
b	Constant
β	Growth parameter ($= \frac{\alpha}{2\sqrt{D_{11}}}$)
c	Constant
C	Concentration in moles/unit volume
ΔC	Carbon potential (equation 96)
γ	Activity coefficient
d_i	Width of i^{th} layer in a layer diffusion couple
D_{ik}	Diffusion coefficient describing flow of component i on a concentration gradient of component k
e	Constant
E	Internal energy
ϵ	Atom pair interaction energy
f	Constant
F	Gibbs free energy
F^*	Free energy of mixing
J_i	Flux of component i
J_i^A	Flux of component i measured with respect to reference frame A.
k	Boltzmann constant
L_{ik}	Mobility describing flow of component i on a chemical potential gradient due to component k

λ Lattice spacing (section IId)

λ A parameter ($= x/\sqrt{t}$)

M Phenomenological coefficient (equation 105)

ΔMn Manganese potential (equation 96)

n_i Number of atoms of species i

n_i^k Number of moles of component i per atom plane k

N Mole fraction

η Number of atom pairs

P Pressure

P_{ik} A transformation matrix

R Gas constant

S Entropy

σ Local rate of entropy production

t Time

T Absolute temperature

μ Chemical potential

μ_{ik} $= \partial\mu_i'/\partial C_k$

v Phase boundary velocity

V Volume

ν Atomic jump frequency

W Thermodynamic probability

X Generalized thermodynamic force

X_i^A Force due to component i measured in frame of reference A (section IIb).

TABLE I: INTERACTION PARAMETERS IN BINARY AND TERNARY AUSTENITES

Alloy	ϵ_{11}/kT	$(\epsilon_{12} - \epsilon_{31})/kT$
Fe-C	0·44	-
Fe-C-Si	0·44	1·97
Fe-C-Mn	0·44	- 0·67
Fe-C-Ni	0·44	0·82

TABLE II: ANALYSES OF ALLOYS

	Concentration (wt%)						
Alloy	Si	Mn	S	P	Cu	Cr	Aℓ
Melting stock	0·02	0·01	0·01	0·01	-	-	-
Fe- 3·2 Mn	0·035	3·16	0·014	0·011	0·001	0·018	0·010
Fe- 1·5 Mn	0·04	1·52	0·015	0·002	0·005	0·010	-
Fe- 1·9 Si	1·90*	0·015	0·014	0·007	-	0·011	-
Fe- 1·5 Si	1·50	0·18	-	0·08	-	0·01	-

*corrected slightly for SiO_2 content

TABLE III: ANALYTICAL RESULTS FOR DIFFUSION LAYER COUPLES

Couple		Temp. °C	N_1^i	N_2^i	N_1^o	D_{12}/D_{11}	Remarks
Fe-C-Si	1	853	0·0229 ± .00042	0·0364	0·0317 ± .00030	0·170 ± 0·010	
	2	915	0·0236 ± .00023	0·0364	0·0329 ± ·00035	0·166 ± 0·008	
	3		0·0064 ± ·00019	0·0369	0·0092 ± ·00027	0·052(5) ± 0·006	
	4*		0·0092 ± ·00042	0·0292	0·0120 ± ·00041	0·072 ± 0·013	Annealed $t = 1.7\left(\frac{d_1^2}{D_{11}}\right)$
	5		0·0111 ± ·00029	0·0368	0·0166 ± ·00024	0·101 ± 0·007	
	6	988	0·0123 ± ·00019	0·0368	0·0176 ± ·00023	0·100 ± 0·006	Annealed $t = 28\left(\frac{d_1^2}{D_{11}}\right)$
	7		0·0155 ± ·00019	0·0367	0·0216 ± ·00023	0·116 ± 0·007	
	8		0·0211 ± ·00016	0·0365	0·0297 ± ·00045	0·167 ± 0·009	
	9		0.0258 ± ·00045	0·0364	0·0358 ± ·00020	0·195 ± 0·010	
	10	1058	0·0163 ± ·00050	0·0366	0·0230 ± ·00041	0·129 ± 0·013	
Fe-C-Mn	11	795	0·0274 ± ·00026	0·0315	0·0244 ± ·00021	-0·109 ± 0·012	
	12	853	0·0298 ± ·00016	0·0314	0·0271 ± ·00019	-0·096 ± 0·009	
	13	915	0·0278 ± ·00043	0·0314	0·0254 ± ·00046	-0·087 ± 0·021	
	14		0·0095 ± ·00012	0·0319	0·0086 ± ·00012	-0·032(6) ± 0·006	
	15		0·0165 ± ·00015	0·0317	0·0153 ± ·00030	-0·043(5) ± 0·012	
	16	988	0·0210 ± ·00035	0·0316	0·0193 ± ·00025	-0·057 ± 0·014	
	17		0·0296 ± ·00039	0·0314	0·0272 ± ·00019	-0·085(4) ± 0·015	
	18		0·0313 ± ·00038	0·0313	0·0283 ± ·00010	-0·106(7) ± 0·013	

*The iron-silicon alloy used in couple No.4 was a transformer iron, rather than the vacuum melted alloy used in couples 1-3 and 5-10. The analysis is reported in table II.

TABLE IV: MEASURED FERRITE GROWTH PARAMETERS

Alloy	Temperature (°C)	$\alpha \left(\frac{cm}{\sqrt{sec}} \times 10^{-6}\right)$
Fe-0.367 wt% C	792	71 ± 5
1·52 wt% Mn, 0·210 wt% C	760	6·8 ± 0·6
	735	10·4 ± 0·5
	725	18 ± 1 (minimum value)
1·52 wt% Mn, 0·335 wt% C	741	6·3(4) ± 0·6
	725	8·7(3) ± 0·6
1·52 wt% Mn, 0·405 wt% C	760	0
	741	5·2(3) ± 0·4
	725	7·3(2) ± 0·5
3·16 wt% Mn, 0·282 wt% C	752	0
	745	2·25 ± 0·2
	742	3·10 ± 0·2
	733	5·10 ± 0·2

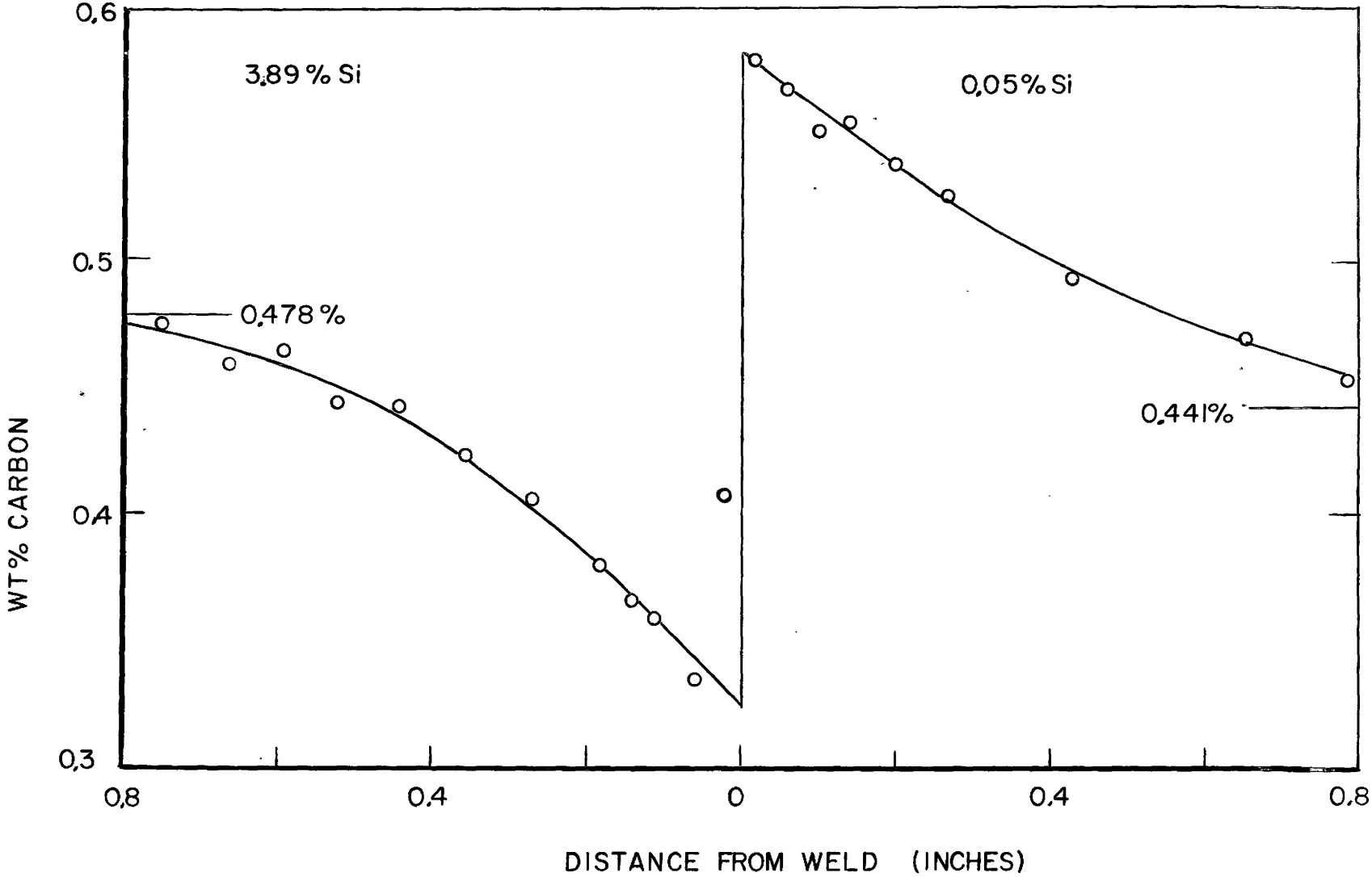

Figure 1. Penetration curve for an iron-carbon-silicon diffusion couple, after Darken[3].

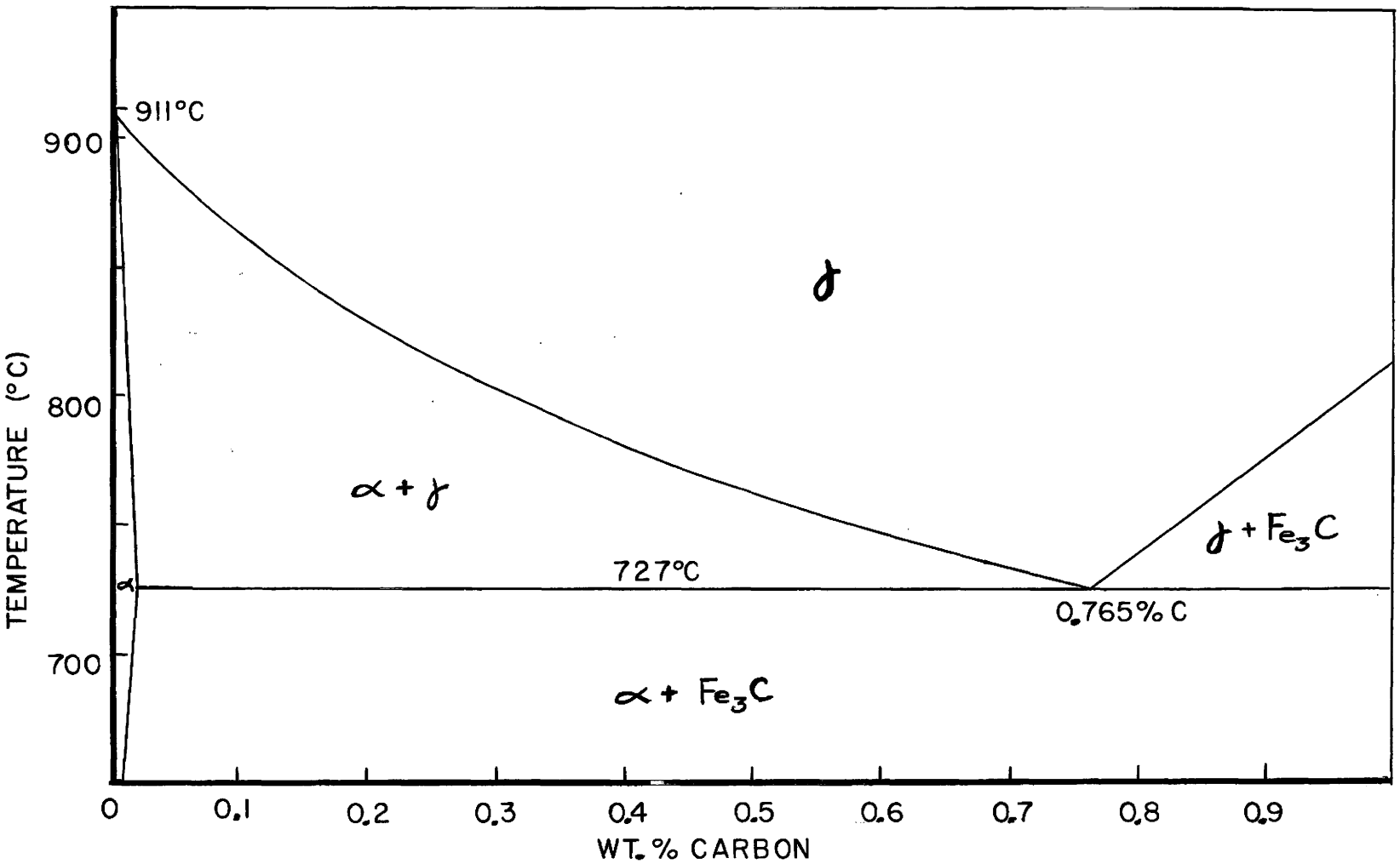

Figure 2. Portion of the Fe-Fe_3C constitution diagram.

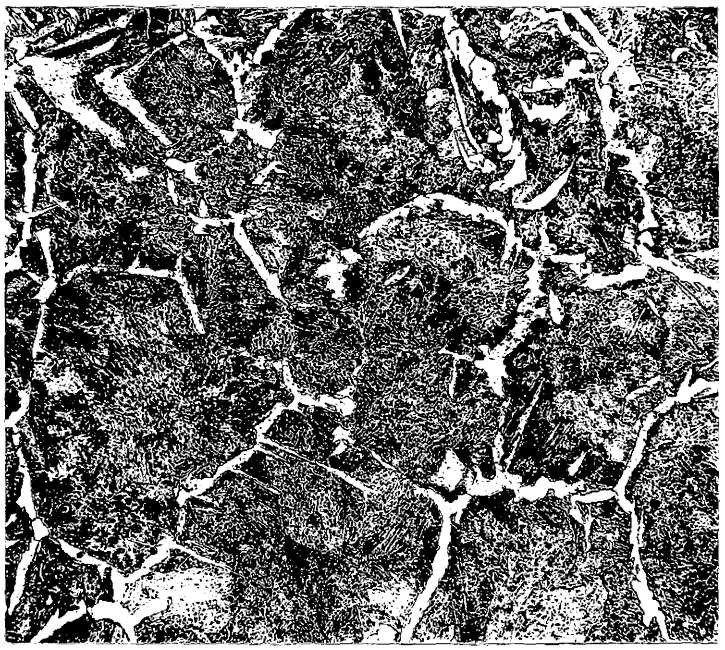

Figure 3. Micrograph showing grain boundary and Widmanstatten ferrite (X 125).

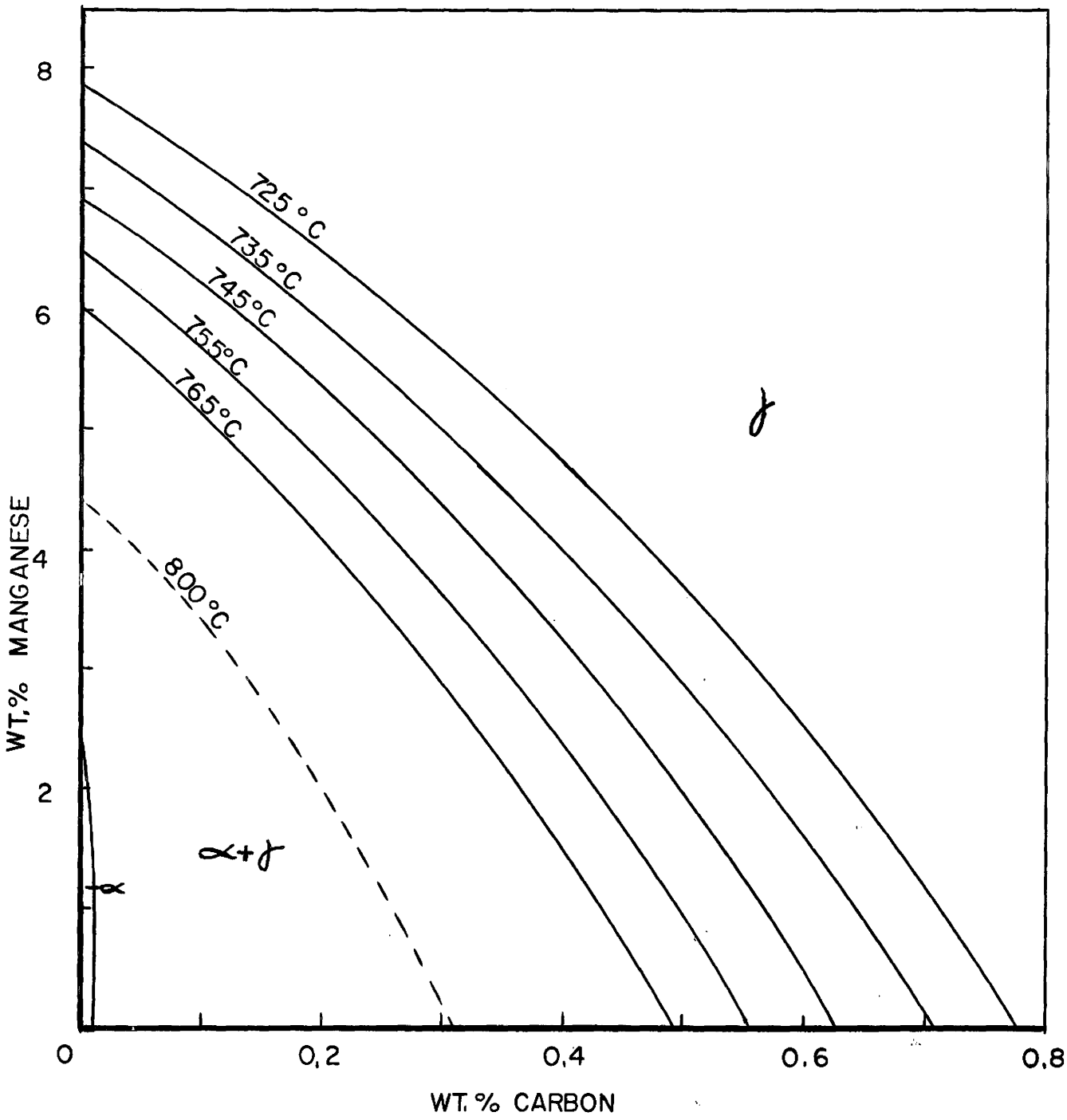

Figure 4. Austenite to austenite + ferrite surface of the iron, carbon, manganese constitution diagram.

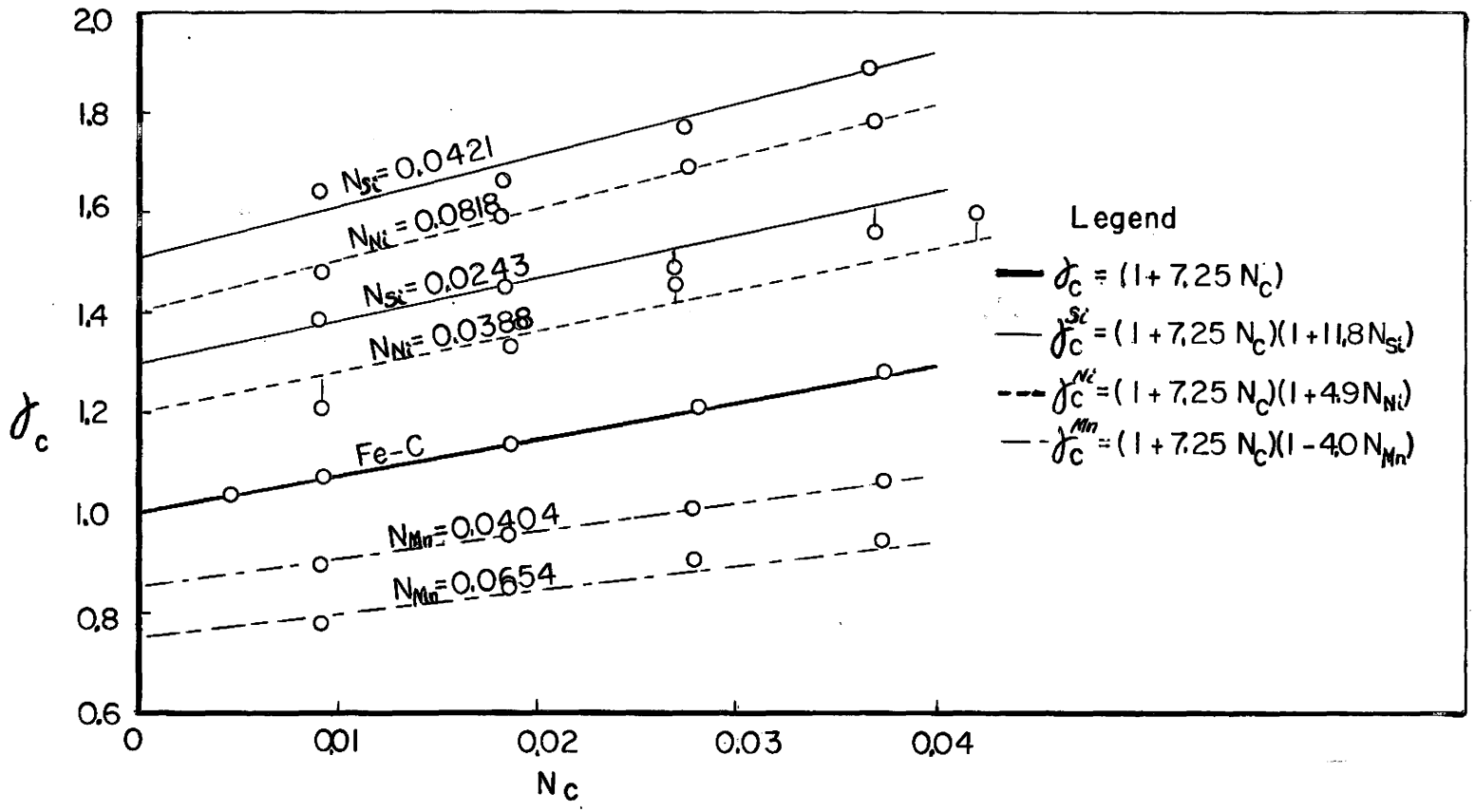

Figure 5. Analytic representation of experimental activity data for the ternary systems Fe-C-Si, Fe-C-Mn, Fe-C-Ni. γc is the activity coefficient (ac/Nc) with standard state defined at infinite dilution in the binary Fe-C alloy. Experimental points have been adjusted slightly from constant weight per cent to constant mole fraction.

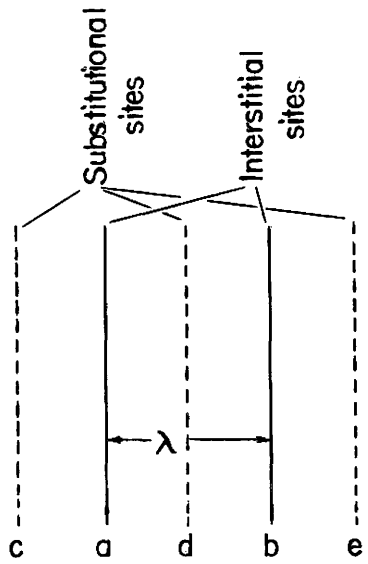

Figure 6. Schematic representation of jump configuration in a ternary system containing an interstitial component.

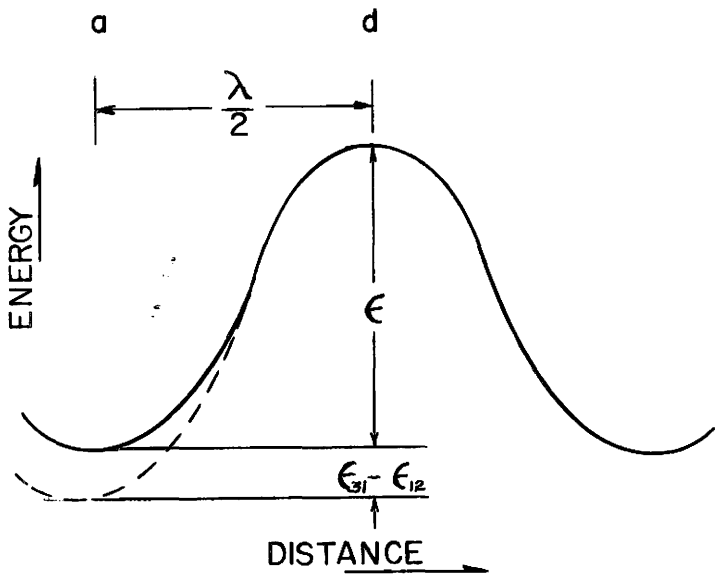

Figure 7. Schematic representation of the energy relationships involved in the jump of an interstitial atom from site to site in a ternary alloy.

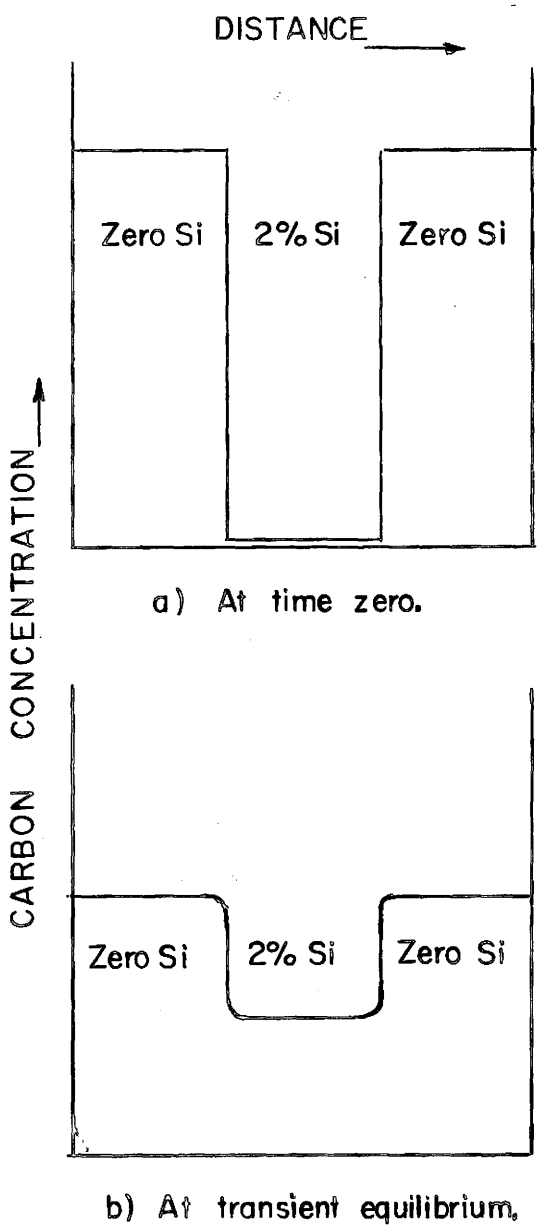

Figure 8. Initial and final solute distributions (schematic) in a layer diffusion couple.

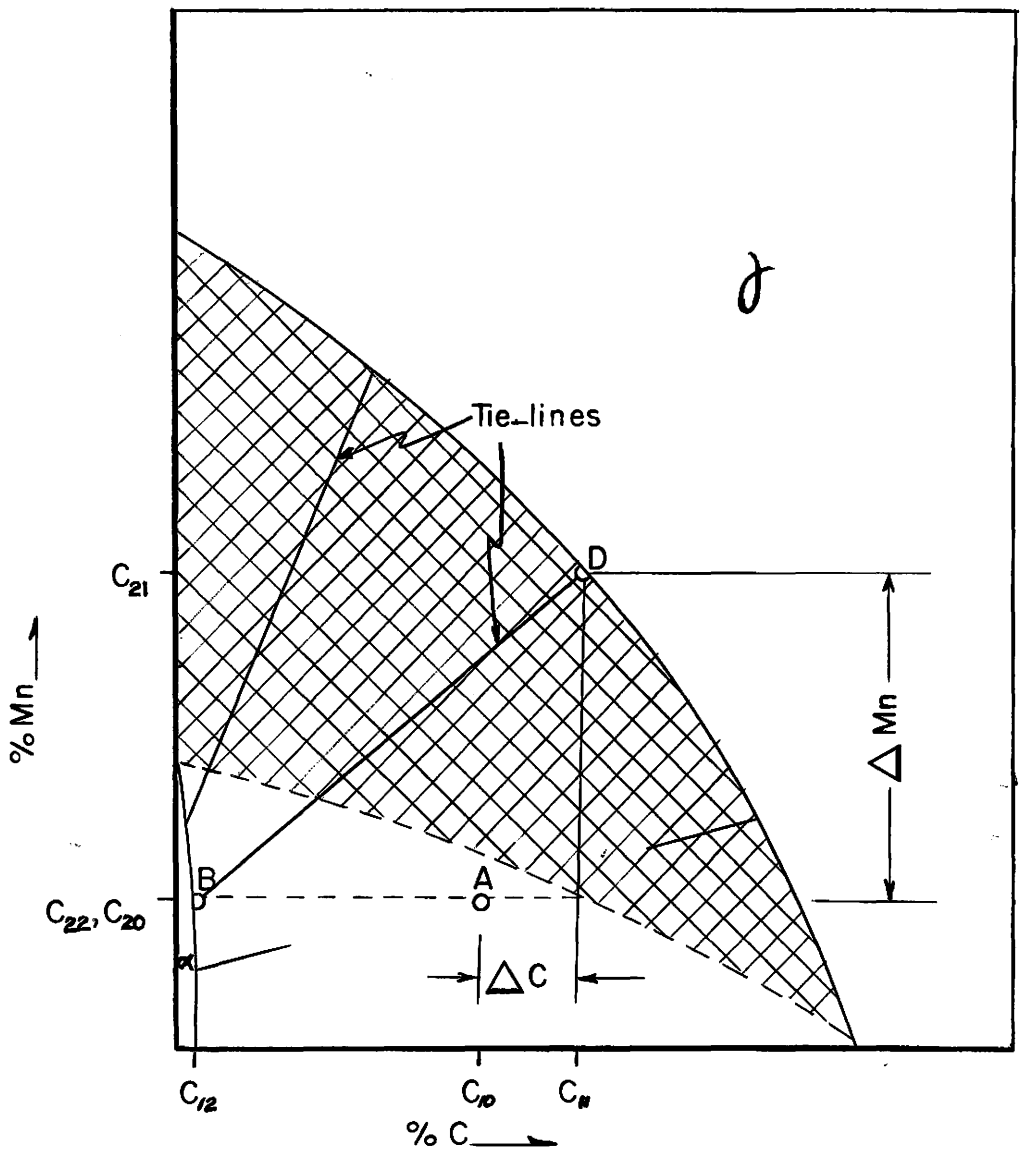

Figure 9. Schematic isothermal section of the Fe-C-Mn constitution diagram.

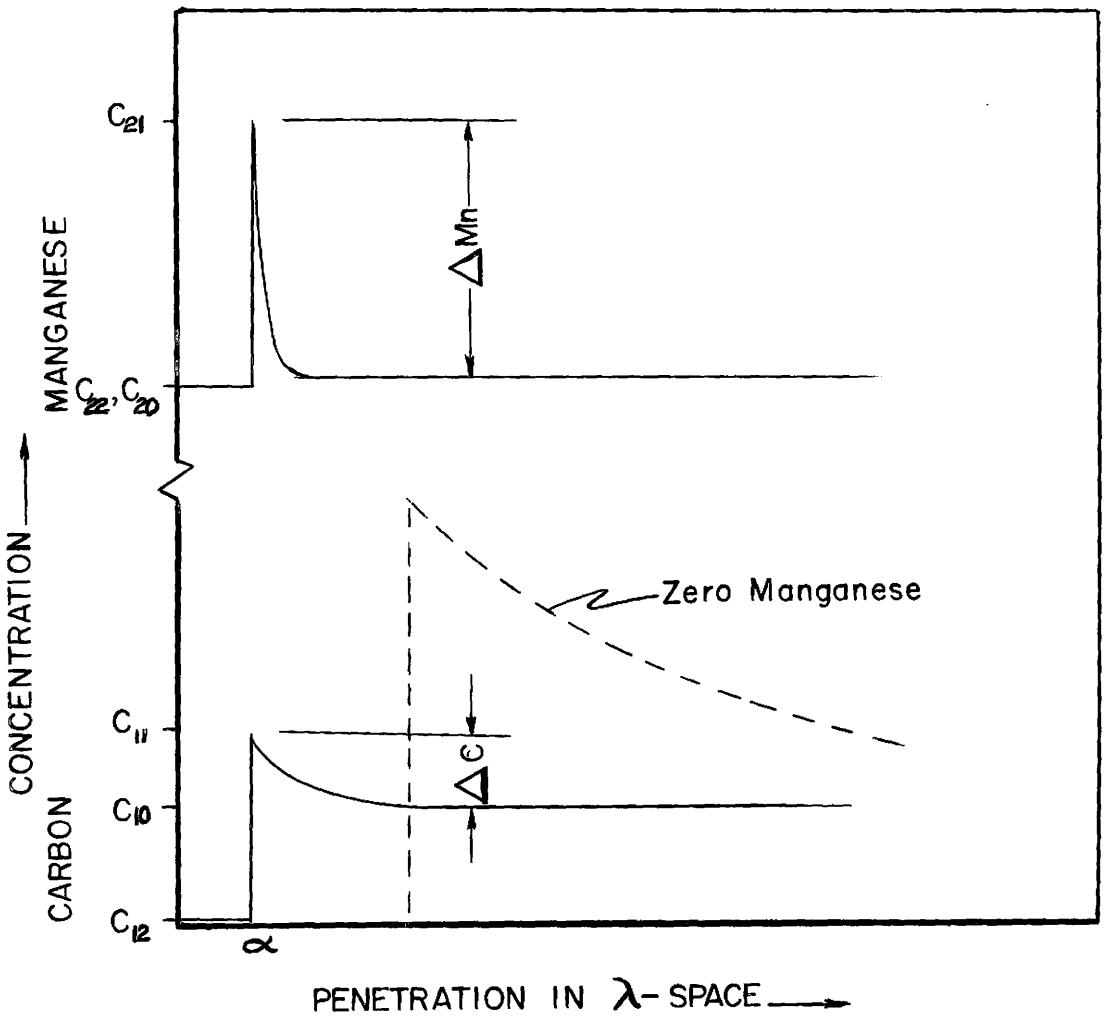

Figure 10. Schematic penetration curves for ferrite growth in a ternary Fe-C-Mn austenite.

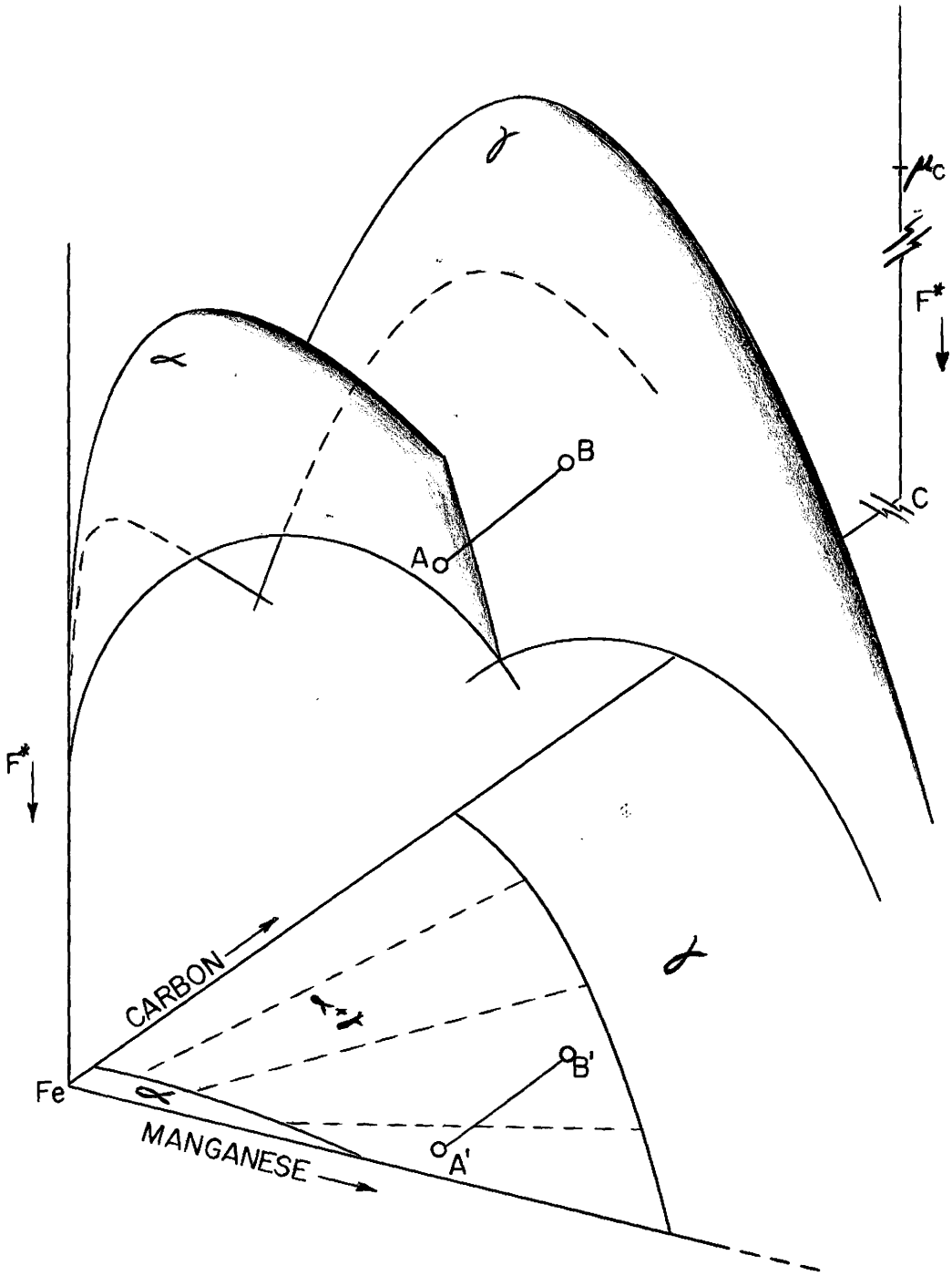

Figure 11. Schematic isothermal free energy surfaces for ferrite and austenite in the ternary Fe-C-Mn system.

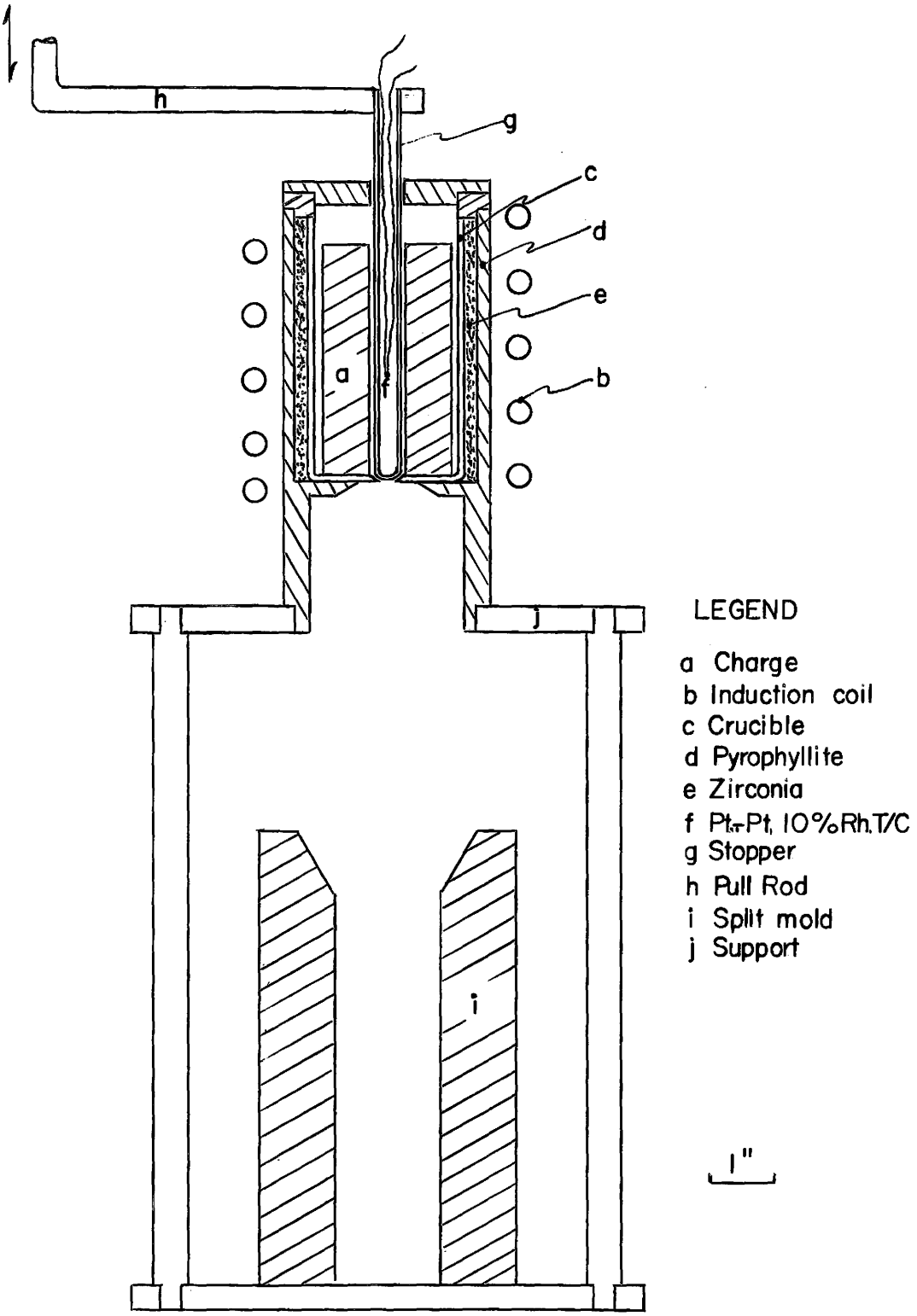

Figure 12. Melting and casting apparatus.

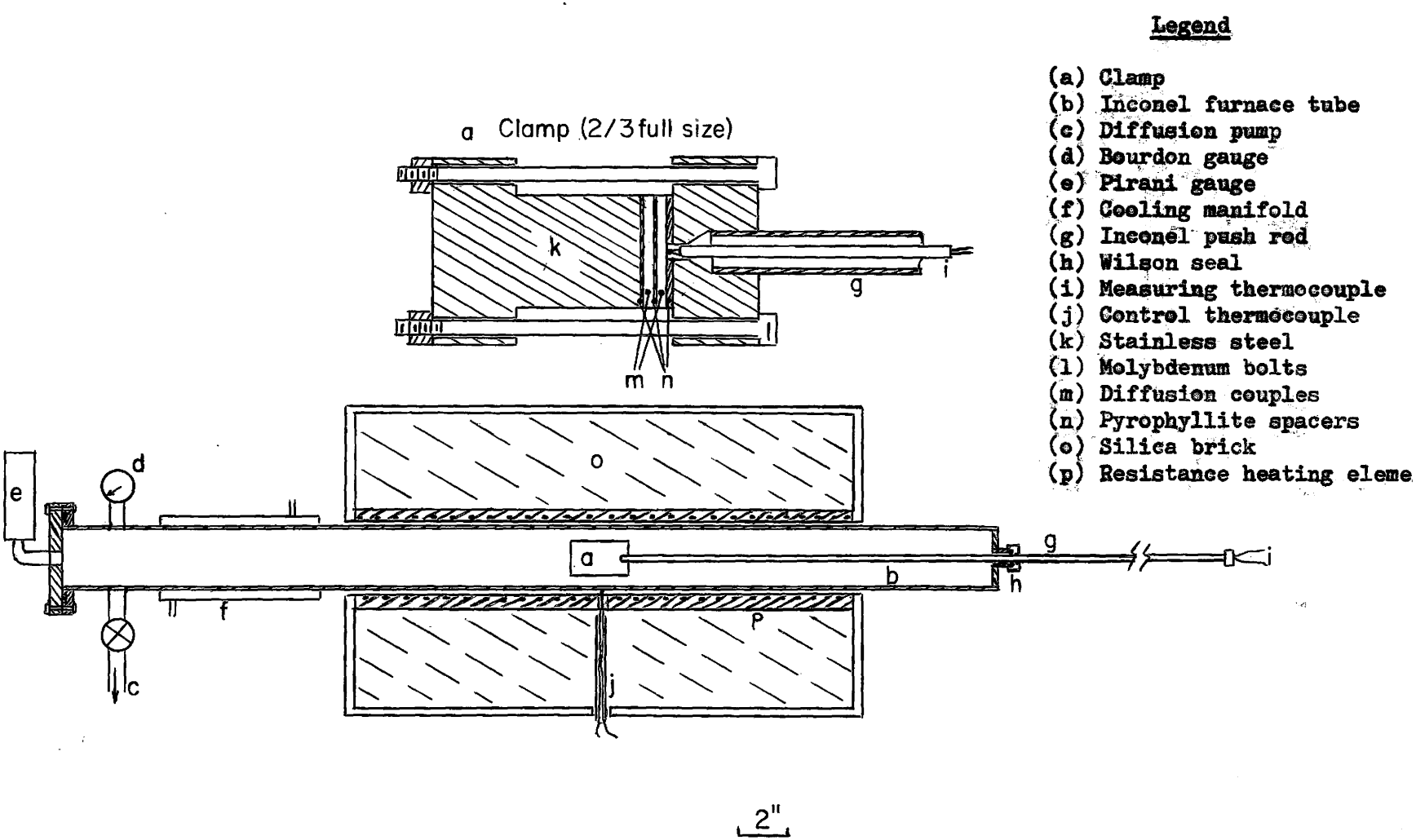

Figure 13. Annealing furnace and clamp.

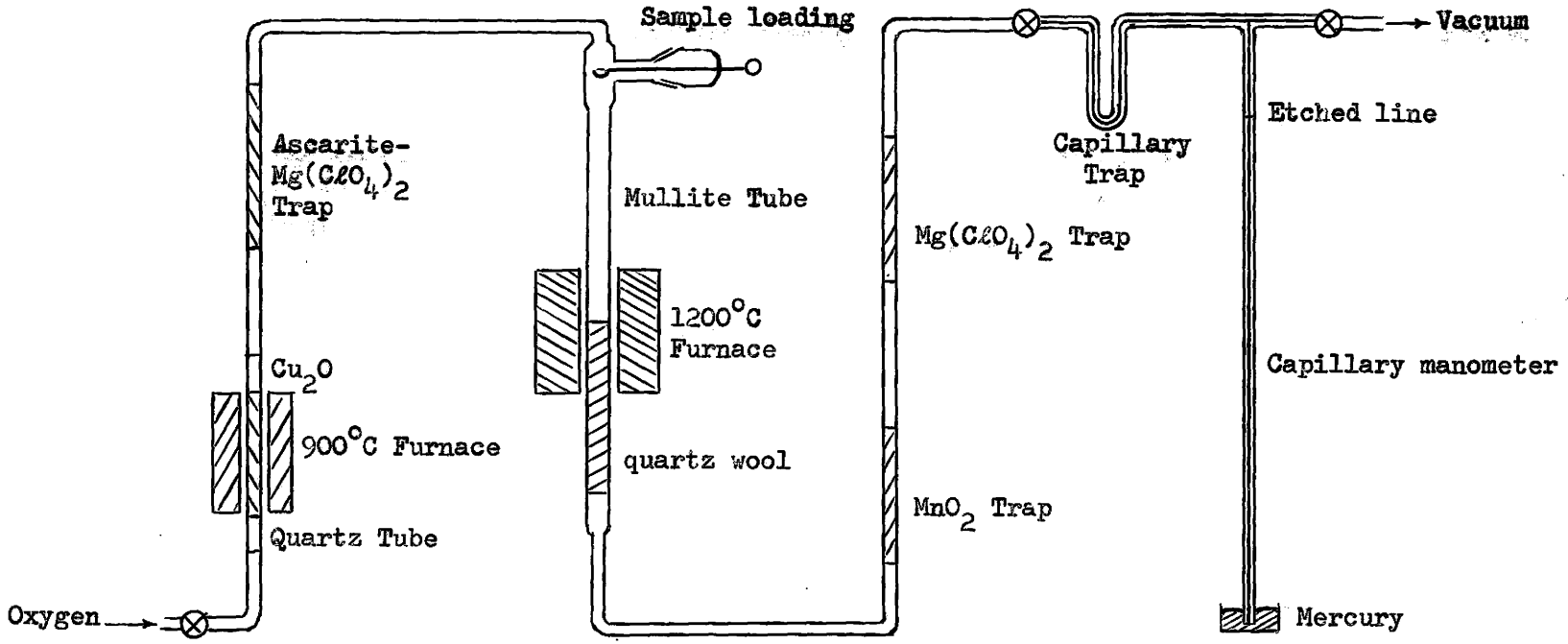

Figure 14. Microanalytic apparatus for carbon determination.

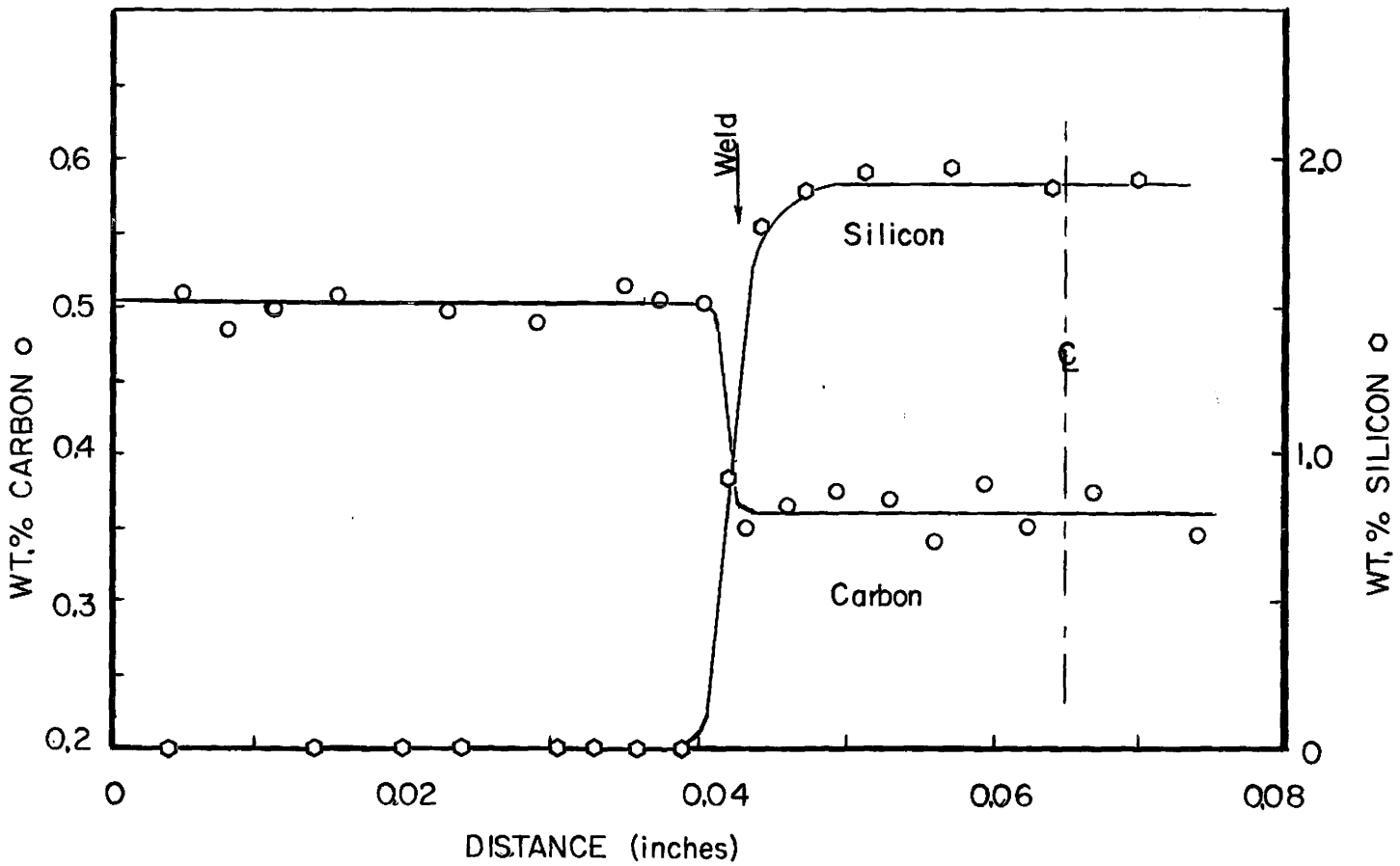

Figure 15. Penetration curve for Fe-C-Si layer diffusion couple in the transient equilibrium state.

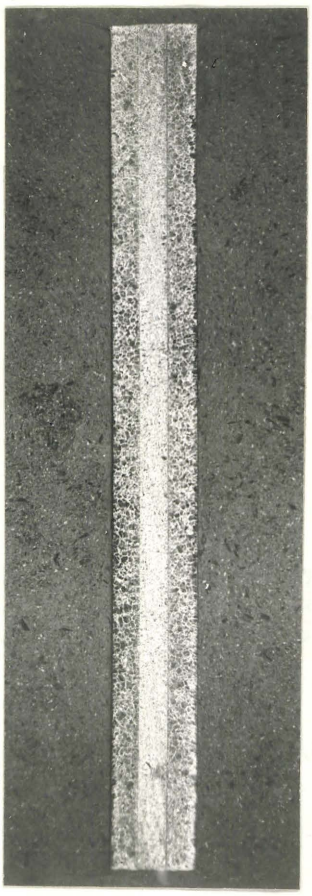

Figure 16. Macrograph of a cross section of a typical "transient equilibrium" diffusion layer couple (X 4.5).

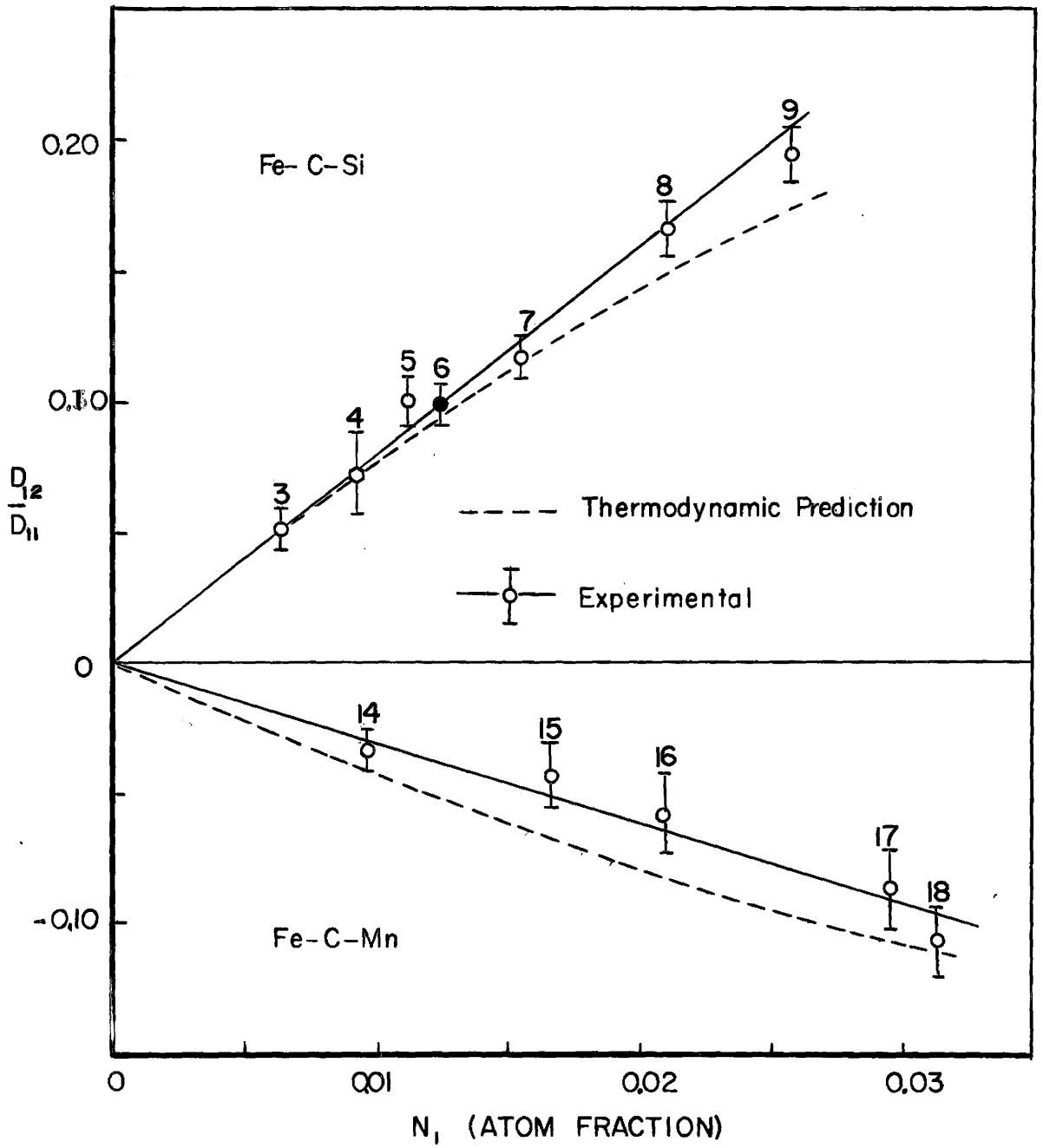

Figure 17. The interstitial concentration dependence of D_{12}/D_{11} in Fe-C-Si and Fe-C-Mn. The hexagonal point was obtained from a couple which was held at temperature for one-quarter of the usual diffusion time, the solid point from a couple annealed four times the usual diffusion time.

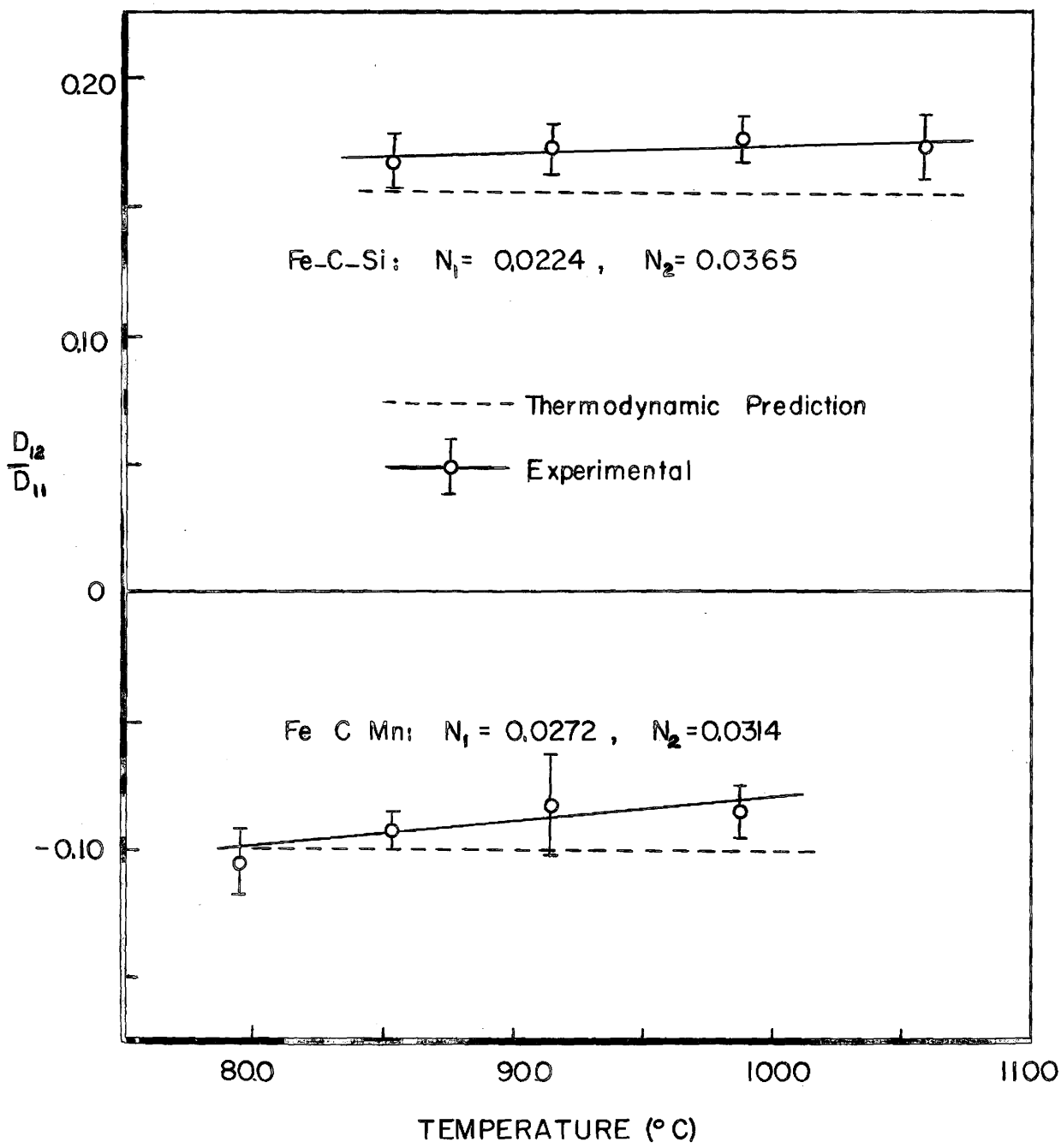

Figure 18. The temperature dependence of D_{12}/D_{11} in Fe-C-Si and Fe-C-Mn.

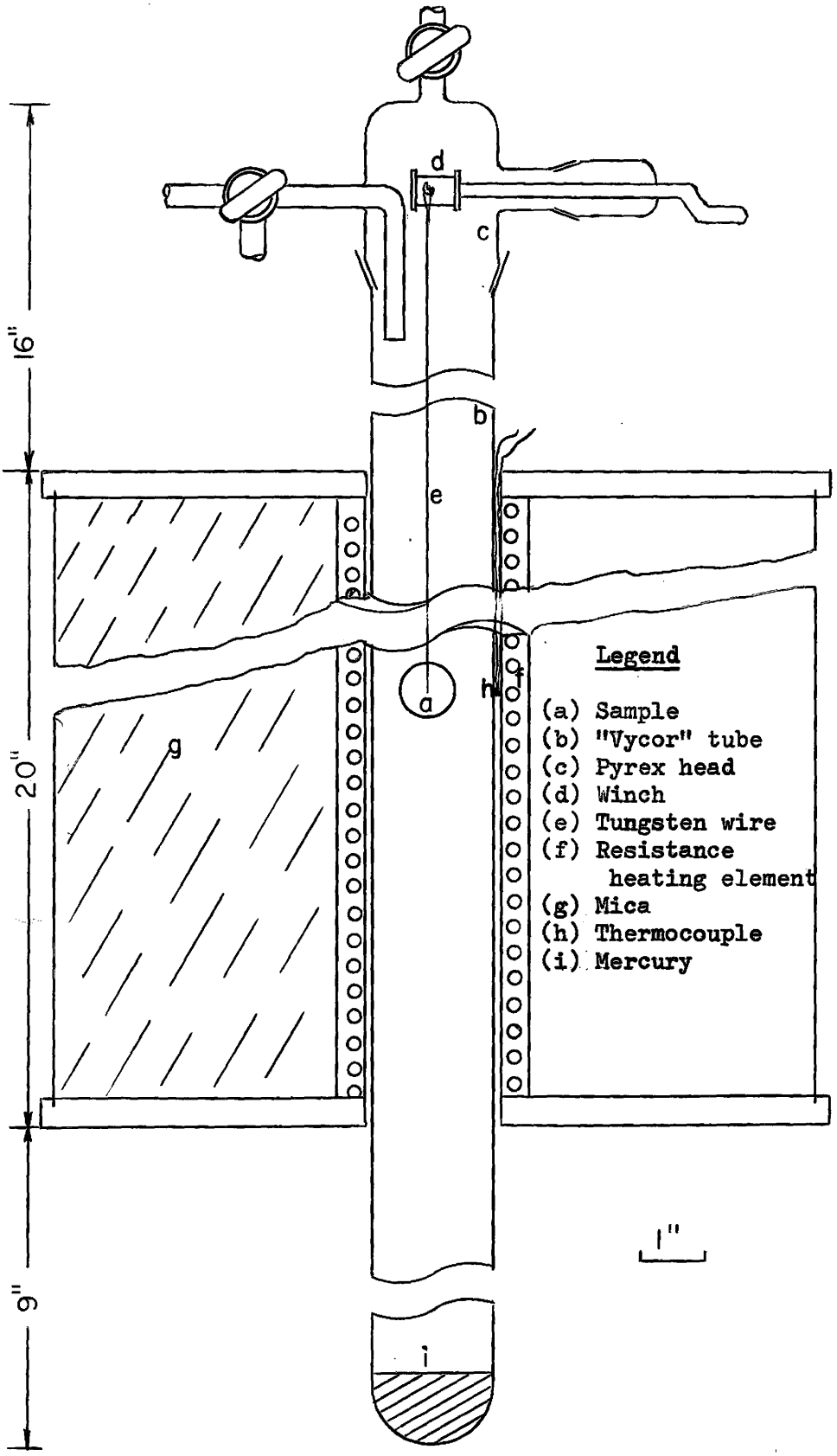

Figure 19. Quenching furnace

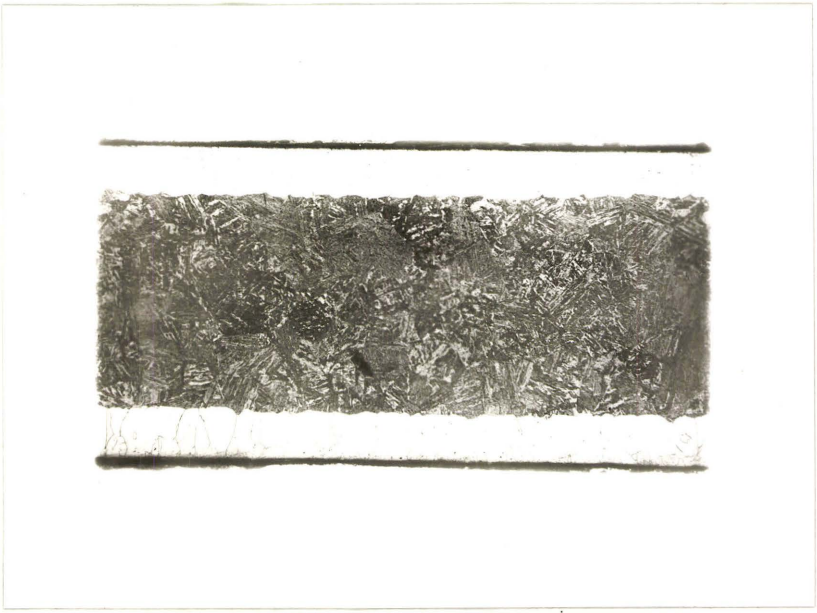

Figure 20. Macrograph of a binary ferrite-austenite diffusion couple (X 16).

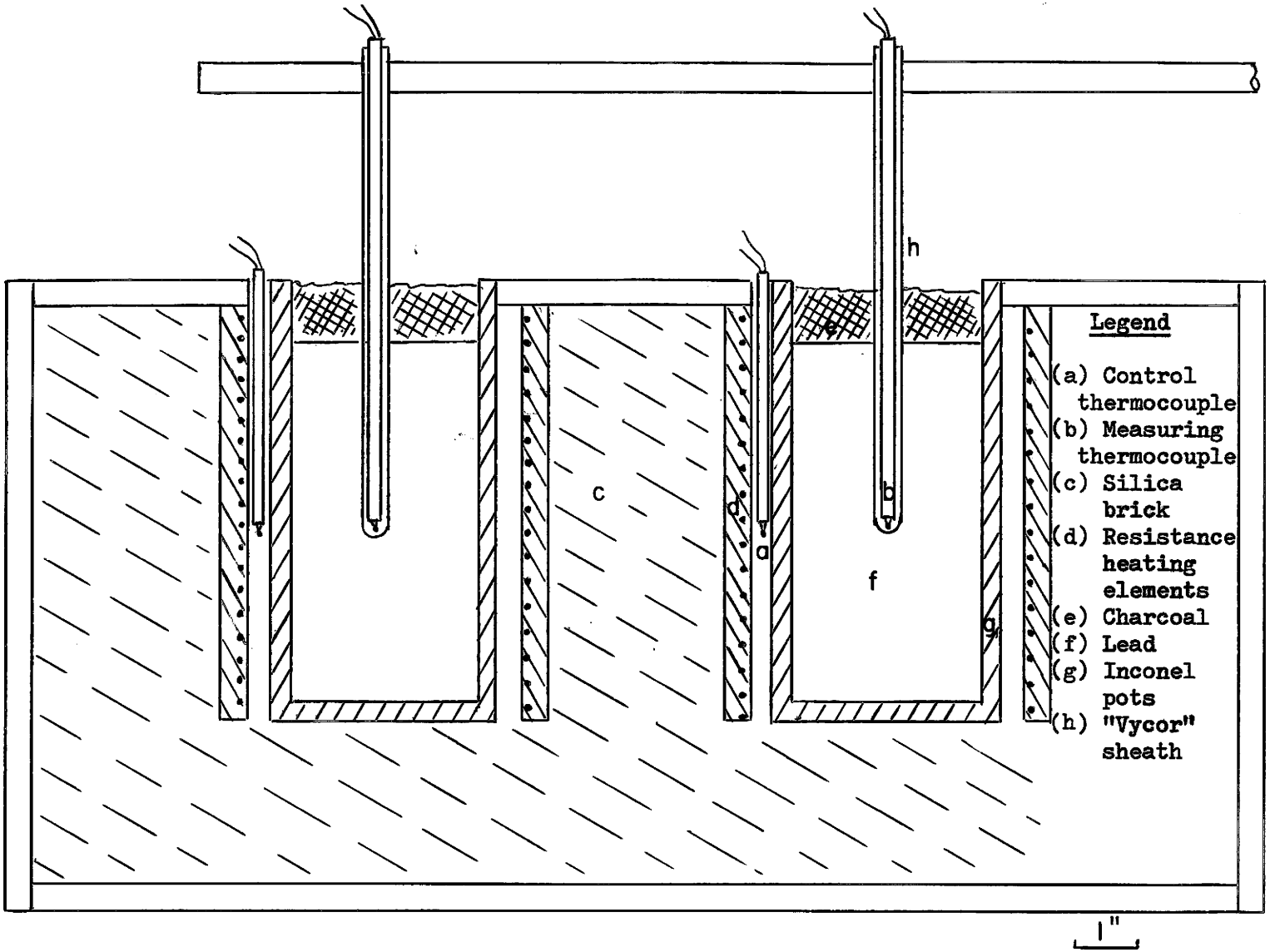

Figure 21. Lead baths

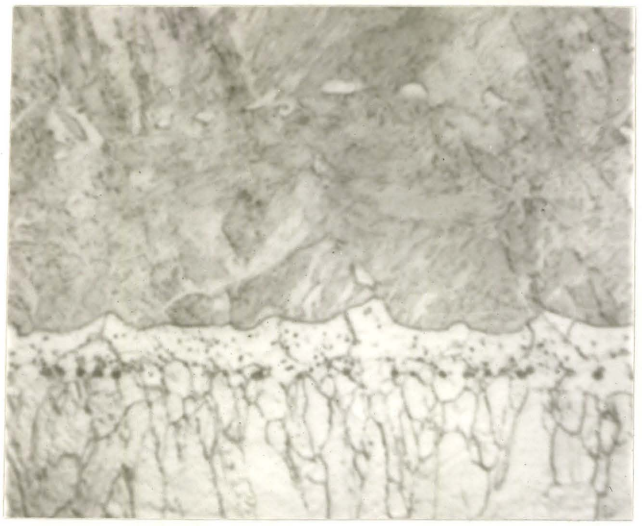

(a) Typical ternary diffusion couple, — showing pores delineating the original interface (X 2240)

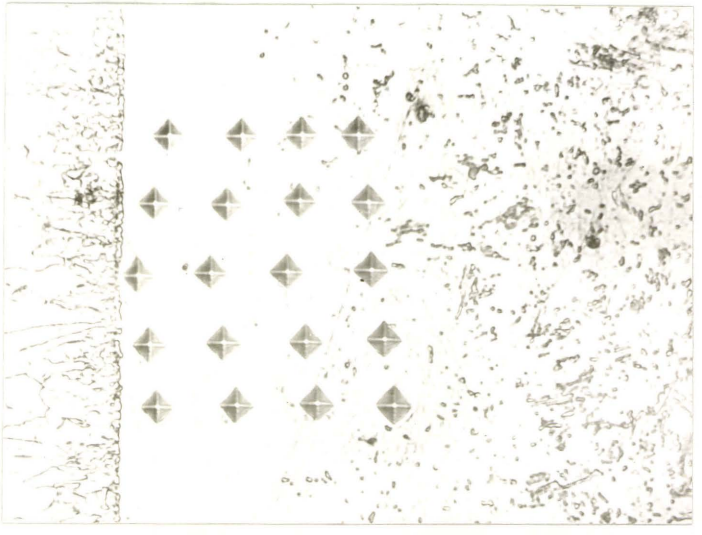

(b) 0·282% C, 3·16 Mn, annealed 22 minutes at 742°C, showing carbon gradient near the interface (X 570). The microhardness indentations were made using a 32 gram load.

Figure 22. Micrographs of ternary Fe-C-Mn ferrite-austenite diffusion couples.

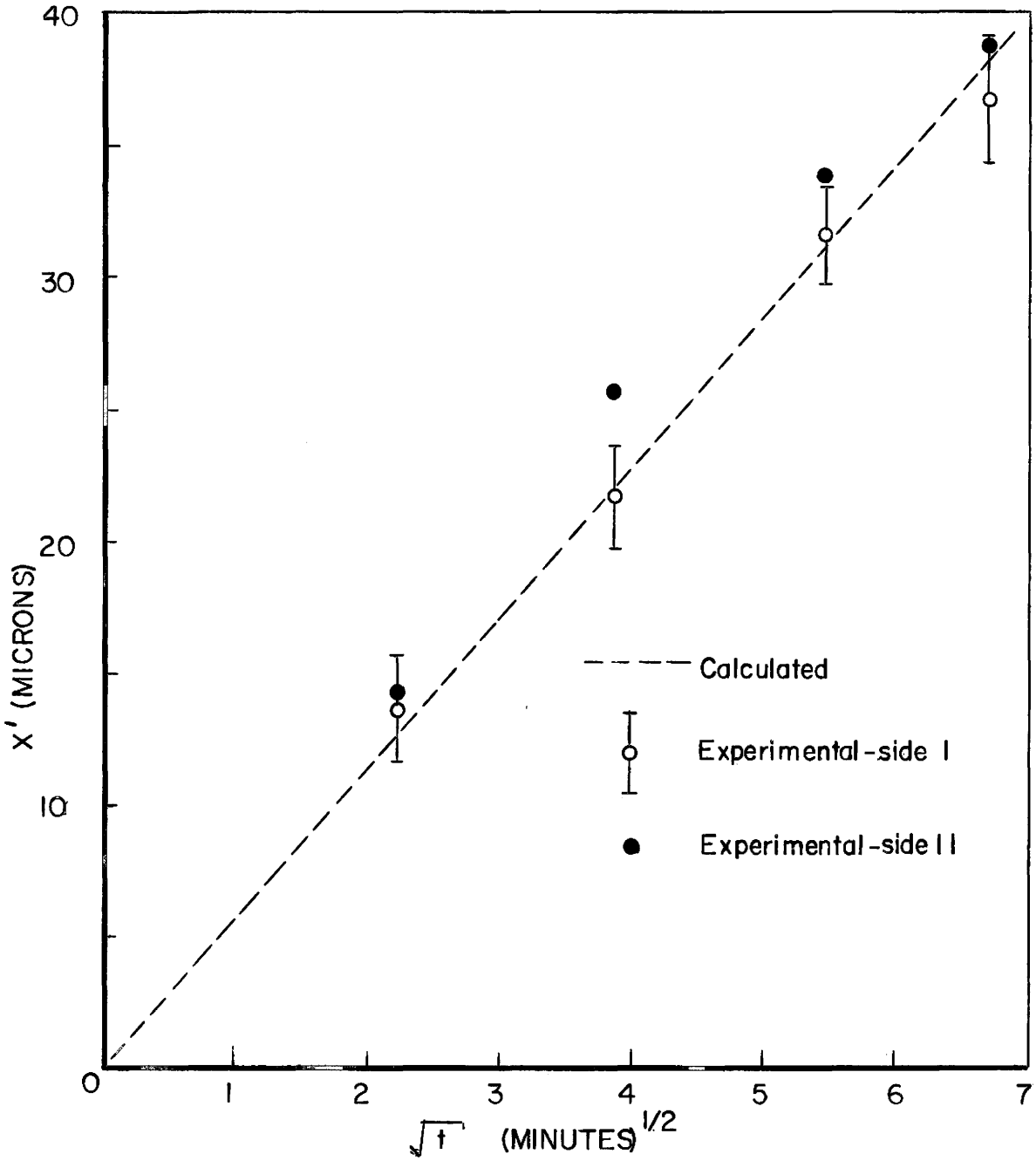

Figure 23. Austenite growth data for binary ferrite - 0.567%C austenite diffusion couple. (Temperature 792°C).

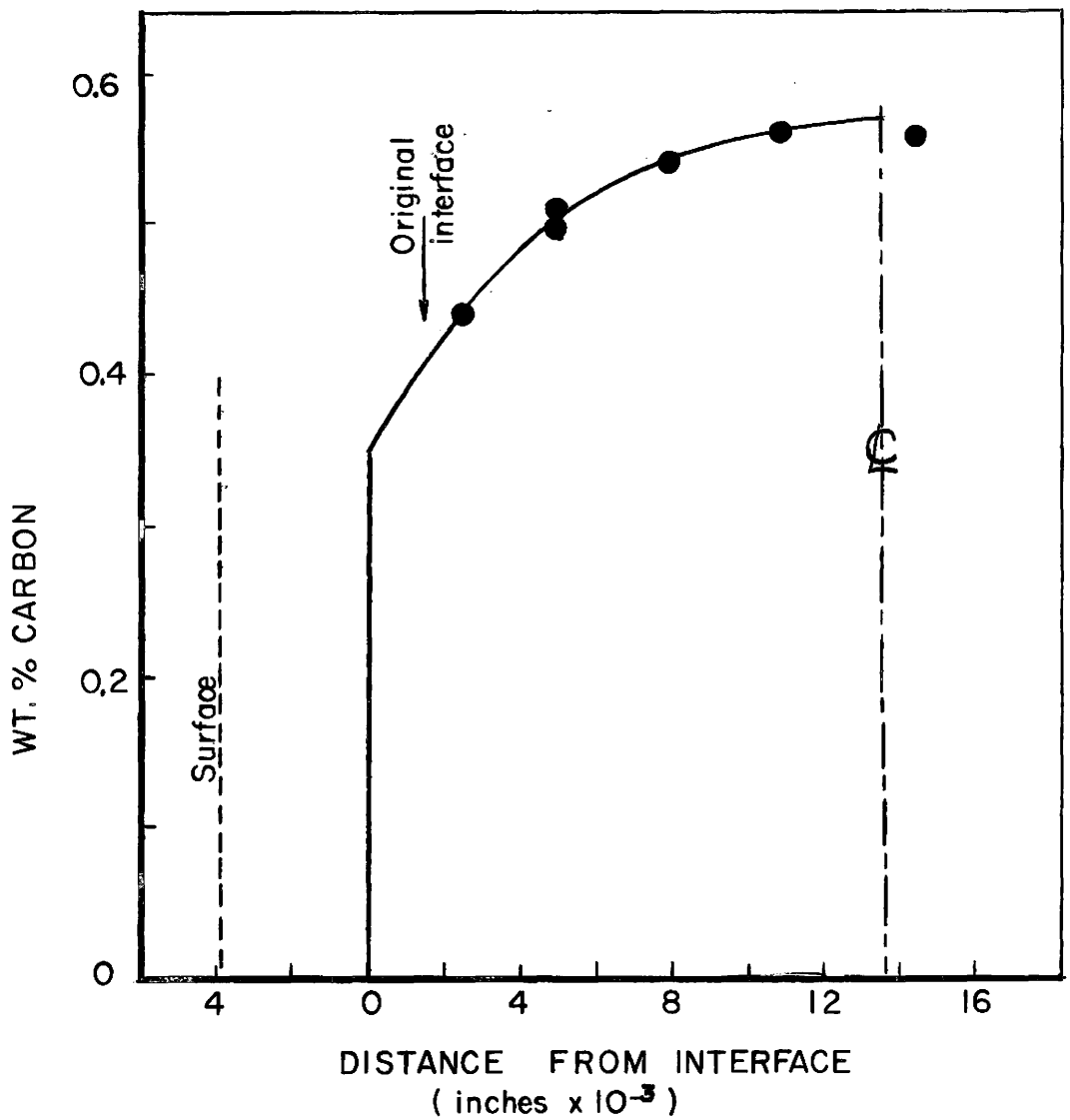

Figure 24. Penetration curve for binary ferrite-austenite diffusion couple.

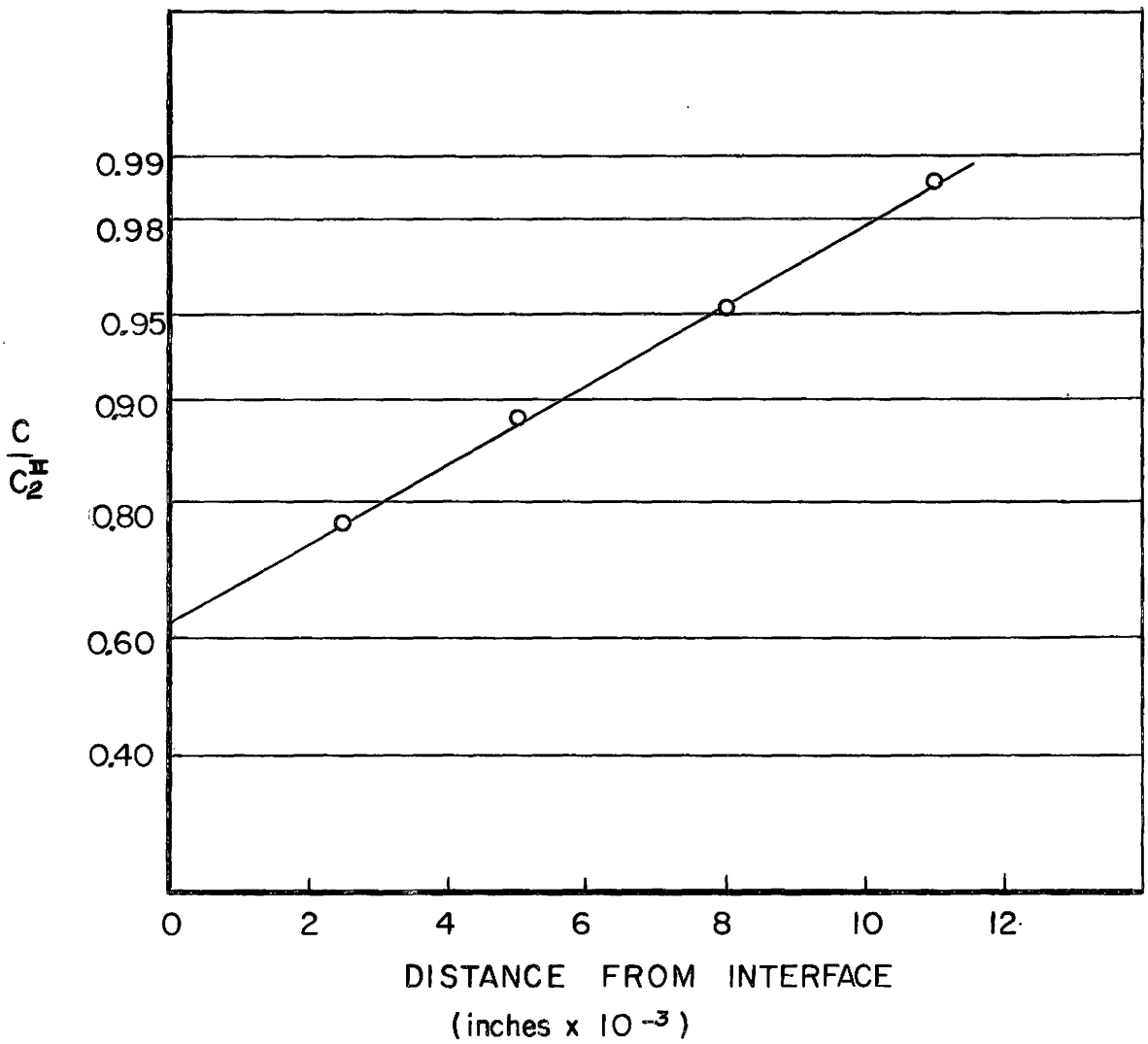

Figure 25. Penetration curve for binary ferrite-austenite diffusion couple. The vertical axis is a probability scale.

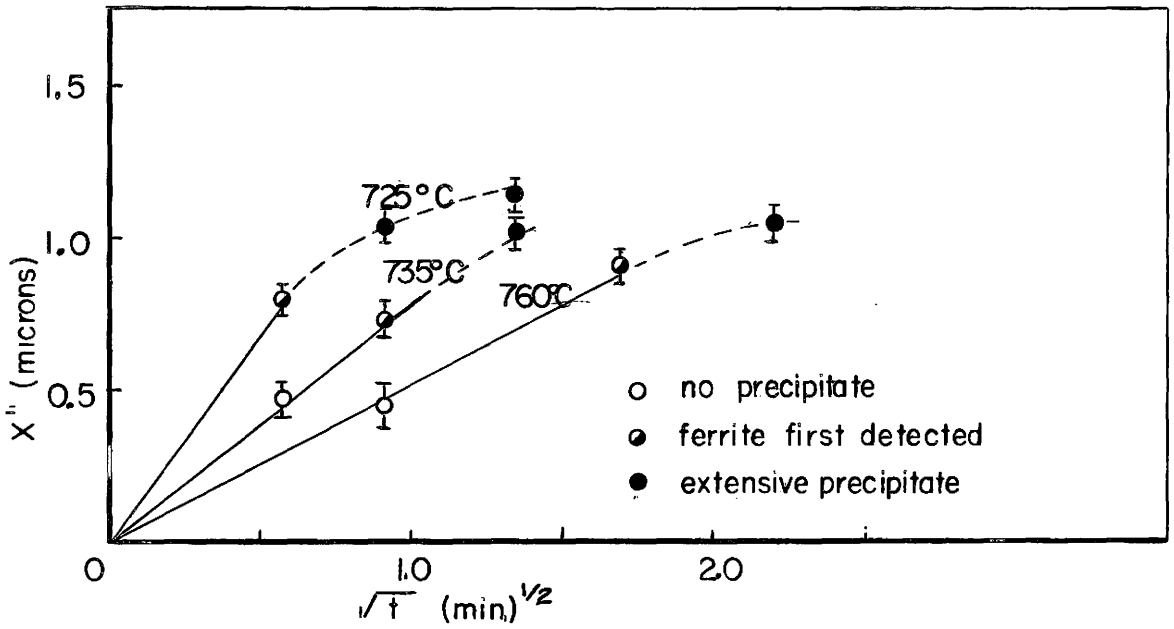

Figure 26. Ferrite growth data for ternary 1.52% Mn, 0.210% C diffusion couples.

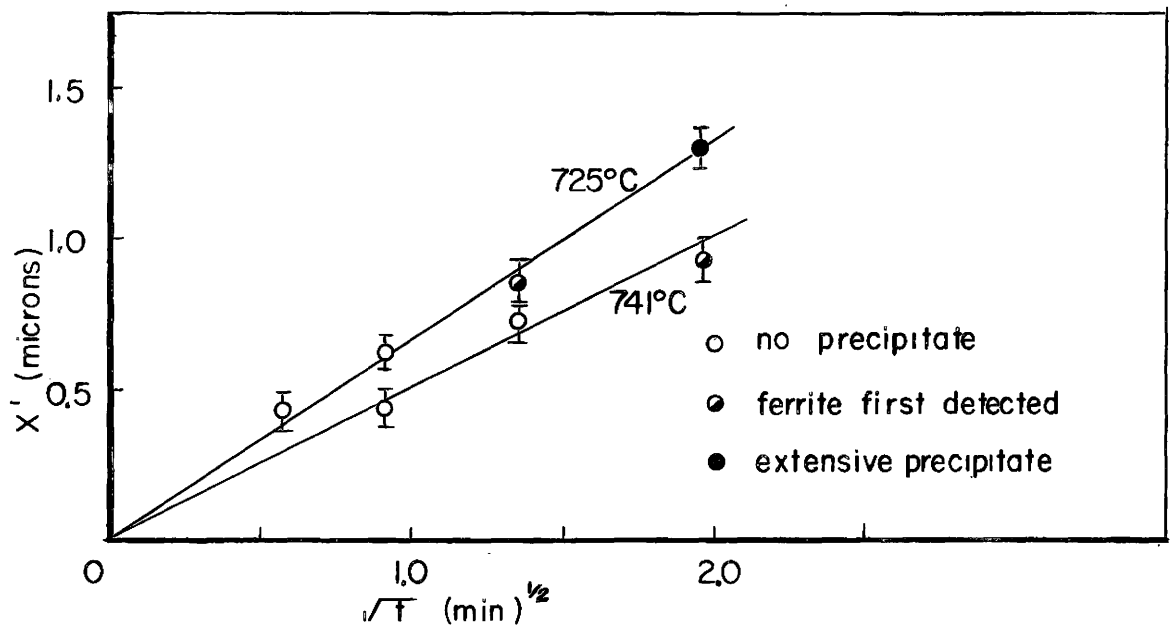

Figure 27. Ferrite growth data for ternary 1.52% Mn, 0.335% C diffusion couples.

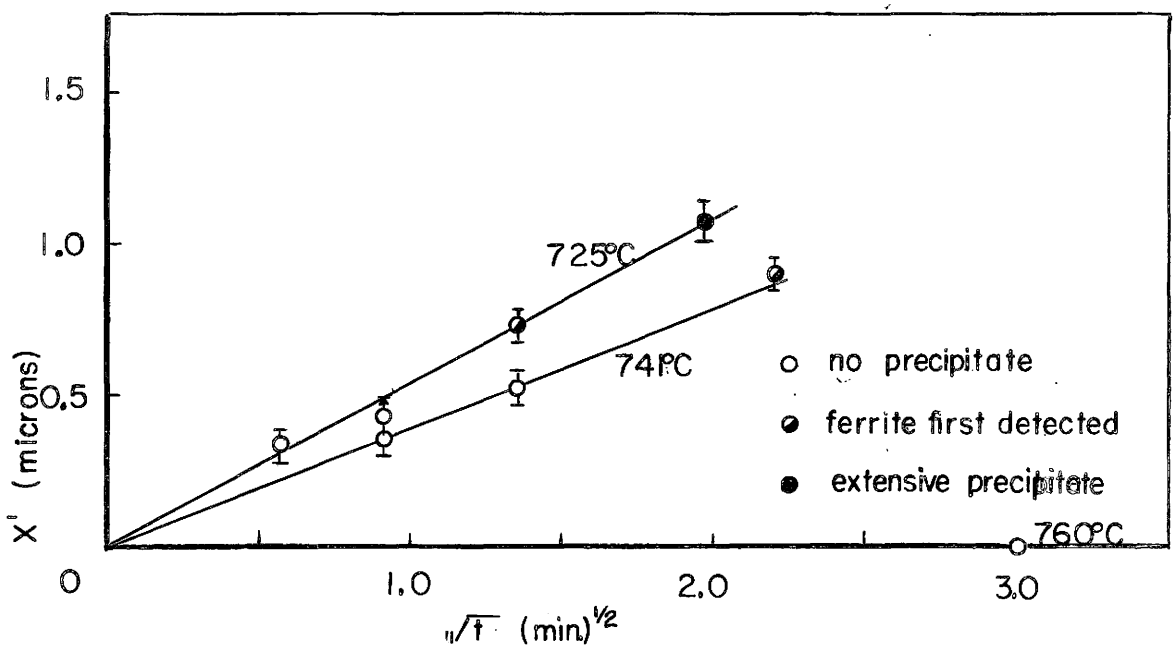

Figure 28. Ferrite growth data for ternary 1·52% Mn, 0·405% C diffusion couples.

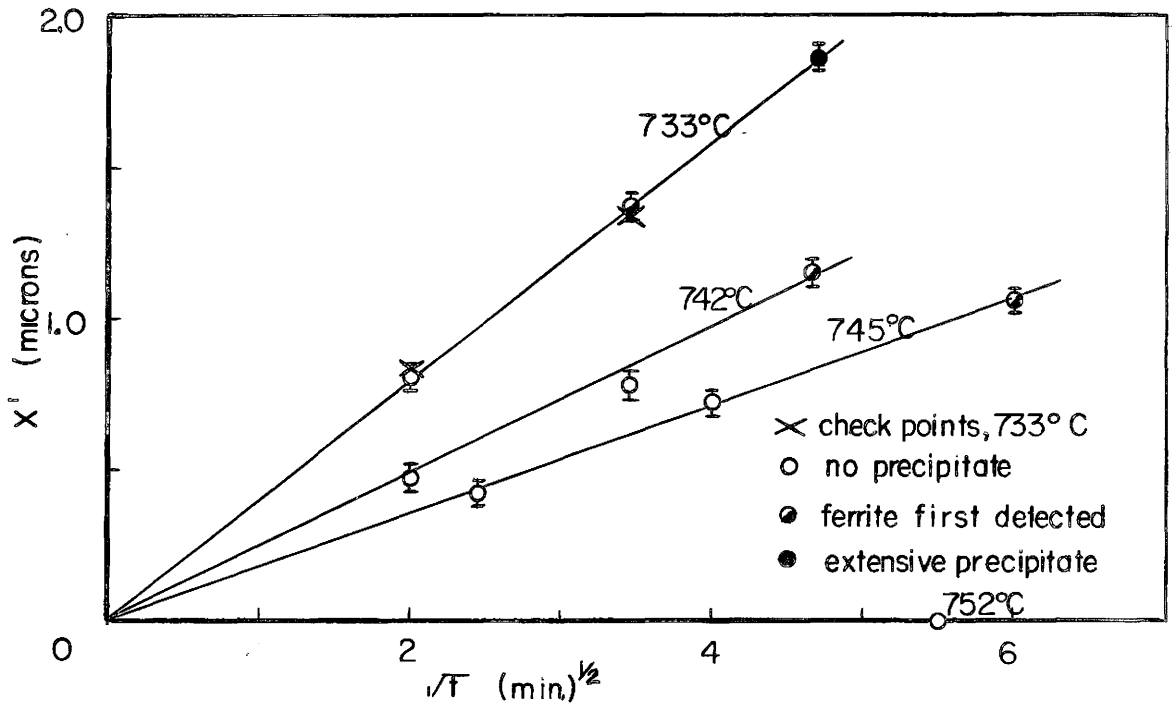

Figure 29. Ferrite growth data for ternary 3·16% Mn, 0·282% C diffusion couples.

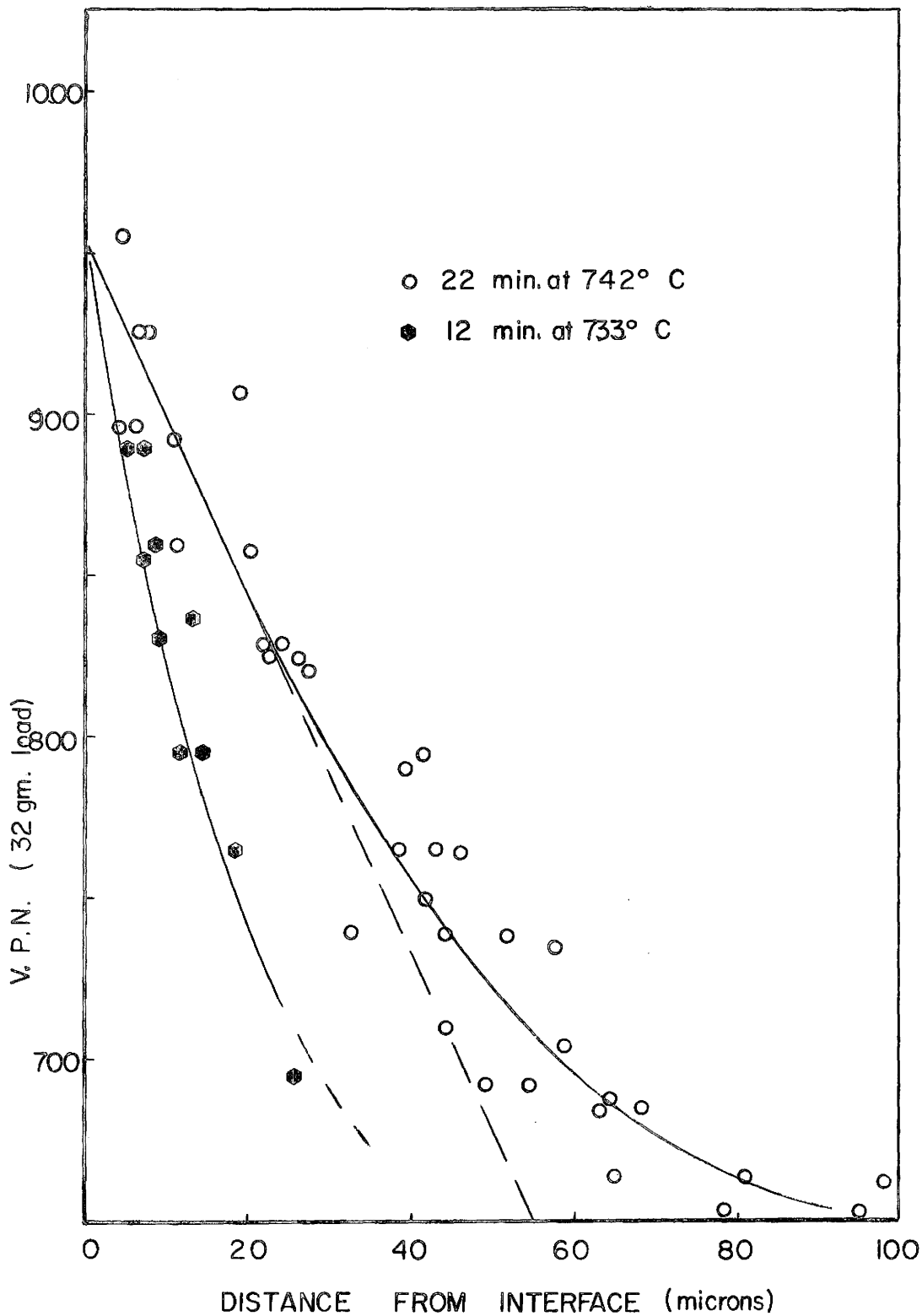

Figure 30. Microhardness traverses of 0·282 wt% C, 3·16 wt% Mn, diffusion couples.

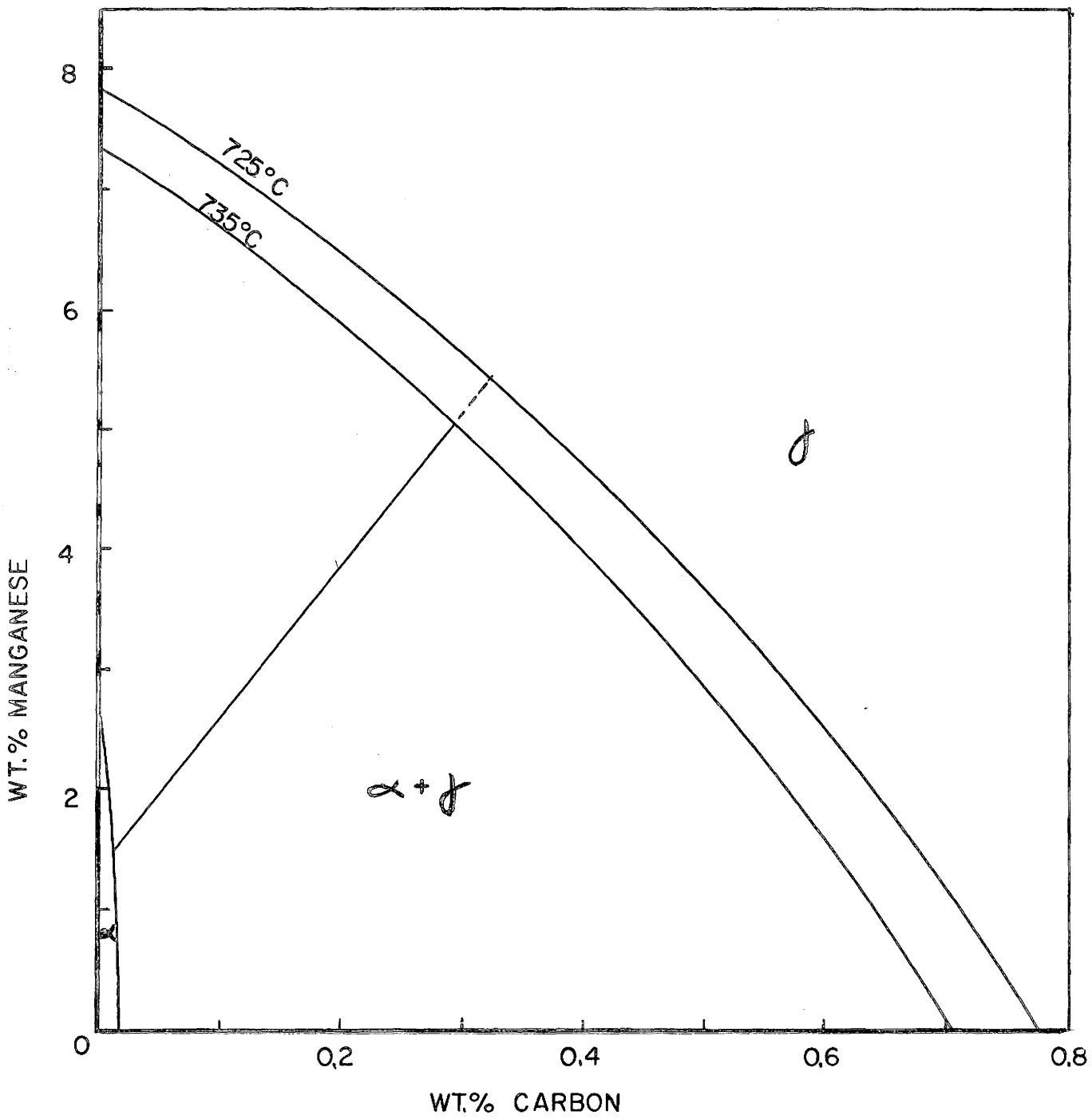

Figure 31. Iron, carbon, manganese constitution diagram, showing equilibrium tie-line.

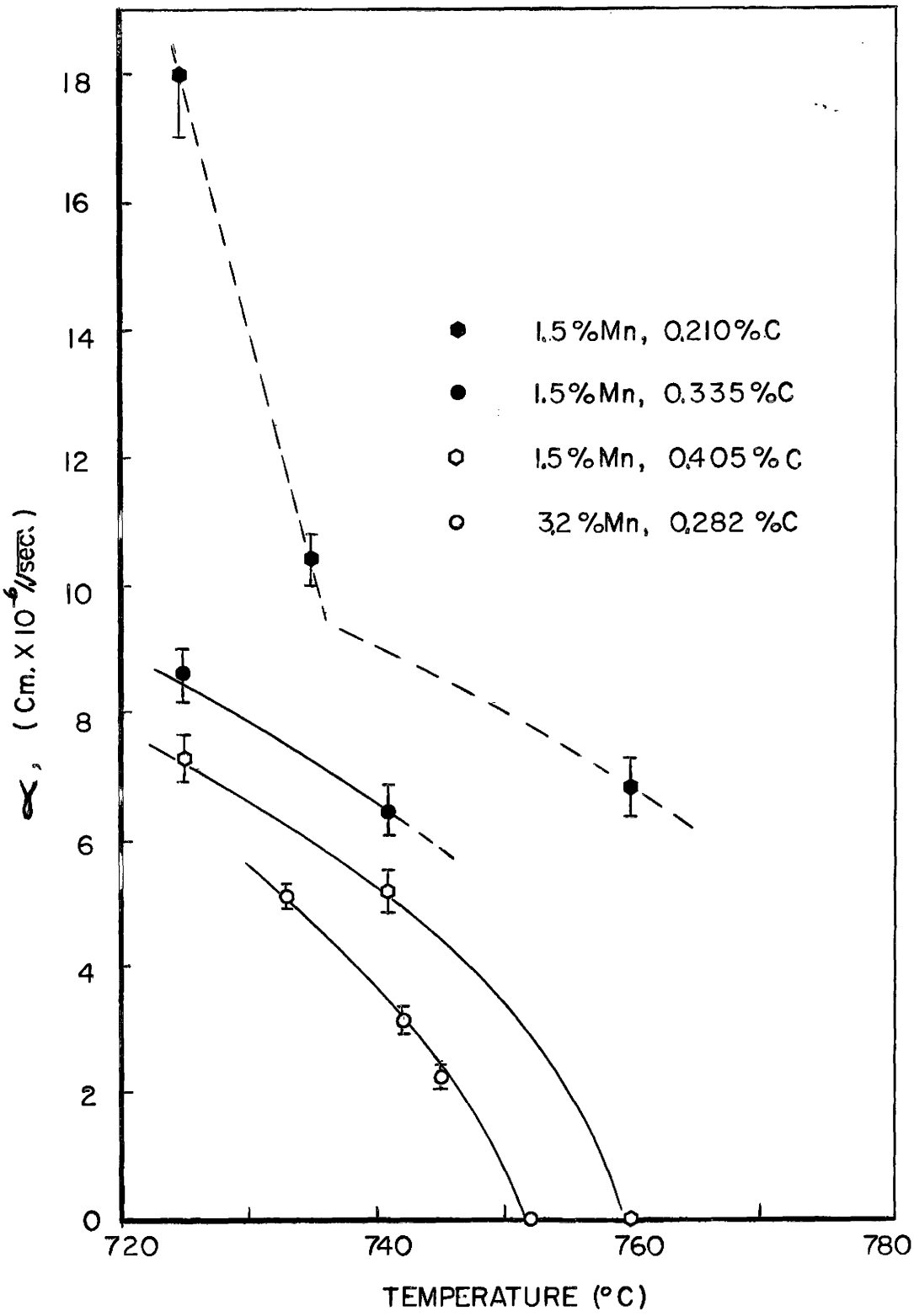

Figure 32. Summary of ferrite growth data for all ternary compositions studied. Each line shows the variation of the ferrite growth rate (for a particular composition) with temperature.

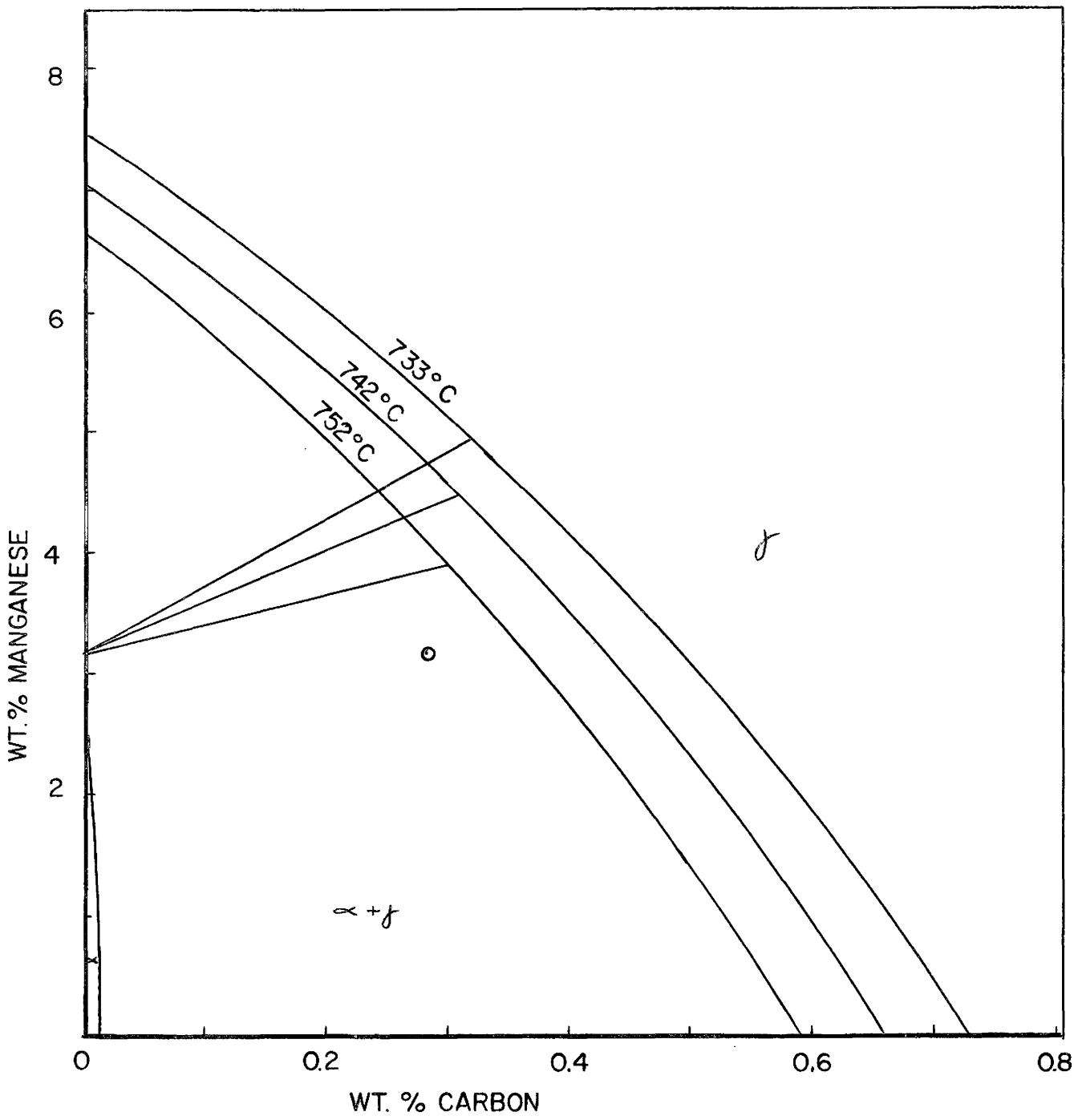

Figure 33. Calculated "constrained" tie-lines for ferrite growth in 0·282 wt% C, 3·16 wt% Mn austenite.